Theses and dissertations

1-1-2010

Using electrical resistance tomography to characterize and optimize the mixing of micron sized polymeric particles in a slurry reactor

Parisa Tahvildarian
Ryerson University

USING ELECTRICAL RESISTANCE TOMOGRAPHY TO CHARACTERIZE AND OPTIMIZE THE MIXING OF MICRON SIZED POLYMERIC PARTICLES IN A SLURRY REACTOR

by

Parisa Tahvildarian

B.Sc. Chemical Engineering, Sharif University of Technology, Iran, 1996

A Thesis presented to Ryerson University in Partial Fulfillment of the Requirements for the Degree of Master of Applied Science in the Program of Chemical Engineering

Toronto, Ontario, Canada, 2010

AUTHOR'S DECLARATION

I hereby declare that I am the sole author of this thesis.

I authorize Ryerson University to lend this thesis to other institutions or individuals for the purpose of scholarly research.

Parisa Tahvildarian

I further authorize Ryerson University to reproduce this thesis by photocopying or by other means, in total or parts, at the request of other institutions or individuals for the purpose of scholarly research.

Parisa Tahvildarian

BORROWER'S PAGE

Ryerson University requires the signatures of all persons using or photocopying this thesis. Please sign below, and give address and date.

To Hossein

for his love and support

and

my little angels, Parmis and Adrin

Abstract

Using Electrical Resistance Tomography to Characterize and Optimize the Mixing of Micron Sized Polymeric Particles in a Slurry Reactor.
Presented by Parisa Tahvildarian as a Master of Applied Science Thesis in Chemical Engineering, Ryerson University, Toronto, Canada, 2010.

A solid-liquid mixing system has a significant role in the suspension polymerization, crystallization, adsorption, and solid-catalyzed reactions. In this study, Electrical Resistance Tomography (ERT) was employed to investigate the effect of the particle size, the design parameters such as impeller type, impeller clearance and impeller diameter as well as operating conditions such as impeller speed, impeller pumping mode, and solids concentration on the mixing of micron sized latex particles in a slurry reactor. The ERT data were used to calculate the concentration profile and the degree of homogeneity in three dimensions, as a function of design parameters and operating conditions within the reactor.

In this work, tap water and latex particles (5.2 µm, 8.5 µm, 9.1 µm) were used as liquid and solid phase, respectively. Six axial impellers were utilized (A310, A100, A200, A320, A315, 3AM) with impeller speed (N) varying from 252 rpm to 400 rpm. Impeller diameter to tank diameter ratios (D/T) were in the range of 0.29 to 0.47 while, the impeller clearance (C/T) was changed in the range of $T/3.8$ to $T/2.5$. Impeller pumping was tested in both downward and upward directions. The concentration of latex particles was ranged between 15 wt% and 30 wt%.

This study shows that the level of homogeneity in a solid-liquid mixing system improved with the increase in impeller speed. However, after achieving the maximum level of homogeneity, any further rise in the impeller speed had a detrimental effect on the level of homogeneity. A310 impeller, with D/T ratio of 0.31, demonstrated the highest level of homogeneity while the upward pumping direction was found to be more efficient than the downward one. In addition, a clearance of T/3 proved to create the highest level of homogeneity. Also, the results showed that a rise in the size and concentration of particles decreases the level of homogeneity. Thus, 5.2 µm latex particles with the concentration of 15 wt% demonstrated the highest level of homogeneity.

Applying the findings of this study will lead to improved equipment design, chemical cost reduction, increased production rate, improved quality of products, and more efficient use of power in slurry reactors.

Acknowledgements

Table of Contents

List of Figures

List of Tables

Chapter 1
Literature Review

1.1 Introduction

Solid-liquid mixing processes are widely used in industry, such as coal-water slurries, paper-pulp slurries, polymer dispersions, ion-exchange resins, and sugar crystal slurries. In all these processes, a certain degree of mixing is required to achieve the desired result. Insufficient mixing drives the production process to the poor quality products, low production rate, and higher manufacturing costs, which is far greater than the cost of solving the mixing problem during the production process. Although, the mixing of solid-liquid systems has been extensively studied in the past, the lack of enough information about the optimization of the solid-liquid mixing, especially the mixing of micron sized particles in a liquid is realized.

This project, with the collaboration of Xerox Research Center of Canada, aims to optimize the mixing of micron sized latex particles in a slurry reactor. To optimize this mixing process, Electrical Resistance Tomography is used to investigate the effect of design parameters (e.g. impeller type, impeller clearance, impeller diameter), operating conditions (e.g. impeller speed, impeller pumping mode), particle size and solids concentration on the level of homogeneity. Afterwards, the optimum value for each variable is recommended. The results of this study are expected to improve the quality of products, decrease manufacturing costs, and lead to more efficient use of power in slurry reactors.

1.2 Solid-Liquid Mixing

Solid-liquid mixing is one of the most common industrial processes that increases the degree of homogeneity and the rate of the mass transfer between two phases (Paul *et al.*, 2004). The objective of a solid-liquid mixing is to produce a homogeneous mixture efficiently in terms of time and power consumption (Peker *et al.,* 2008). To optimize the solid-liquid mixing process, the type of impeller, shaft, baffle, impeller clearance, impeller diameter, impeller speed, impeller pumping direction, concentration of solid particles, and particle size have to be considered (Montante *et al.,* 2001). Despite the vast researches have been done so far, there is still a lack of

enough information about the prediction of fluid dynamics in a solid-liquid mixing process (Angst & Kraume, 2006).

1.3 State of Suspension

The solid suspension condition is characterized in three different areas: on-bottom for partial suspension (some solids rest on the bottom of the vessel for short periods), off-bottom for complete suspension (all solids are off the bottom of the vessel), and homogenous for uniform suspension (solid particles suspended uniformly throughout the vessel) (Sardeshpande *et al*., 2009).

The state of solids suspension depends on the impeller speed. At low impeller speed, most particles sit on the bottom of the vessel. The increasing of the impeller speed causes only parts of solids to get suspended to a certain level (Kraume, 1992 and Bujlaski *et al*., 1999). Therefore, at this state, the total surface area of particles is not used for mass transfer (Baldi *et al.,* 1977). A further increase in impeller speed leads to complete suspension at which all solids get suspended in a way that no particle sits on the bottom of the vessel for more than 1 to 2 s and a boundary layer get visible between the suspended particles and clear liquid area. At this state, maximum solids surface area exposes to the liquid for the mass transfer, however the solids distribution may not be uniform throughout the vessel. The impeller speed at this stage is called just suspended impeller speed *Njs*. The increasing of the impeller speed beyond the *Njs* reduces the height of the clear liquid and increases the height of the suspended area. The slurry height criterion to determine *Njs* is provided once the height of the suspension gets to 90% of the liquid height. Finally, the raise of impeller speed leads to uniform distribution of solids throughout the vessel (Kraume, 1992 and Bujlaski *et al*., 1999) at which, solids concentration is consistent throughout the vessel. The impeller speed at this stage is called critical impeller speed for homogenous suspension. Figure 1.1 presents three different states of solids suspension.
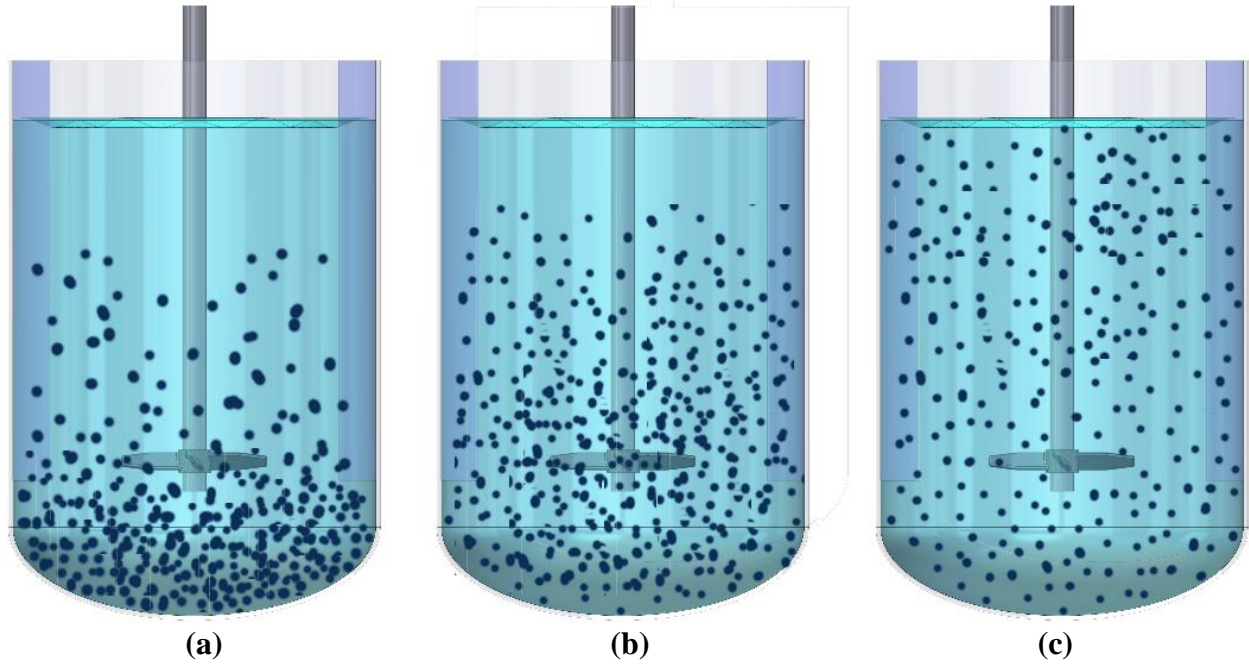
Figure 1.1 Degree of suspension (a) partial suspension, (b) complete suspension (just suspended), (c) uniform suspension

1.4 Just Suspended Impeller Speed

In all solid-liquid mixing processes, *Njs* is the minimum impeller speed required to suspend all particles and is estimated by Zwietering correlation (1985) as follow:

$$Njs = S v^{0.1} \left(\frac{g_c \, (\rho_s - \rho_l)}{\rho_l} \right)^{0.45} X^{0.13} \, d_p^{\,0.2} \, D^{\,-0.85}$$

(1.1)

where D is the impeller diameter; d_p is the particle diameter; X presents the mass ratio of suspended solids to liquid; S is the dimensionless number which is a function of impeller type; *Njs* shows the impeller speed for "just suspended particles"; v is the kinematic viscosity of the liquid; g_c presents the gravitational acceleration constant; ρ_s and ρ_l are the density of particles and the density of liquid, respectively.

1.4.1 Different Methods of Measuring Just Suspended Impeller Speed

Several visual and non-visual experimental methods have been proposed to determine the just suspended impeller speed. These methods are elaborated on their procedures as follows:

1.4.1.1 Visual Methods

Zwietering (1985) offered a visual observation technique to measure *Njs.* Using a tank with transparent wall and a mirror placed underneath of the tank, he observed the motion of solids on the bottom of the tank. To aid the observation, he illuminated the bottom of the tank with photoflood light. *Njs* was determined as the impeller speed at which no solids was remained at rest on the bottom of the tank for more than 1 or 2 s. This method is very subjective and can determine *Njs* with an accuracy of ±5%.

 Einenkel and Mersmann (1977) introduced another visual technique. They visually determined the height of the interface between the solid-liquid suspension and the clear liquid. They determined *Njs* as the speed at which the height from the bottom of the tank to the interface (boundary layer between the slurry and clear liquid) was 90% of the total liquid height. This method does not appear to be accurate because the fine particles come to the top of the tank before the last particle lifts off the tank bottom. According to Kraume (1992), this speed had approximately 20–25% deviation from that predicted by Zwietering's (1958) method.

Hicks *et al*. (1997) determined *Njs*, measuring the settled bed height visually at different impeller speeds. According to his method, *Njs* is defined as the impeller speed at which the height of the settled bed is zero. The defect of this method is that, the bed surface is usually uneven due to the complex flow pattern in the mixing vessel. Therefore, the bed height is measured at a plane just above the tank bottom and at a point half way between the two consecutive baffles. In this method, only with a skilled observation, a reproducibility of ±5% is obtained. For solids concentration above 8 w/w%, this method is not reliable (Oldshue and Sharma, 1992). The accuracy of all mentioned visual methods depends on the subjective evaluation. Also, these visual measurements require transparent tank wall, which is possible for the laboratory scale but impractical for the large scale installations. The only advantage of the mentioned visual methods is their simplicities.

1.4.1.2 Power Consumption Method

Rewatkar *et al*. (1991) presented another method based on the measuring of the variation in power consumption with respect to the impeller speed. This method is very useful when the mixing vessel is opaque and the visual observation method cannot be used. As the impeller speed

increases, more particles get suspended. Thus, more energy is dissipated at solid-liquid interface. As a results, the power consumption and power number increase. After all solid particles are suspended; any further increase in the impeller speed doesn't change the power number. Therefore, the impeller speed at which the power number approaches a constant value is called *Njs*. Figure 1.2 shows the change of the power number with the increase of the impeller speed.
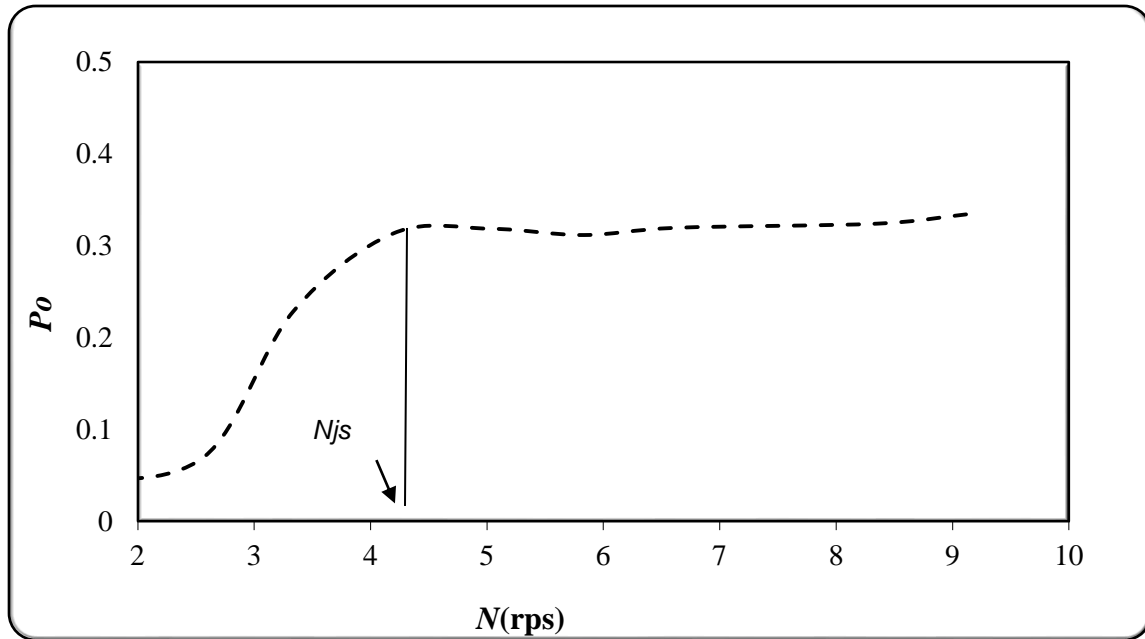
Figure 1.2 The impeller speed versus power number

1.4.1.3 Mixing Time Method

This method is based on the measurement of mixing time (θ_{mix}) with respect to the impeller speed in the clear liquid and in the solid-liquid system, keeping all other geometrical and operating parameters constant (Raghava Rao and Joshi, 1988; Rewatkar *et al.*, 1991). In this method, the curve of mixing time versus impeller speed for solid-liquid system is compared to that for the single-phase (only liquid) system. *Njs* is the impeller speed at which the difference between the mixing times in the presence and absence of solids is the maximum.

1.4.1.4 Concentration Method (Local Value of Concentration)

Bourne and Sharma (1974) and Musil (1976) measured *Njs* based on the measurement of the local concentration. They observed that at low impeller speed, most of the particles sit on the

bottom of the tank and cause low solids concentration above the bottom of the tank. As the impeller speed increases, the particles gradually start suspending and the solids concentration just above the bottom of the vessel increases. Bourne, Sharma and Musil proposed that *Njs* is the impeller speed at which the particles concentration just above the bottom of the tank is maximum or independent on the impeller speed. This method is also called the concentration peak method.

1.4.1.5   Concentration Method (Overall Value of Concentration)

Brucato *et al*. (1997) revised the pressure measurement technique developed by Biddulph (1990) to obtain the overall value of the solids concentration in the vessel. The suspension of particles causes the pressure at the bottom of the tank to change. He used a pressure probe to measure the pressure variation at the bottom of the tank and realized that the pressure variation is directly proportional to the mass of the suspended solids. The pressure reading was calibrated to get the value of the solids concentration in the vessel. This way, *Njs* is the impeller speed at which the particles concentration in the tank is maximum or independent on the impeller speed

All mentioned methods were developed to measure minimum impeller speed required to suspend all particles. To have a homogenous solid-liquid system, the impeller speed should be greater than *Njs*. Mixing process is evaluated with respect to the mixing quality and cost. To achieve the efficient mixing with minimum cost, mixing time and power consumption need to be considered.

1.5 Mixing Time

Mixing time is one of the important parameters used to design a mixing system and is the time needed to obtain a desired degree of homogeneity, after the addition of solid particles to a tank (Jahoda and Machon, 1994; Bouaifi and Roustan, 2001). Mixing time is influenced by solids concentration (Raghav Rao *et al*., 1988; Harrop *et al.,* 1997), impeller diameter and off- bottom clearance and impeller speed (Kuzmani´c et al., 2008), however there is still the lack of sufficient information about the effect of solids on the mixing time (Raghav Rao *et al*., 1988; Harrop *et al.,* 1997).

Kuzmani´c *et al*. (2008) and Raghav Rao and Joshi (2008) investigated the effect of solids concentration on the mixing time. They realized that as the solids concentration increases, the

fluid circulation velocity reduces and the mixing time increases. Raghav Rao and Joshi (1988) developed a correlation for the dimensionless mixing time as follow:

$$(N\theta)_{CS} = CX^{0.19}d^{0.11}\frac{T^{0.32}}{D^{1.15}}$$

(1.2)

where $(N\theta)_{CS}$, d, T, D, C, and X, are dimensionless mixing time at critical impeller speed, particle size, tank diameter, impeller diameter, clearance and solid concentration, respectively.

1.5.1 Experimental Methods to Measure the Mixing Time

So far, several methods, based on the electrical conductivity, concentration measurements, temperature colorimetric, and optical measurement have been developed to measure the mixing time in a vessel (Nere *et al.*, 2003). The most common experimental techniques to measure the mixing time are discussed as follows:

1.5.1.1 Visual Techniques

The simple technique to measure the mixing time is to inject a dye to the mixing vessel and observe how the dye moves throughout the mixing vessel (Shervin *et al.,* 1991). Another technique used commonly is called dye decolonization (Menisher *et al*., 1999). In fact, one chemical colors the contents of the mixing tank and the addition of the second chemical removes the color (Fox and Gex, 1956). This simple technique is used infrequently in the industry because the industrial vessels are non-transparent (Nere *et al*., 2003). Also, this visual technique provides an approximation for mixing time in mixing tanks (Paul *et al.,* 2004).

1.5.1.2 Conductivity Probe Technique

In this technique, a single-point sensor (a probe) is used to measure the conductivity of the solution. Using a proper calibration, this conductivity is converted to the concentration (Kramers *et al.,* 1953). In this method, the tracer has to be an electrolytic solution. This method is very accurate however, it is very easy and cheap to use. The probe can only measure the local conductivity, and the calculated mixing time depends on the probe position. In addition, for non-conducting systems and systems where rheological properties are sensitive to tracer concentration, this technique is not suitable.

1.5.1.3   Light Intersection Imaging Technique (Laser-induced Fluorescence)

In this technique, a laser sheet generator, which is directed toward the mixing tank and a fluorescent indicator (as a trace) are used to measure the mixing time. After adding the tracer, it glows only at the plane of the laser sheet. The mixing time is obtained as the time required for achieving an image with homogeneous color throughout. This technique requires a transparent vessel; therefore, it cannot be used in the industry (Hackl and Wurian, 1979 and Distelhoff *et al.,* 1997).

1.5.1.4   Liquid-Crystal Thermography (LCT)

The principle of this technique is the coloring of thermochromatic liquid crystals (LCs) and observing a different color once they expose to a different temperature. The crystals are suspended in the mixing tank. After sending a thermal pulse, the mixing of this thermal pulse transmits different colors to the liquid crystals in various parts of the vessel. These colors are analyzed either visually or by a camera. This method is fast but difficult to be used because the color response of the crystals is not perfect. In addition, since this technique needs transparent vessels, it is not generally applicable in the industry (Lee and Yianneskis, 1997).

1.5.1.5   Radioactive Liquid Tracer Technique

In this technique, a pulse of a radioactive liquid tracer is injected into the vessel and the profile of the tracer concentration is monitored (Pant *et al.,* 2001). Without disturbing the flow pattern, this technique can be used at high temperature conditions and non-transparent vessels (Nere *et al.*, 2003). The use of this technique is restrained by its unavailability, transportation difficulty, and health hazards.

1.5.1.6   Computer Tomography with Coherent Light

This technique requires radiations from four lines to calculate the concentration field in a mixing vessel. First, an object which is marked by a dye is exposed to the radiation with a monochromic light, and a 2D image is generated. After irradiation in different directions, the image of the object is reconstructed in horizontal planes using mathematical techniques. Using the image analysis, the negatives of the black and white films are scanned, processed and used for the tomographic reconstruction. This way, the concentration profiles of mixing performance are

obtained from which the mixing time is calculated. This technique requires a transparent vessel; thus, it cannot be used in industry (Zlokarnik, 2001).

1.5.1.7 Thermocouple-based Technique

In this method, a liquid, with a different temperature from the bulk, is added to a mixing tank. Then, the temperature of the different points in the bulk is monitored over the time using thermocouple. In this method, the probes output is used to calculate the mixing time. This technique is applicable for non-transparent and/or non-conducting liquid but is not suitable for the fluids, whose properties such as viscosity are very sensitive to temperature changes (Masiuk and Lacki, 1993).

1.5.1.8 Electrical Resistance/Impedance Tomography (ERT)

The electrical tomography technique is based on the reconstruction of the electrical conductivity distribution in the mixing tank (Williams *et al.,* 1993; Mann *et al.,* 1997; Holden *et al.,* 1998). A number of equally spaced electrodes are installed on the periphery of the vessel wall. To measure the conductivity distribution and then the mixing time, the electrical current is injected into two adjacent electrodes and then the voltage is measured between the other adjacent electrode pairs (adjacent strategy). Then, the local distribution of the electrical conductivity is reconstructed topographically using the back projection algorithm. Afterwards, ERT data are used to obtain concentration profile and mixing time in the vessel.

The purpose of a mixing process is to achieve the desired level of homogeneity with the minimum cost. Thus, to reduce the cost of a mixing process, the power consumption has to be concerned.

1.6 Power Consumption

Power input is an important parameter for mixing systems. It is the energy transformed from an impeller to a fluid per unit time. The impeller power in a homogeneous liquid depends on the geometry of impeller and tank, the density and viscosity of the liquid, the impeller speed and the gravitational force (Tatterson, 1991):

$$P = f(\mu, \rho, N, D, T, g) \tag{1.3}$$

where *P, μ, ρ, D, T, N,* and *g* are power, fluid viscosity, fluid density, impeller diameter, tank diameter, impeller speed, and gravitational acceleration, respectively.

Applying dimensional analysis, the following equation is obtained (Skelland, 1967):

$$\frac{P}{\rho N^3 D^5} = f\left(\frac{\rho N D^2}{\mu}, \frac{N^2 D}{g}\right) = f(\text{Re}, Fr) \tag{1.4}$$

According to Equation 1.4, dimensionless power coefficient, $P/\rho N^3 D^5$, is a function of both Reynolds number (Re) and Froude number (*Fr*) for a fluid and is referred to power number, P_o, as follows:

$$P_o = \frac{P}{\rho N^3 D^5} = f(\text{Re}, Fr) \tag{1.5}$$

$$Fr = \frac{D N^2}{g} \tag{1.6}$$

$$\text{Re} = \frac{\rho N D^2}{\mu} \tag{1.7}$$

1.7 Settling Velocity of Particles

Settling velocity of particles is the velocity after acceleration from zero to steady state at which the drag force balances the buoyancy and gravitational forces without interaction between solid particles. This constant velocity is referred to terminal velocity (Guiraud *et al.*, 1997). Oldshue (1983) defined three regimes to describe the effect of settling velocity on the particles suspension. He realized that for the settling velocity of particles in the range of 0.1-0.6 ft/min, 4-8 ft/min, and 16-60 ft/min, the suspension of particles is easy, moderate and hard, respectively

Perry & Green (1984) offered an equation to calculate the terminal velocity for spherical particles as follows:

$$V_t = \left(\frac{4\, g_c\, d_p\, (\rho_s - \rho_l)}{3\, C_D \rho_l} \right)^{\frac{1}{2}} \tag{1.8}$$

where, g_c is the gravitational constant, d_p is the particle diameter, ρ_s is the particle density, ρ_l is the liquid density and C_D is the drag coefficient, which is a function of particle Reynolds number:

$$\mathrm{Re}_p = \left(\frac{\rho_l\, V_t\, d_p}{\mu} \right) \tag{1.9}$$

In laminar regime, the drag coefficient is a function of particle Reynolds number as follow:

$$C_D = \left(\frac{24}{\mathrm{Re}_p} \right) \tag{1.10}$$

For the Newtonian fluid in the turbulent regime ($Re_p > 1000$), the drag coefficient is a constant value (0.445). Thus, the terminal velocity is estimated as follow:

$$V_t = 1.73 \left(\frac{g_c\, d_p\, (\rho_s - \rho_l)}{\rho_l} \right)^{\frac{1}{2}} \tag{1.11}$$

A mixing process is influenced by operating conditions and design parameters. To achieve a homogenous solid-liquid suspension with the minimum power consumption and cost, the operating conditions and design parameters have to be concerned.

1.8 The Effect of Design Parameters on the Mixing Process

Design parameters, such as the geometry of the tank, impeller type, impeller clearance, impeller diameter, and concentration have significant effects on the mixing performance. In the following sections, the effects of designed parameters are investigated.

1.8.1 The Bottom Shape of the Vessel

Geometry of a mixing vessel, dimension, and bottom shape are important design parameters of a mixing process. Dish-bottomed vessels are preferred to flat-bottomed vessels. In fact, the bottom shape of a vessel not only affects the location of dead zones but also influences the just suspended impeller speed. In a flat-bottomed vessel, dead zones are in the corner between the bottom of the tank and the tank wall. In a dish-bottomed vessel dead zones are under the impeller position or between the center of the tank and the periphery of the bottom. Just suspended impeller speed is 10 to 20% higher in a flat-bottomed vessel than that in a dish-bottomed vessel. As a result, a dish-bottomed vessel is preferred to a flat-bottomed vessel (Bittorf and Kresta, 2003).

In addition, the best geometric proportion of a mixing vessel is a tank with height equal to diameter. Tall tanks with height greater than diameter (Z/T > 1) need multiple impellers to create motion (McDonough, 1992). For a solid suspension system, if Z/T >1.5, the use of the multiple impellers is necessary (Paul *et al*., 2004).

1.8.2 Shaft

The shaft can be installed in three different positions: on the bottom, on the top and on the side of a tank. Top-entry shafts are very common in industrial applications however; side-entry shafts are suitable for blending homogenous fluids or slurries of solid particles (King, 1992). Bottom-entry shafts are rarely utilized. They are used mainly with dished-bottomed tanks. If the shaft is installed on the top, sealing to prevent leakage is not required. Also, the pumping rates of top-entry shafts are higher and blending times are shorter than that of the side-entry shafts. Also, if the shaft is installed on the side of the tank, the presence of baffle is not required because the shaft may prevent the vortices.

1.8.3 Baffle

Mixing vessels are sometimes equipped with baffles, usually located at or near the walls. The function of a baffle is to inhibit liquid swirl, minimize tangential flow, and develop the axial-flow pattern. Most of the mixing vessels are equipped with four baffles and are called "fully baffled" mixing vessels. Adding any more baffles to a "fully baffled" mixing vessel doesn't

seriously increase the power consumption of impellers (Rushton, 1947). Most common baffles are made in the form of straight flat plates of metal that sit along the side of vertically oriented cylindrical vessel and called standard baffles. Baffle width is a function of viscosity. For very high viscous fluids, baffles are not necessary, due to enough resistance to flow at the walls. As the viscosity decreases, the presence of the baffle with large width becomes essential (Ulbrecht and Patterson, 1985).

1.8.4 Impeller Type

Since mixing processes have significant effects on the most of the chemical industries, the selection of a proper impeller is very crucial (Kramers *et al*., 1953). Generally, there is not a unique impeller to meet all process specifications (Oldshue and Tood, 1981). Determination of the most effective impeller is based on the knowing of the process requirements and physical properties of materials to be mixed (Wu and Pullum, 2001). Depends on the generated flow, impellers are categorized in two groups: axial-flow impellers and radial-flow impellers. Axial-flow impellers such as propellers, marine-type and pitch-blade impellers release fluid parallel to the impeller shaft (in a vertical direction) (Oldshue, 1983). They are used in homogenization process (Thring and Edwards, 1990), solid-liquid suspension, blending and convective heat transfer (Myers *et al.*, 1996). Unlike axial-flow impellers, radial-flow impellers such as disc turbine (Rushton), hollow-blade turbine (Scaba) and flat-blade impeller release fluid to the wall of the tank in radial direction (horizontal direction) (Oldshue, 1983). After leaving the blade tips, the flow is cleaved into two equal flows (up and down) and consequently, generates strong top-to-bottom flows, above and below the impeller with the equal suctions. Radial-flow impellers exert shear stress to a fluid to remove the boundary layer between various phases such as the mixing of immiscible or viscous fluids (Figure 1.3) (Thring and Edwards, 1990).
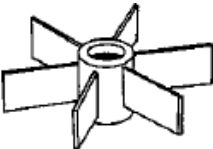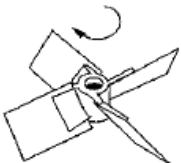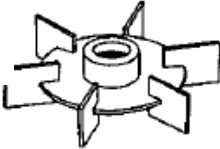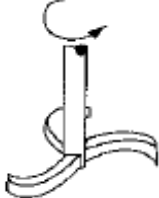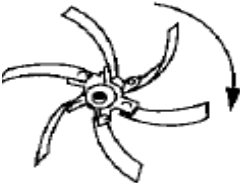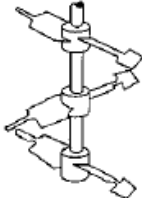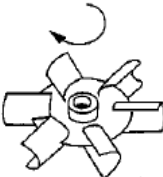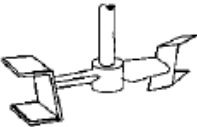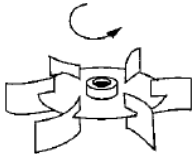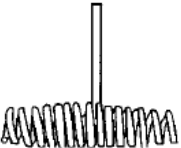
Impellers can further classified as propellers, hydrofoils, and high efficiency impellers. Hydrofoils and propellers generate high flow and low shear rate. They are generally employed for solids suspension, and heat transfer applications with moderate viscosity (McDonough, 1992). High efficiency impellers such as paddle, anchors, helical and spirals are suitable for the mixing of viscous fluids. Turbines are used in gas-liquid, liquid-liquid dispersions and other

mass transfer applications (Harnby *et al*., 1997). Table 1.1 presents different axial and radial-flow impellers used in the industry.

(a) (b)
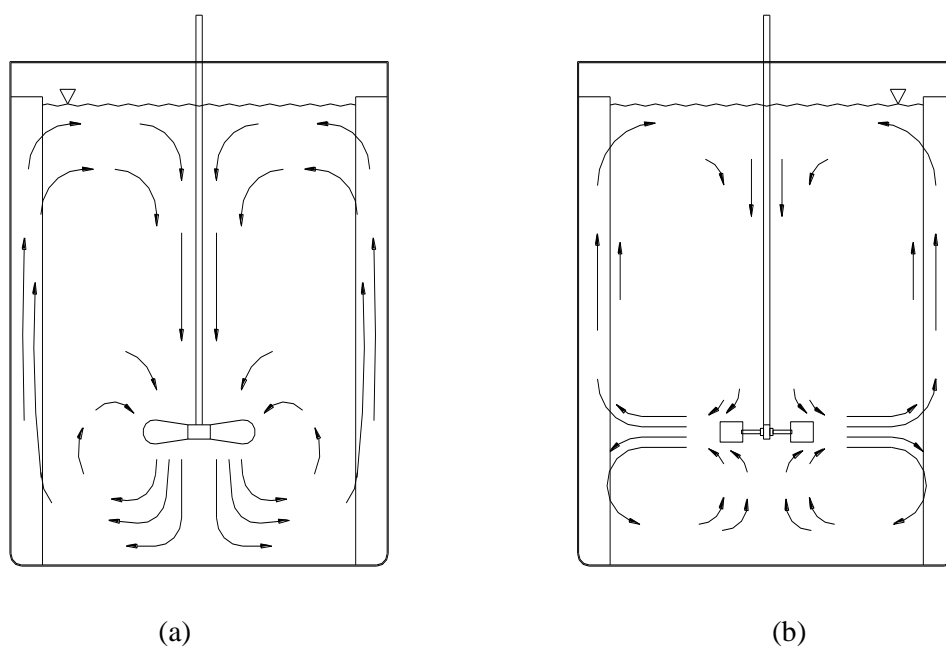
Figure 1.3 Flow patterns in a baffled tank, generated by: (a) axial-flow impeller, and (b) radial-flow impeller

Table 1.1 Different axial and radial- flow impellers

Axial –Flow Impellers	Radial-Flow Impellers
Propeller (A100)	Open flat blade
Pitched blade turbine	Disk style Rushton
Pfaudler retreat curve	Back swept open
Ekato MIG	Scaba SRGT
Ekato INTERMIG	Chemineer CD 6 Smith
	Spring impeller

1.8.5 Clearance

Clearance is the distance from the bottom of a vessel to the impeller location and has an important impact on the mixing quality. Improper location of an impeller results in staged flow pattern and non-uniform distribution of the added material.

A large clearance generates deep vortex, which induces the air entrainment into the system and the splash of the fluid around (Paul *et al*., 2004). It causes a flow transition in which the flow direction at the bottom of a tank reverses from outward to inward. Thus, the velocity at the bottom of the tank decreases and the outflow of the impeller changes from axial to radial-flow pattern (Jaworsky *et al*., 1991). Therefore, complete solids suspension becomes much more difficult to achieve. In addition, this flow reversal results in the impractical increase in just suspended impeller speed, which cannot be easily correlated with Zwietering equation (Bakker *et al*., 1994).

On the other hand, for the impeller located very close to the bottom of the tank, the axial-flow pattern, generated with the downward pumping impeller, is similar to the radial-flow pattern. This phenomenon leads to a pumping reduction and a higher shear. For solid suspensions, this situation makes the bottom of the tank clear from the suspension of the particles however; it decreases the level of homogeneity in the entire of the tank (Paul *et al*., 2004).

1.8.6 Impeller Diameter

An important ratio in mixing vessel design is impeller to tank diameter ratio (D/T), which is selected from 0.16 to 0.98 (McCabe, 2005). When the impeller to tank diameter ratio is too small, the velocity at the vessel base, close to the tank wall, is too small to suspend the solids, contrary for the large D/T ratio, the outflow of the impeller mostly turns into a radial- flow pattern and causes solids to settle at the center of the vessel base (Bakker *et al*., 1994). The diameter of the impellers which produce bulk motion such as helical ribbons, screws, and anchors should be close to the tank diameter. In addition, the diameter of the impellers which generate turbulent flow such as axial and radial impellers should be one-fourth to one-half of the tank diameter (Tatterson, 1991).

1.9 Effect of Impeller Pumping Direction

Impeller pumping direction influences the level of homogeneity in a solid-liquid system. For the same clearance, the impeller pumping direction changes just suspended impeller speed and affects the state of the suspension. When the impeller is pumping upward, the fluid velocities, close to the liquid surface, increase. Thus, this pumping mode can be effective for entrainment of floating solids and gas dispersion. Also, it is a productive mechanism to incorporate lighter solids on the liquid surface, near the wall. As the impeller pumping direction switches into downward, the dynamic head effect is changed. Thus, the fluid is directed to the bottom of the tank (Selima *et al.*, 2008). Downward pumping mode is an effective mechanism to suspend heavy particles settled on the bottom of the tank (Paul *et al.*, 2004).

1.10 Effect of Concentration

The concentration of solid particles can change the level of homogeneity. In fact, the increase of the solids concentration causes the increase of particles number and viscosity. As the concentration increases the hindered settling velocity develops due to the firstly, the increase of the particle-particle interaction, secondly, the interaction of particles with upward flow of the liquid, which is generated by the settling of the particles, thirdly, the increase of the viscosity and density. This phenomenon causes the reduction of the settling velocity and the development of the hindered velocity (Paul *et al.*, 2004).

Maude (1958) derived an empirical correlation for the hindered velocity as follows:

$$V_{ts} = V_t \left(1 - x\right)^n \tag{1.12}$$

where V_{ts} is the hindered settling velocity for mono dispersed solid, V_t is the free settling velocity, x is the volume fraction of solids in the slurry. For $Re_p < 0.3$, n is 4.64; for

$0.3 < Re_p \leq 1000$, $n = 4.375 \ Re_p^{-0.0875}$; for $Re_p > 1000$, n is 2.33.

1.11 Effect of Particle Size

The size of particles in a solid-liquid suspension has a prominent effect on the mixing performance. The settling velocity of large particles is greater than that of smaller ones (Paul *et al*., 2004). 5Thus, particle size can change the level of homogeneity.

Generally, the particles utilized in industrial applications have a size distribution. Baldi *et al*. (1978) recommended the mass-mean diameter dp, calculated from the size distribution as follows:

$$dp = \frac{\sum_{i=1}^{n} n_i d_i^4}{\sum_{i=1}^{n} n_i d_i^3} \qquad (1.13)$$

where dp is the average particle diameter and n_i is number or mass fraction of the particle with d_i size. The particle size distribution and power consumption were experimentally measured for different size diameter from 0.2-0.9 mm (Angst & Kraume, 2006).

n_i is calculated from the weight percent data as follow:

$$n_i = \frac{mass\,of\,solids\,in\,i^{th}\,size\,class}{mass\,of\,particle\,of\,diameter\,d_i} \qquad (1.14)$$

In spite of the studies have been done on the mass- mean diameter, in practice, the largest particle size is used to achieve the desired process result (Paul *et al*., 2004).

1.12 Research Objective

Literature review of solid-liquid suspensions not only shows the lack of enough experimental information about the mixing hydrodynamic of suspensions but also, discloses the shortage of experimental works on the micron sized particles. Having taken the significance of solid-liquid mixing, this study employs ERT to investigate, experimentally, the effect of the following parameters on the mixing of fine particles suspension ($dp < 10$ μm):

- Designed related parameters
    - Effect of impeller type
    - Effect of impeller clearance
    - Effect of impeller diameter
- Operating condition related parameters
    - Effect of impeller speed
    - Effect of impeller pumping mode
    - Effect of particle concentration
- Effect of particle size

Applying the finding of this study will lead to improved equipment design, chemical cost reduction, increased production rate, improved quality of products, and more efficient use of power in slurry reactors.

Chapter 2
Electrical Resistance Tomography

Tomography is a technique to obtain the concentration profile inside a process. Recently, the application of tomography, a reliable tool to observe the behavior of numerous fluids in industry, has been increased (Reimers *et al*., 1984).

According to Yan *et al.* (2005) and Dierick *et al*. (2005) the different tomographic instrumentations currently used in medical and engineering area are as follows:

X-ray tomographic system, infrared tomographic system, Gamma-ray tomographic system, electrical tomography system, positron emission tomography (PET), magnetic resonance imaging (MRI), sonic or ultrasonic tomographic system, optical fiber process tomography (OFPT) and high-speed neutron tomography.

Depends on the physical properties of fluids (the status of matter and composition), process condition, desired resolution, equipment size and cost, different types of the tomography system are used. University of Manchester Institute of Science and Technology (UMIST) in England developed and applied electrical techniques to investigate different processes which contain conducting fluids (Williams and Beck, 1995). The tomography system, developed by this institute is based on the measurement of capacitance (ECT), resistance (ERT), and electromagnetic (EMT). In these systems, sensors are located around a vessel or pipe and emit the signals through the vessel. Also, in order to derive the information and make a cross-sectional image, the presence of an algorithm to reconstruct a tomographic image at many locations of measurement is necessary (Williams and Beck, 1995).

2.1 The Components of a Tomography System

Hoyle (2005) and Williams and Beck (1995) presented the components of a process tomographic instrument as follows:

- Hardware: sensors signal/data control

- – Software: signal reconstruction, display and interpretation facilities, generation of output control signals to process hardware

The two important steps in using tomographic techniques are: process imaging and image processing. Process imaging is involved in observing event inside a closed process. Image processing is involved in mathematically manipulating digitized images to derive information about the process. Among different types of the tomography's systems, electrical tomography is the most popular method due to its high-speed potential and simplicity and inexpensiveness (Scott *et al.,* 2001).

2.2 Electrical Tomography

According to Scott *et al.* (2001), electrical tomography uses electrostatic fields to image the conductive properties of a medium. Different types of electrical tomography are electrical capacitance tomography (ECT), electrical inductance (magnetic) tomography (EMT), electrical impendence tomography (EIT). Electrical resistance tomography (ERT) is a specific kind of electrical impendence tomography (EIT).

In this study, ERT is used to investigate the mixing of micron sized polymeric particles in a slurry reactor.

2.3 Electrical Resistance Tomography

The purpose of ERT is to measure electrical signals sending from different sensing electrodes and reconstruct the conducting properties. In this technology, multiple electrodes are installed around the periphery of a vessel. These electrodes are in contact with the fluid but don't disturb the process flow pattern. Current is injected to the interested area using the sending electrodes. Then, the voltage is created on a number of electrodes and is converted to the conductivity distribution using an algorithm (e.g. back projection algorithm) (Williams and Beck, 1995). Thus, the conductivity and concentration distribution will be measured without any influence on the process (Williams and Beck, 1995). In the case of using ERT system two factors should be concerned (Mewes and Schmitz, 2000):

  i. The spatial resolution

    ii.   Image quality

The spatial resolution refers to the percentage of the diameter of the cross-section (Mewes and Schmitz, 2000). Also, the accuracy and precision of a reconstructed image depends on the image quality. In fact, the method used to reconstruct an image can affect the quality of that image. For example, for dynamic processes if the measurement speed increases, capture rate will increase. As a result, noise level increases, which in turn results in the reduction of the image quality (Mewes and Schmitz, 2000).

2.3.1 Different Parts of ERT system

A typical ERT system consists of three main parts (Dickin and Wang, 1996):

1. Sensing system

2. Data acquisition system

3. Image reconstruction system/host computer

2.3.1.1 Sensing System

ERT is used to acquire the resistance distribution in the domain of interest. To receive resistance distribution inside a vessel, there are multiple equally axially spaced rings of electrodes located around a vessel. Each ring consists of 16 equally spaced rectangular or circular stainless plates (electrodes) formed into a circular ring. Without any disturbance of flow pattern, each electrode contacts the inner conductive fluid on the front surface. Other possible arrangements of electrodes are a set of electrodes sitting around a square cross-section and a vertical series of electrodes. To reduce the irrelevant environmental noise and interference, the electrodes are connected to the data acquisition system by co-axial cables. To ensure all voltage measurements are fixed against a common ground source, one electrode is required to connect to the ground source. This electrode is in contact with the internal fluid but located away from the measurement electrodes (Dickin and Wang 1996).

Depends on the process application variety of materials are used to fabricate electrodes. To achieve reliable measurements, the physical sensors must be more conductive than the electrolyte; otherwise reliable measurements are not achieved. Normally the electrodes are

metallic because they are fabricated and installed easily. Also, they have low cost and resistance against abrasion and corrosion. They are usually fabricated from stainless steel, brass, silver, silver palladium alloy, gold, or platinum (Paulson *et al.,* 1992).

The size of electrodes is another important factor in tomography technology that should be concerned. The size of electrodes depends on vessel diameter, range of measured conductivity, velocity of materials and required imaging speed (Mann *et al*., 1997). Despite of the different available structures of electrodes, the same optimized size of electrodes is used for both current injection and voltage measurement because of its simplicity (Fransolet *et al*., 2005).

2.3.1.2 Data-Acquisition System (DAS)

One of the required components of an ERT system is a stable data acquisition system (DAS) which is connected to electrodes. DAS obtains the quantitative data and discloses the state of the conductivity distribution inside a vessel. In order to observe any small change of conductivity in real-time, data acquisition should be done accurately and quickly (Williams and Beck, 1995).

Data acquisition system is responsible for the 6 following functions: 1-signal measurement, 2-demodulation, 3-filter and control, 4-waveform generation and synchronization, 5-multiplexer control and 6-power supply. A schematic diagram of the ERT data acquisition system is illustrated in Figure 2.1 (Holden *et al.,* 1998):
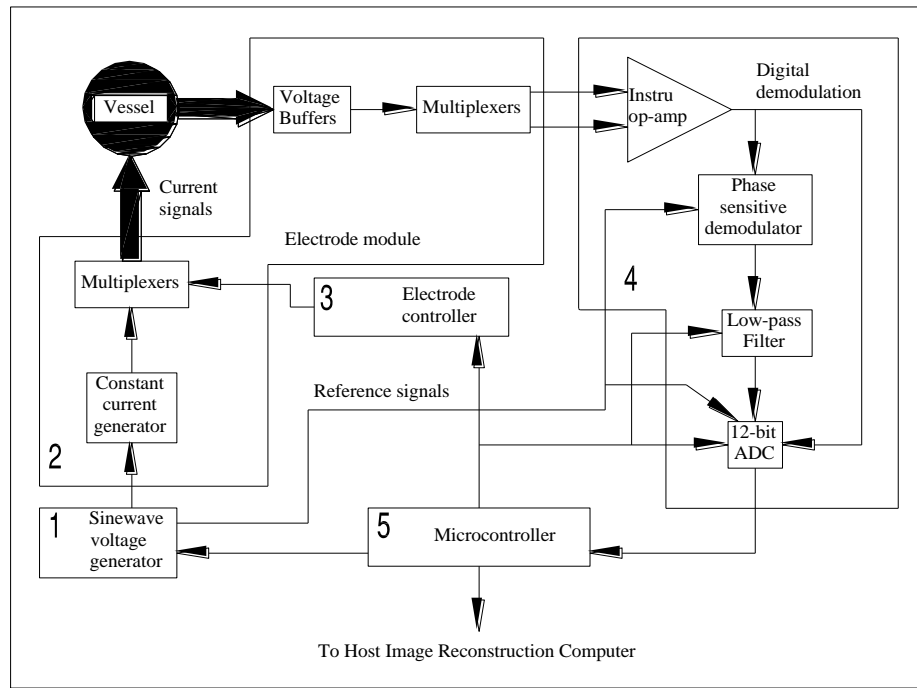
Figure 2.1 Different components of a data acquisition system

The digital "stir-case" function generators are responsible for the generating of staircase wave. Then a digital to analogue converter (DAC) converts the digital pattern to analogue. Afterward, the analogue pattern is filtered to eliminate unwanted harmonics. The output of this stage is a sine wave voltage that sends to a voltage- to- current convertor. Multiplexers (MUX) are the parts of the DAS system which share the current source and voltage measurement stages between any numbers of electrodes.

To generate a zero potential in the conducting region inside a vessel and eliminate the high common-mode voltage from the current-driven electrodes, an extra-grounded floating measurement (GFM) lead is connected to one of the unused electrodes, as a ground electrode, on the vessel. The other end of the lead is linked to the output of the common-mode voltage. Then all unwanted components are removed from the sine wave generator by a filter and using an analogue-to-digital converter (ADC) a desirable signal-to-noise (SNR) can be attained (Beck *et al*., 1993).

2.3.1.3   Data Collection Strategies

The four main strategies to investigate conductivity distribution in a vessel and obtain the maximum information are as follows:

a. Adjacent   b. Opposite   c. Diagonal   d. Conducting boundary

a.   Adjacent Strategy

This strategy is commonly for sensors with insulating boundaries. In this strategy, current is injected using a pair of neighbouring electrodes and voltage differences are measured, using all other pairs of neighbouring electrodes. To repeat this process, current is injected using all other possible pairs of neighbouring electrodes until all the independent measurements have been made. However, this strategy requires minimal hardware to implement and image reconstruction, it is very sensitive to measurement error and noise because of the non-uniformity of the current distribution and low current density at the center of the vessel (Mann *et al*., 1997; Kaminoyama, 2005).

In this strategy, the total number of independent measurements (*M*) is obtained by:

$$M = \frac{N(N-3)}{2} \tag{2.1}$$

where *N* is number of electrodes.

b.   The Opposite Strategy

In this strategy, current is applied through diametrically opposed electrodes. The electrode adjacent to the current-injecting electrode is the voltage reference electrode. The voltages are measured with respect to the reference at all electrodes except the current-injecting ones. To obtain the next set of data, the current is applied to the next pair of opposite electrodes in the clockwise direction. The whole procedure is repeated until all independent measurements have been made. Comparing to the adjacent strategy, the opposite strategy is less sensitive to conductivity changes at the boundary because most of the current flows through the central part of the region (Hua *et al*., 1993). Due to the less number of independent current projections, which can be applied, the opposite strategy has less image resolution than adjacent strategy

(Dickin and Wang, 1996). In this strategy, the total number of independent measurements (*M*) is obtained by (Viergever and Todd-Pokropek, 1988):

$$M = \frac{N}{4}\left(\frac{3N}{2} - 1\right)$$ (2.2)

c. The Diagonal Strategy

In this strategy, electrode 1 and 2 are fixed as the current reference and the voltage reference, respectively. Then, the current is sent successively to electrodes 3, 5, 7, 9... .Afterwards, respecting to the electrode 2, voltages from all electrodes except the current electrodes are measured. Then the current reference and voltage reference are changed to electrode 4 and electrode 3, respectively. Sending current through electrodes 6, 8... 16 and 2, voltage is measured on all other electrodes but the current-injecting ones. Compared to adjacent method, the diagonal strategy releases an image with better quality because it does not yield a high sensitivity in the periphery (Dickin and Wang, 1996).

d. The Conducting Boundary Strategy

In this strategy, only two electrodes are used for the measurements. The proportionately large surface area of the conducting boundary is used as the current sink to decrease the common-mode voltage across the electrodes doing the measurement. This measurement strategy allows ERT system to be used for process vessels and pipelines with electrically conducting boundaries. Compared to the adjacent strategy, this strategy has a considerable lower common-mode voltage component (Dickin and Wang, 1996).

Depends on the process, the strategy which has good distinguishability and high sensitivity to conductivity changes has to be used. The distinguishability is calculated by (Gisser *et al.*, 1987):

$$\delta = \delta(i) = \frac{\|R(\sigma_1) - R(\sigma_2)\|}{\|i\|} \geq \varepsilon$$ (2.3)

where, *i*, *ε*, σ_1, σ_2, *R* are current, precision of measurements, two conductivities and a nonlinear functional associated with the resultant boundary voltage, respectively.

2.3.1.4 Imaging Reconstruction

According to Pinheiro *et al*. (1999) and Mann *et al.* (1996), after obtaining the measurements from a set of electrodes sitting on the periphery of a vessel, an image reconstruction algorithm is applied to determine the interior distribution of the resistance in the process vessel. The algorithm, which can be used both on and off-line, exists in the host computer connected to the data acquisition system. There are two algorithms called qualitative algorithm, in which the reconstructed images are ascribed to dynamic and quantitative algorithm, in which the reconstructed images are ascribed to static.

In the qualitative algorithm, images are capable to show relative change in resistivity against an initially achieved set of reference data, which are usually obtained before the start of the experiment under quiescent conditions. Also, this algorithm releases an image showing the values of resistivity or conductivity for each pixel.

To proceed the image reconstruction two problems needs to be solved: first forward problem and second inverse problem. For instance, the determination of electrical measurements changes when the electrical conductivity of one pixel only in the cross section is changed, by a known amount, is called forward problem. On the other hand, determination of the electrical conductivity of each pixel within an image from a set of electrical measurements is called inverse problem. In fact, the electrical measurements taken at the boundary of a process vessel are not enough to solve inverse problem directly therefore, forward problem needs to be solved first (ITS, 2006). Poisson's equation is a model developed to solve the forward problem in a source free conducting in homogeneous domain Γ as follow (Williams and Beck, 1995):

$$\nabla.\{\sigma(x,y)\nabla V(x,y)\}=0 \quad in\ \Gamma \tag{2.4}$$

where, $\sigma(x,y)$ is a conductivity distribution, $V(x,y)$ is voltage correspond to the steady-state injected current. For the boundary conditions:

$V=0$ *(ground electrode)*

$$\int \sigma \left(\frac{\delta V}{\delta n} \right) = +I \qquad on\ Source\ (input)\ electrode$$

$$\int \sigma \left(\frac{\delta V}{\delta n} \right) = -I \qquad on\ sink\ (output)\ electrode$$

where I is the current applied on the electrode and n is the outward unit normal to the sensor.

In order to solve the Poisson's equation, finite element is used. An automatic mesh generator program creates the circular-shaped mesh (combination of triangular- or quadrilateral-shaped elements). Therefore, FEM converts the Poisson's equation to a series of simultaneous equations presenting the behaviour of each of the element. There are 14 pairs of electrodes in a 16-electrode system. These electrodes are used for current injection in adjacent protocol, therefore (Dickin and Wang, 1996):

$$AV_{(i)} = b_{(i)} \quad (i = 1,...,14) \tag{2.5}$$

where, A is the system's stiffness matrix of $N \times N$ entries and N presents the number of nodes within finite-element mesh, $V_{(i)}$ denotes a vector representing the N unknown nodal potentials and $b_{(i)}$ is $N \times 1$ vector showing the boundary conditions as described above.

After solving the forward problem, the inverse problem has to be solved using iterative or non-iterative methods. Iterative methods, Newton Raphson (non-linear) and Parametric Model methods are based on the sensitivity conjugate gradient and have the flexibility in the measurement protocol. They are more accurate but time consuming and costly, compared to non-iterative methods. Non- iterative method, linear back projection method, is a single step method. It can be executed in one step using a pre-calculated pixel sensitivity matrix that is stored in the computer's memory. Also, it has low computational cost and immunity to the sensor noise. In addition, the image is simply reconstructed by a matrix /vector multiplication operation that can be executed very fast on modern computers provided with floating-point units (Tapp and Williams, 2000). Despite of the mentioned advantages of this method, the 3-D distribution of real electric fields and the LBP algorithm cause the accuracy of the imaging data from the 2-D presumption to be reduced (Mann *et al*., 1996). P2000 system (Industrial Tomography Systems-

ITS, Manchester, UK) comes with a qualitative, non-iterative algorithm on linear back-projection.

The linear back projection algorithm, defined by Geselowitz (1971) and improved by Kotre (1989), uses a sensitivity coefficient weighting procedure for the qualitative algorithm. The reason this method is called Linear back projection (LBP) method is that the potential difference on the surface is back projected to a resistivity value in the area between two equipotential lines. This method is used to convert the voltage measurements to conductivity values using sensitivity matrix (Dickin *et al.*, 1996):

$$S_{(e,M)} = \frac{1}{\beta^{(e)}} \frac{V_{(e,M)} - V_{(M)low}}{-V_{(M)high} - V_{(M)low}} \tag{2.6}$$

where, e is number of the elements and M presents number of measurements in a horizontal cross section, $V_{(M)low}$ is voltage where all elements were occupied by the lower resistance phase, $V_{(M)high}$ denotes voltage where all elements are occupied by the higher resistance phase and $V_{(e,M)}$ presents voltage where only the eth element is occupied by the higher resistance phase.

To construct the electrical resistance distribution graphically, the sensitivity matrix, $S_{(e,M)}$, and the boundary conditions based on the measured voltages $V_{(M)\,meas}$ are used.

$$P_{(e)} = \frac{\displaystyle\sum_{M=1}^{104} S_{(e,M)} V_{(M)meas}}{\displaystyle\sum_{M=1}^{104} S_{(e,M)}} - P_{(e)\,ref} \tag{2.7}$$

where, $P_{(e)}$ is change in the electrical resistance from the initial state for each element, ignoring the effect of the initial resistance distribution due to the impeller, baffles and etc. The flowchart of an image reconstruction is shown in Figure 2.2:

Start

Set up of the boundary condition

Analyze voltages by the FEM

$$AV=b$$

Calculate sensitivity matrix

$$S_{(e,M)} = \frac{1}{\beta^{(e)}} \frac{V_{(e,M)} - V_{(M)low}}{-V_{(M)high} - V_{(M)low}}$$

Analyze electrical resistance distribution

$$P_{(e)} = \frac{\sum_{M=1}^{104} S_{(e,M)} V_{(M)meas}}{\sum_{M=1}^{104} S_{(e,M)}} - P_{(e)ref}$$

Output reconstruction of images
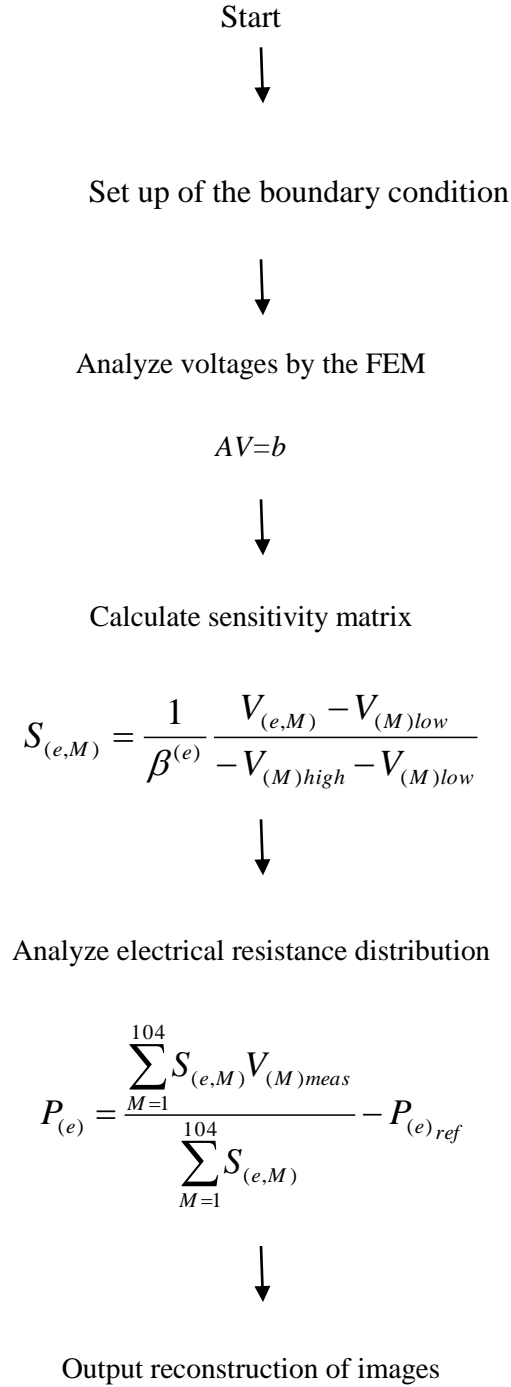
Figure 2.2 Image reconstruction flow chart (source: Kamiyama *et al*., 2005)

The calculated conductivity was then converted to solid concentration through Maxwell's equation (ITS, 2006):

$$X_V = \frac{2\sigma_l + \sigma_s - 2\sigma_{mc} - \left(\dfrac{2\sigma_{mc}\, 2\sigma_s}{2\sigma_l}\right)}{\sigma_{mc} - \left(\dfrac{\sigma_s}{\sigma_l}\right)\sigma_{mc} + 2(\sigma_l - \sigma_s)} \tag{2.8}$$

where, X_V, σ_l, σ_s and σ_{mc} are the volume fraction of the dispersed materials, the conductivity of the continuous phase, the conductivity of the dispersed phase and the reconstructed measured conductivity, respectively. In this study, σ_s was considered zero for the latex particle during the experiments hence Equation 2.8 is further simplified as follows:

$$X_V = \frac{\sigma_l - \sigma_{mc}}{\sigma_l + 0.5(\sigma_{mc})} \tag{2.9}$$

Chapter 3
Experimental Setup and Procedure

3.1 Experimental Set up

In this study, a fully baffled cylinder tank with dish shape bottom and with a diameter (T) of 38.1 cm was selected to mix the suspension. To improve the mixing performance, the width of baffles (B) and the clearance to the tank wall were selected 2.5 cm ($B = T/12$) and 3.8 cm ($T/10$), respectively. To send the AC current to the inner conductive fluid and measure the potential difference across the vessel, the mixing tank was equipped with four sensor planes with the intervals of 8.6 cm between them. Planes were numbered from top to bottom. Each plane consists of 16 simple equally spaced circular stainless plates (electrodes), with the diameter of 2.0 cm, formed into a circular ring. The lowest plane was located 8 cm above the bottom of the tank. A single ground electrode was located between the plane number 3 and 4, on which the base reference was taken. This setup was equipped with a torque meter (Staiger Mohilo, Germany) a data acquisition system (DAS) (Industrial Tomography Systems 2000, UK) and a computer (Pentium IV, CPU 2 GH, 512 MB RAM) (Figure 3.1). The settings of DAS, for all experiments, were: partial gain, 15 mA current, 1 measurement/frame and 4 s/frame temporal resolutions.
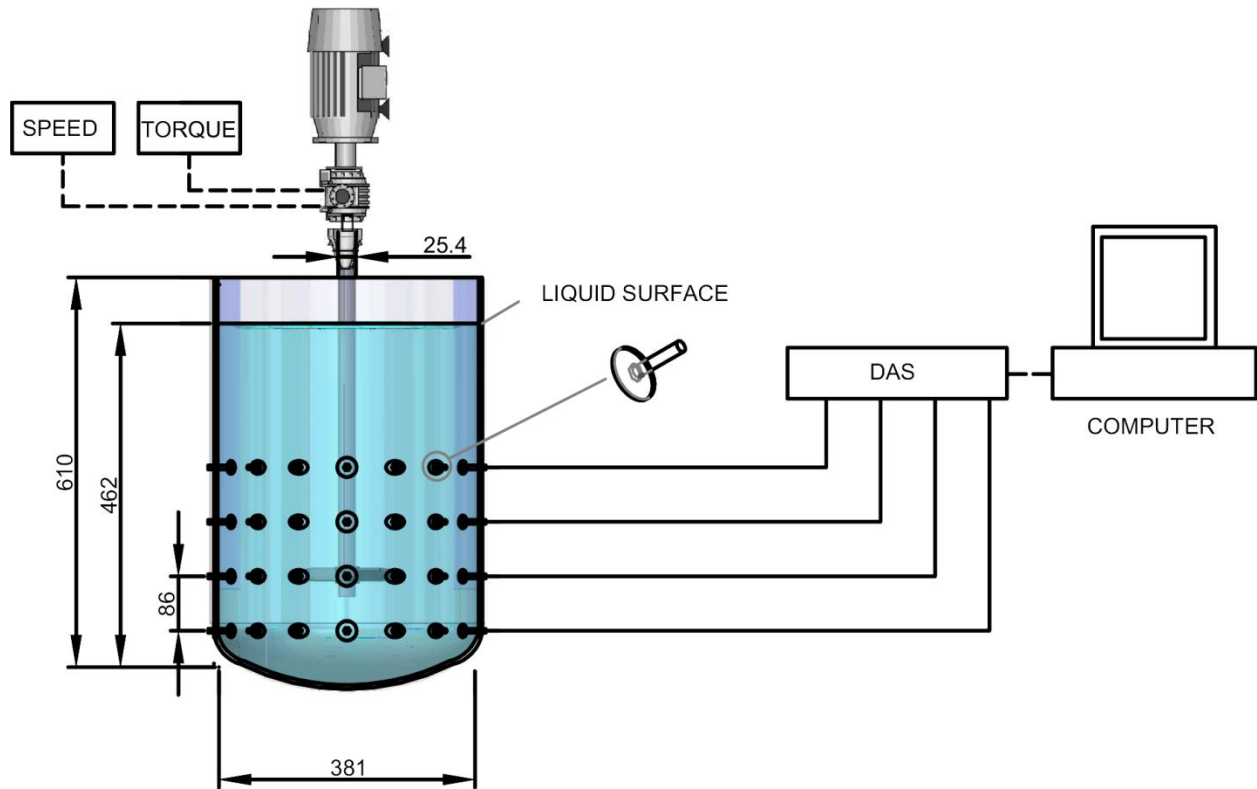
Figure 3.1 Schematic diagram of the experimental setup used in this study (all units in mm)

3.1.1 Impeller Properties

In this study, six axial impellers A100, A200, A320, A315, A310 and 3AM each with a diameter of 17.8 cm were used. A hydrofoil impeller, A310, with the clearance of T/3 was used as the main impeller. The properties of theses impellers are as follows (Paul *et al*., 2004):

A100 (marine propeller) is a three rounded and twisted blade impeller with a blade angle of 45$^{\text{o}}$. This impeller generates an axial-flow directing to the bottom of the tank and has a high discharge capacity with low head. It is recommended for the low viscosity applications requiring moderate pumping.

A200 (pitched blade turbine) is a four blade impeller with a blade angle of 45$^{\text{o}}$. This impeller generates an axial-flow pattern and is efficient for the low to medium viscosity and flow controlled applications.

A320 (Hydrofoil) is a three twisted blade impeller with the blade angle of 45° and is recommended for the high viscosity applications which require a high flow.

A310 is a three twisted blade impeller with the blade angle of 45°. The top edge of each blade is straight while the bottom edge is tapered at the end. The blade tip of this impeller removes any tendency for the flow to re-circulate around the tips and generates a uniform velocity across the entire discharge area. This impeller is very efficient for the low viscosity and the flow controlled applications.

3AM is a three twisted blade impeller with a blade angle of 45°. The top and bottom edge of each blade is tapered at the end. The blade tip of this impeller also removes any tendency for the flow to re-circulate around the tips and generates a uniform velocity across the entire discharge area. This impeller is very efficient for the low viscosity and the flow controlled applications.

A315 (hydrofoil impeller) is a four twisted blade impeller with a blade angle of 45°. The high solidity of this impeller makes it very efficient for the gas dispersion in viscous systems and a solid- liquid suspension.

3.1.2 Solid-Liquid Suspension

In this study, tap water was used as the medium phase and polystyrene latex particles (provided by Xerox Research Center of Canada), with three different sizes of 5.2, 8.5 and 9.1 μm, were used as the solid phase (Figure 3.2). The tank was filled up with tap water up to a height (*H*), equal to 1.2 times the tank diameter (38.1 cm). Using a conductivity meter (OAKTON conductivity meter, EUTECH Instrument, Germany), the conductivity of the water was measured (324 μS/cm) and kept constant throughout the experiments. Variable frequency drive was used to adjust the impeller speed to the desired rpm.
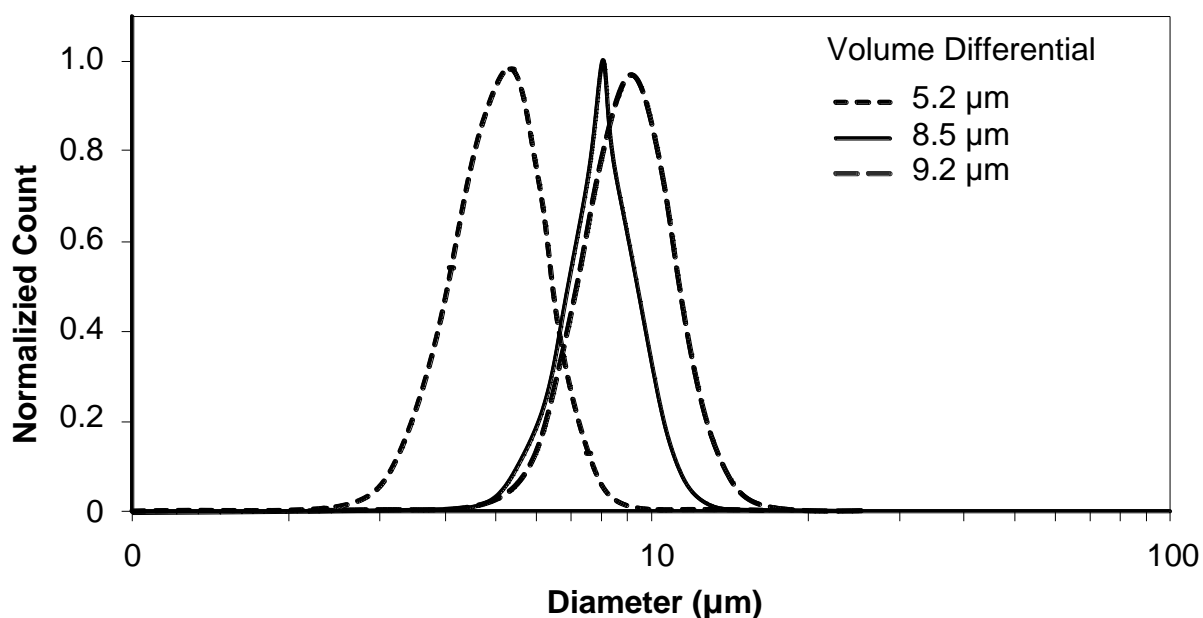
Figure 3.2 Polystyrene latex particle size distribution (Xerox Research Center of Canada)

3.1.3 Solid Particle Properties

The solid particles used in this study were polystyrene latex particles with the refractive index of 1.51 (Windholz *et al.,* 1989). The physical properties of particles, such as water content, shape, particles size reported by the manufacturer and density, are listed in Table 3.1.

Table 3.1 Particles specifications

Particle Type	Particle Size (µm)	Shape	Density (g/cm^3)	Water Content (%)
Polystyrene latex	5.2	Spherical	1.05	17.8
Polystyrene latex	8.5	Spherical	1.05	17.8
Polystyrene latex	9.1	Spherical	1.05	17.8

3.1.4 Rheology of the Solid Suspension

The working fluids were the polystyrene latex particle suspensions with the concentrations of 15 wt%, 20 wt%, 25 wt%, and 30 wt%. Rheological properties of the suspensions were measured at room temperature (22 ± 0.5^{0}C) by a Bohlin CVOR Rheometer 150 (Malvern instruments, USA) using a cup and bob measuring system. The shear rate required for applying in the rheometer was obtained using Metzner-Otto relationship. In this relationship, the local shear rate in the flow is proportional to the mixer speed as follows (Metzner and Taylor, 1960):

$$\dot{\gamma}_{ave} = K_s.N \tag{3.1}$$

where K_s is proportionality constant, $\dot{\gamma}_{ave}$ is the shear rate (s^{-1}) and N is the impeller speed (rps).

The K value, for the A310 impeller, was reported as 10 (Paul *et al.*, 2004). The minimum applied shear rate was (0.14 s^{-1}). This is the minimum shear rate which could be generated by the rheometer. The maximum impeller speed used for all experiments was 400 rpm. Thus, the maximum shear rate applied in the rheometer was 57s^{-1}. Therefore the range of shear rate applied in the rheometer covered the range of impeller speed used in the mixing system. The required measurement temperature was the same as the bulk fluid temperature (22 ± 0.5^{0}C) in the tank.

The rheology of the suspension was modeled best (with good regression coefficients) by the Newtonian model. Figure 3.3 presents this model while Table 3.2 lists the obtained data. In the Newtonian fluids, the shear stress is directly proportional to the shear rate. The proportional

constant is the fluid viscosity. In fact, the plot of the shear stress versus shear rate generates a straight line with the slope being fluid viscosity. Thus, the viscosity is given by:

$$\tau = \mu \cdot \dot{\gamma} \tag{3.2}$$

where τ is the shear stress (Pa), μ is Newtonian viscosity (Pa.s), and $\dot{\gamma}$ is the shear rate (s^{-1}).
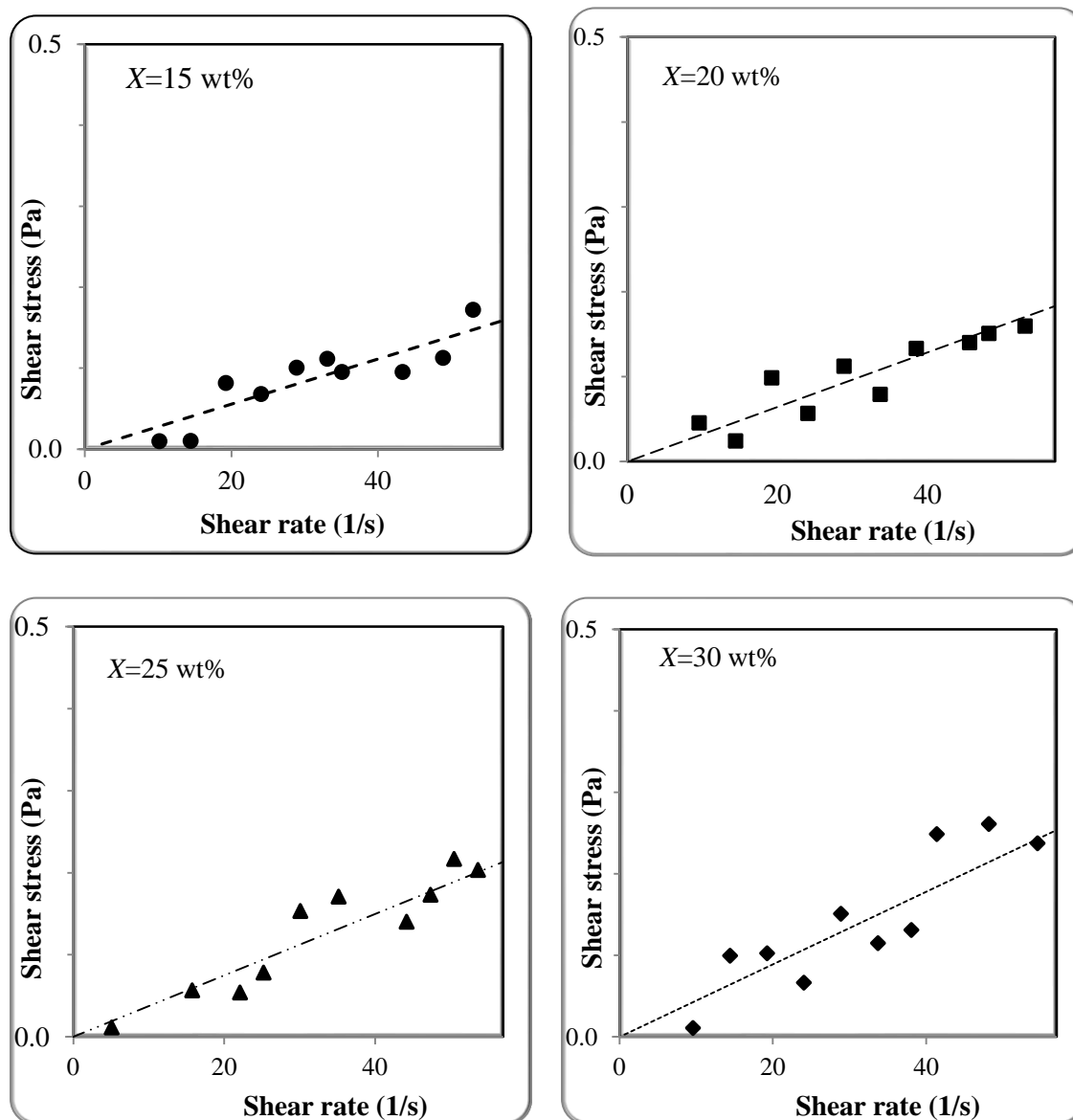
Figure 3.3 Shear stress versus shear rate for polystyrene latex suspension at different concentrations

In response to different impeller speeds, in this work, when measuring the mixing times, 50 ml of 5 w/v% salt solution was added to the 15 wt% polystyrene latex suspension. Therefore, any change in the rheology of the 15 wt% solution, after the injection of salt solution, has to be concerned.

3.1.5 The Effect of Salt Solution on the Rheological Properties of the Suspensions

In this section, the effect of 50 ml of 5 w/v% salt solution on the rheological properties of 15 wt% polystyrene latex suspension was evaluated. The obtained data were listed in Table 3.2 and were fitted with Newtonian model (Figure 3.4). This figure shows that 50 ml of 5 w/v% salt solutions had no significant effect on the viscosity of 15 wt% concentration of polystyrene suspension.
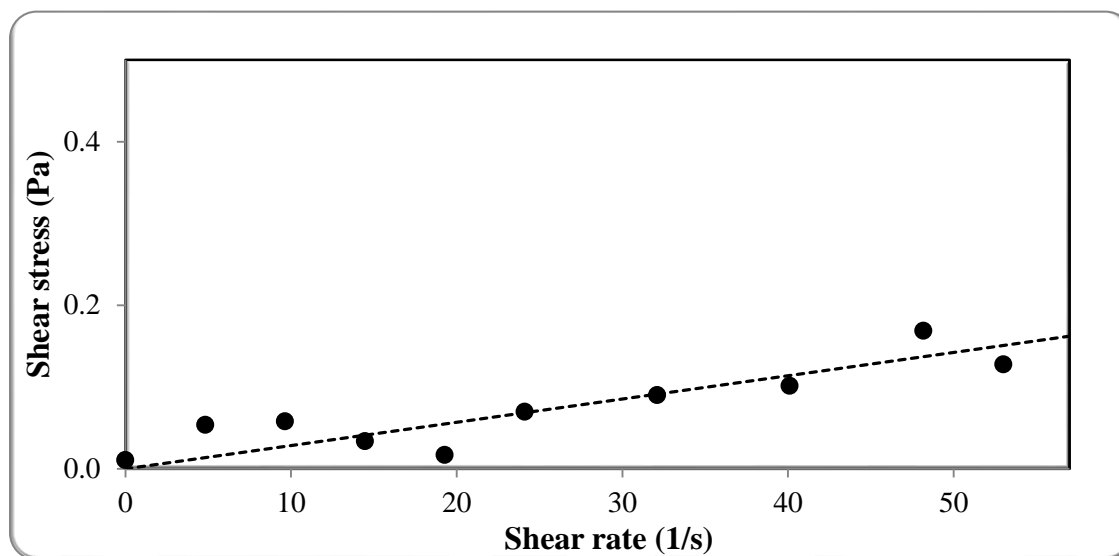
Figure 3.4 Effect of 50 ml of 5 wt% of salt solution on the polystyrene latex suspension, *X*=15 wt%.

Table 3.2 Rheological properties of different concentrations of polystyrene latex suspensions

Polystyrene latex suspension			Polystyrene latex suspension with salt	
Concentration (wt%)	Viscosity (Pa.s)	Regression Coefficient (R^2)	Viscosity (Pa.s)	Regression Coefficient (R^2)
15 %	0.0027	0.9103	0.0028	0.9186
20 %	0.0032	0.9106		
25%	0.0037	0.9175		
30 %	0.0047	0.9191		

3.1.6 Experimental Protocol

In this study, according to the literature review, a range of experimental conditions was defined for each variable. The applied impellers were limited to only axial-impellers, recommended primarily for the solid-liquid mixing in the literature. The impeller speed ranged from just suspended impeller speed (252 rpm) to the impeller speed at which the descending of the homogeneity was obvious (400 rpm). The impeller clearance was limited between the lowest position on the shaft (T/3.8) and the clearance at which the homogeneity started to drop (T/2.5). In order to study the behaviour of different size of particles in a mixing vessel, the narrow distribution of three various particle sizes of polystyrene latex (5.2, 8.5 and 9.1 µm) was used. These three specific sizes were selected due to their availability. Because of the complexity of the experiments, the wide range of particle size distribution was not considered. To investigate the effect of the solid concentration on the mixing process, the suspension was prepared with four different concentrations of 15%, 20%, 25% and 30% wt%. Table 3.3 lists the specification of each run in this study.

Table 3.3 Experimental runs and conditions

Variable/Fixed condition	Run1	Run2	Run3	Run4	Run5	Run6
Impeller speed *N*(rpm)/ all *N, C =* T/3, d_p=5.2 µm, *X* =15 wt%,	252	275	300	328	350	400
Impeller Type/ all *N, C = T*/3, d_p=5.2 µm, *X* =15 wt%,	A100	A200	A315	A320	A310	3AM
Impeller clearance (C) / A310, all *N*, d_p=5.2 µm, *X*=15 wt%	T/3.8	T/3	T/2.5			
Impeller Pumping Mode/A310, C=T/3, all *N*, d_p=5.2 µm, *X*=15 wt%	Downward	Upward				
Impeller diameter to tank diameter ratio (D/T)/A200, all *N* ,*C=T/3*, d_p=5.2 µm, *X*=15 wt%	0.29	0.31	0.39	0.47		
Particle size (*dp*)/ A310, all *N* , *C=T/3, X*=15 wt%	5.1 µm	8.5 µm	9.1 µm			
Solid concentration (*X*)/ A310, all *N, C=T/3,dp=*5.2 µm,	15 wt%	20 wt%	25 wt%	30 wt%		

3.2 Electrical Resistance Tomography

The ERT system consists of three main components: the sensors, the data acquisition system (DAS) and the image reconstruction system.
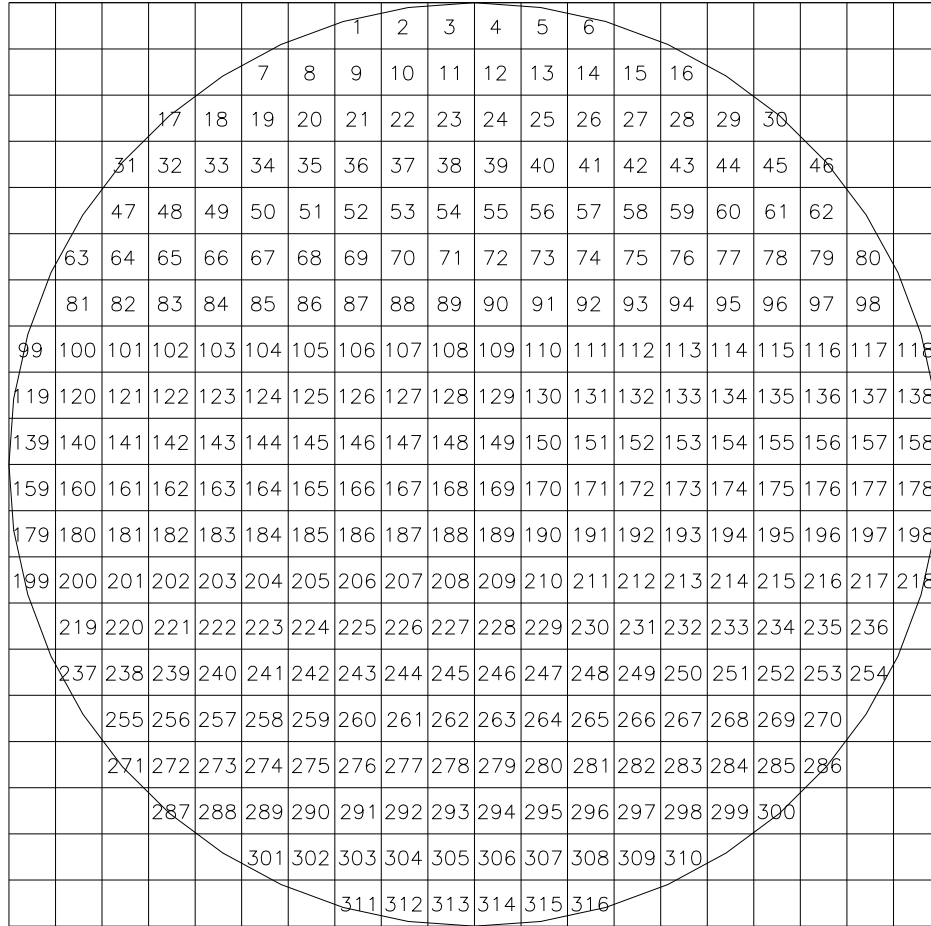
The tank consists of 4 sensor planes with vertical intervals of 8.6 cm between the planes. Each plane consists of 16 equally spaced stainless steel sensors. The planes are numbered from top to bottom. The electrodes are connected to the DAS (Industrial Tomography Systems-ITS, Manchester, UK) using cables.

The function of data acquisition system is to perform the measurement protocol. Using adjacent measurement protocol (Figure 3.5), the AC current is applied between two adjacent electrodes and the potential difference is measured between all other pairs of adjacent electrodes. The AC current is applied to the next pair of electrodes and potential difference is again measured for all other pairs of electrodes. This process is repeated until all combinations of electrodes are used. Based on the $N(N-3)/2$ equation, where N is the number of electrodes per plane, this data collection strategy provides 104 voltage measurements. Therefore, 4 axial plain provides 416 measurements from the solution volume (Barber *et al.,* 1983).
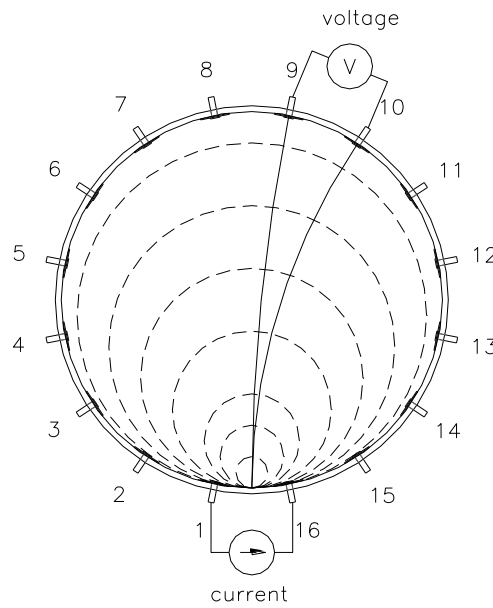
Figure 3.5 Adjacent measurement strategy for the data collection (Pakzad, 2007)

In this work, linear back projection method, a non-iterative image reconstruction algorithm was used to convert the voltage into a 2-D picture of the conductivity. Each tomogram consisted of a 20×20 pixel array and provided 400 spatial elements. The image was generated from pixels inside the vessel; however some of these pixels sit outside the circular boundary of the vessel. In fact, the circular image was constructed using 316 pixels from a 400 pixels square grid. As the vessel had 4 sensing planes, this generated 1264 non-intrusive conductivity probes.

							1	2	3	4	5	6							
					7	8	9	10	11	12	13	14	15	16					
			17	18	19	20	21	22	23	24	25	26	27	28	29	30			
		31	32	33	34	35	36	37	38	39	40	41	42	43	44	45	46		
		47	48	49	50	51	52	53	54	55	56	57	58	59	60	61	62		
	63	64	65	66	67	68	69	70	71	72	73	74	75	76	77	78	79	80	
	81	82	83	84	85	86	87	88	89	90	91	92	93	94	95	96	97	98	
99	100	101	102	103	104	105	106	107	108	109	110	111	112	113	114	115	116	117	118
119	120	121	122	123	124	125	126	127	128	129	130	131	132	133	134	135	136	137	138
139	140	141	142	143	144	145	146	147	148	149	150	151	152	153	154	155	156	157	158
159	160	161	162	163	164	165	166	167	168	169	170	171	172	173	174	175	176	177	178
179	180	181	182	183	184	185	186	187	188	189	190	191	192	193	194	195	196	197	198
199	200	201	202	203	204	205	206	207	208	209	210	211	212	213	214	215	216	217	218
	219	220	221	222	223	224	225	226	227	228	229	230	231	232	233	234	235	236	
	237	238	239	240	241	242	243	244	245	246	247	248	249	250	251	252	253	254	
		255	256	257	258	259	260	261	262	263	264	265	266	267	268	269	270		
		271	272	273	274	275	276	277	278	279	280	281	282	283	284	285	286		
			287	288	289	290	291	292	293	294	295	296	297	298	299	300			
					301	302	303	304	305	306	307	308	309	310					
							311	312	313	314	315	316							

Figure 3.6 Image reconstruction grid Source (Pakzad, 2007)

3.2.1 Material Preparation

To prepare the sample, tap water was used as the medium. The measured conductivity of water was assigned for the reference conductivity. To eliminate the effect of the temperature on the conductivity, all the experiments were conducted at the room temperature. Polystyrene latex particles were kept in room temperature so the temperature would not be a factor when conducting the experiments. During each experiment, the tank was filled with tap water to a height (*H*), equal to 1.2 of the tank diameter and making a volume of about 46 L. To perform the experiment at room temperature and eliminate possible air bubble, the tap water within tank was allowed to sit over the night before performing the experiment. The conductivity of water was measured with conductivity meter reading as 324 μS/cm and was kept constant during all experiments.

3.2.2 Tomography Measuring Steps

To measure the conductivity of the suspension, tomography measurements have to be compared with the reference measurement making it an important part of the experiment. In fact, when taking the reference, the effect of the stirrer and other internals are fixed during the experiment and a constant value (324 μS/cm) is assigned for the conductivity of each pixel in the tank filled with water.

In this study, the injection current and gain map of the tomography machine were calibrated by the Industrial Tomography System (ITS) software. The impeller speed was set to the desired impeller speed using a variable frequency drive (VFD) and the reference measurement was taken using ERT (and saved for future use) to eliminate the effects of the stirrer and other internals. The impeller speed was set to 600 rpm so it doesn't splash the content of tank around and can suspend all particles in the water before they clump together. Impeller was let to reach 600 rpm, before the solids were added. The solid was precisely weighed up to desired weight fraction and was added gradually to the tank once water, equivalent to solid volume, was discharged from the tank. After all solids were added to the tank, the impeller mixed the contents of the tank at 600 rpm for another 3.0 minutes and was stopped. To reach the non-homogeneity state, as a base of the experiment, the content of tank was left stationary for 3.0 hours. After this time, the impeller speed was set to the desired speed (252-400 rpm) and rotated for 6.0 minutes then, 200 frames were measured using ERT system. After the resulting data were time-averaged, the homogeneity was calculated. All experiments were replicated three times using saved references.

3.2.3 ERT Data Post Processing

Figure 3.7 presents a raw data sample taken by ERT. In this figure, the first 200 frames which have the same conductivity for all planes refer to the reference measurement. The distraction of the conductivity from the frame 200 to 250 was caused by removing the volume of water equivalent to solid weight. The weighed latex particles were added about frame 330. Impeller rotation was stopped at frame 400. The sample was left stationary in the tank for 3.0 hours. After 3.0 hours, while the impeller rotation was still stopped, 200 frames were taken. Therefore, frames 400 to 600 refer to the data measurements after 3.0 hours and once the impeller rotation was stopped. Setting the impeller speed to the desired speed (252-400 rpm), the impeller started to rotate. Thus frames 600 to 1200 refer to the data measurements, once the impeller speed was

set to one of the speeds in the experimental conditions (252-400 rpm). The homogeneity calculation was based on the last 200 frames (frames 1000-1200). The resulting data, then were time-averaged before any other calculations.

After data measurements, the released raw data were in the form of voltage measurements. An image reconstruction algorithm (linear back projection algorithm) was applied to convert the voltage into a 2-D conductivity image called tomogram. The tomogram image was generated from pixels inside the vessel. Figure 3.8 shows the tomogram obtained for the 30 wt% solid suspension after being stationary for 3.0 hours (a) and at 316 rpm (b). Due to the sedimentation of the latex particles, Figure 3.8.a shows that the accumulation of non-conductive latex particles (dark blue area in tomogram) on planes 3 and 4 (bottom of the tank) was more than planes 1 and 2 (top part of the tank).

As the impeller speed increased more solid particles were suspended in the upper part of the tank (Figure 3.8.b).
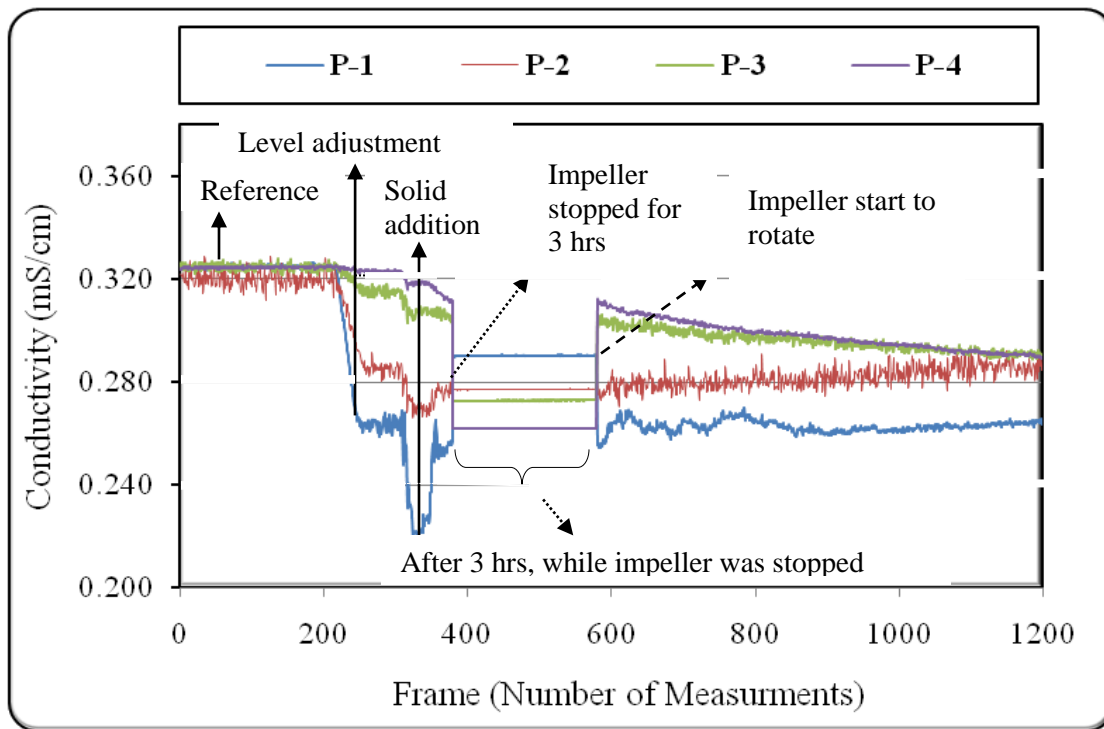

Figure 3.7 ERT data for four tomography planes (A310 impeller, $C = T / 3$, $N = 350$ rpm, $X = 15$ wt%, $dp = 5.2$ μm).
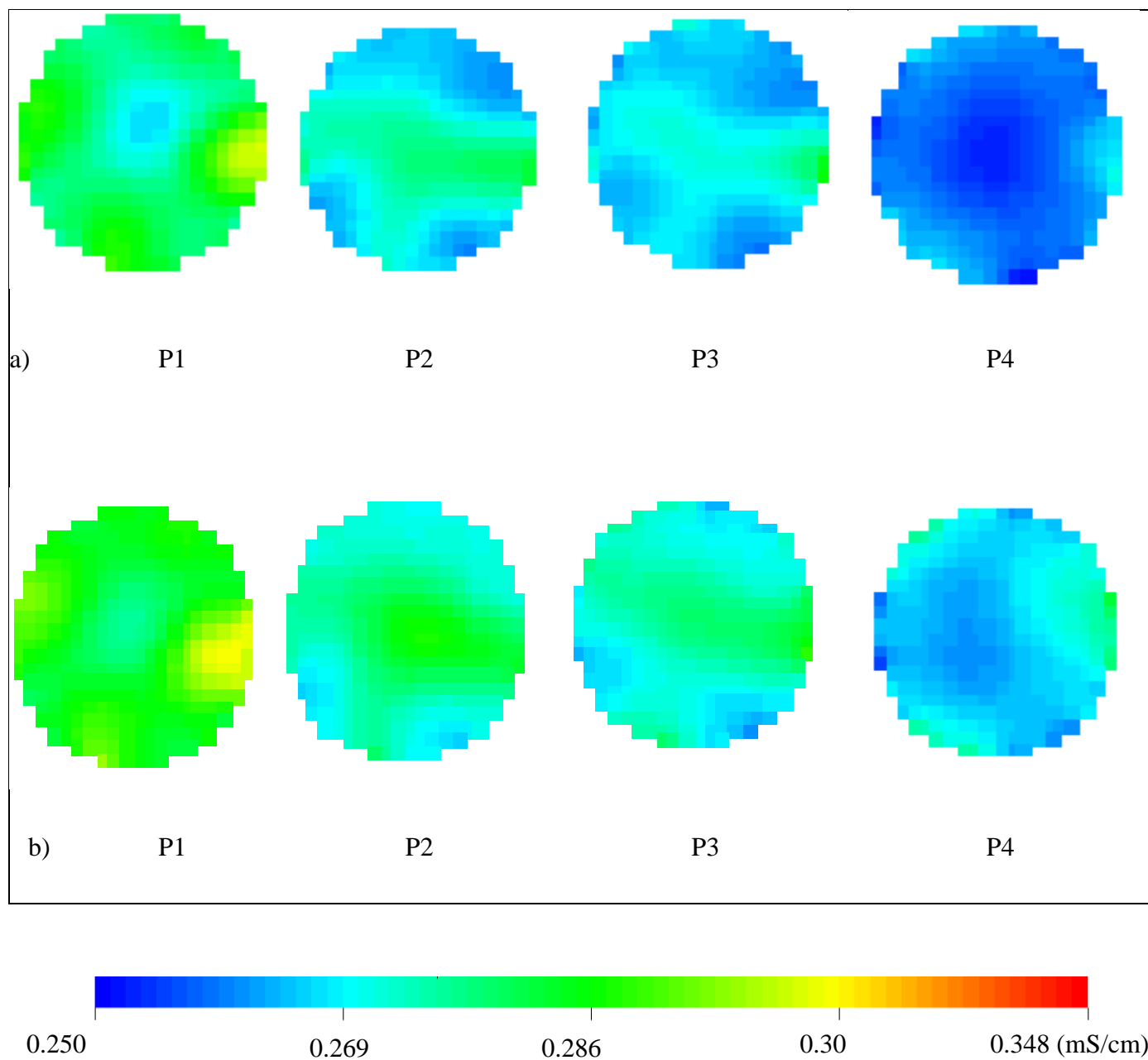
Figure 3.8 Tomograms obtained for the solid suspension (A310 impeller, $X = 30$ wt%, $C = T/3$, $d_p = 5$ µm) a) after leaving stationary for 3.0 hrs b) at 316 rpm

Chapter 4
Results and Discussion

In this chapter, first the just suspended impeller speed is calculated. Afterwards, the effect of impeller speed on the mixing time and the influence of operating conditions and design parameters on the mixing of solid suspension are investigated. Finally, the experimental results are presented, discussed, and compared with previous studies performed so far.

4.1 Shaft Torque

Impeller torque was measured using a rotary torque meter (Staiger Mohilo, Germany) at different impeller speeds. The accuracy of the torque measurement was checked by performing a set of 5 runs at 5 various speeds. Each run was repeated 3 times and the torque measurements were averaged. The random error of the torque sensor, caused by electronic fluctuations and friction, can be defined using standard deviation as follows:

$$\sigma = \sqrt{\frac{1}{N}\sum_{i=1}^{N}\left(M_i - \overline{M}\right)^2} \tag{4.1}$$

where N is the number of measurements, and M is the torque variable and $\overline{M}$ is the mean value of the torque measurements.

Error bars were plotted to show standard deviation in each measurement. Figure 4.1 presents that maximum standard deviation observed in torque measurements was 1.29 %.
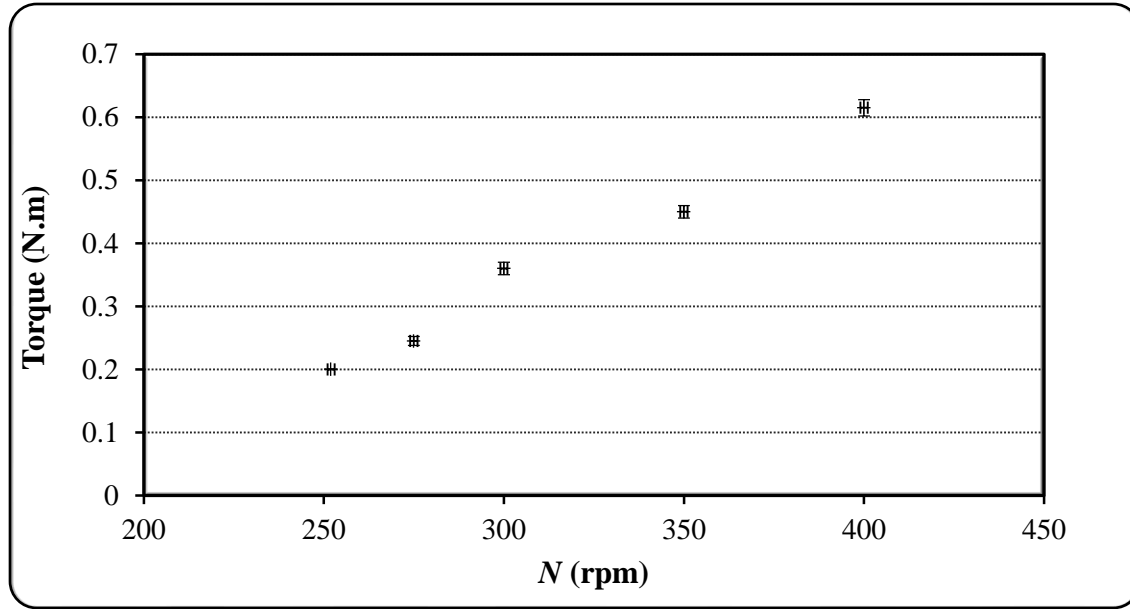
Figure 4.1 Torque versus impeller speed (A310 impeller, $X = 15$ wt%, $C = T / 3$, $dp = 5$ µm)

4.2 Just Suspended Impeller Speed

Just suspended impeller speed is the speed at which all solid particles get suspended in a way that no particle sits on the bottom of the vessel for more than 1 to 2 s (Paul *et al.*, 2004). In speeds below the just suspended impeller speed, some particles are not suspended in the vessel and cause the maximum concentration gradient to occur. Rao and Rewatkar (1988) calculated the just suspended impeller speed from power consumption measurements.

Power consumption is the energy transformed from the agitator to the fluid over a unit time and is a function of flow regime, fluid rheology, tank and impeller geometry. Power consumption is obtained via the torque measurements as follows:

$$P = 2\pi NM \tag{4.2}$$

where N is the impeller speed, M is torque, and P is the power.

Using a torque meter and a tachometer, impeller torque and impeller speed were measured, respectively. The amount of torque lost due to residual torque or friction was subtracted from all torque measurements. Residual torque was measured by operating the empty mixing vessel.

Power number is a dimensionless number and a function of resistance force to the inertia force in a mixing system and is defined as follows:

$$P_o = \frac{P}{\rho N^3 D^5} \qquad \textbf{(4.3)}$$

where ρ, P_o, and D are fluid density, power number, and impeller diameter, respectively.

To determine the just suspended impeller speed, the power consumption was quantified while the impeller speed was gradually increased at constant solid concentration. As the impeller speed was increased more particles were suspended and the power number was increased until all particles were suspended. The power number stayed constant once all particles were suspended. The impeller speed after which the power number stayed constant was called just suspended impeller speed. In this study, the power consumption measurement method was used to obtain the just suspended impeller speed (Njs). Figure 4.2 demonstrates the estimation of just suspended impeller speed in this study. According to this graph, the just suspended impeller speed was determined to be 4.2 rps (252 rpm).
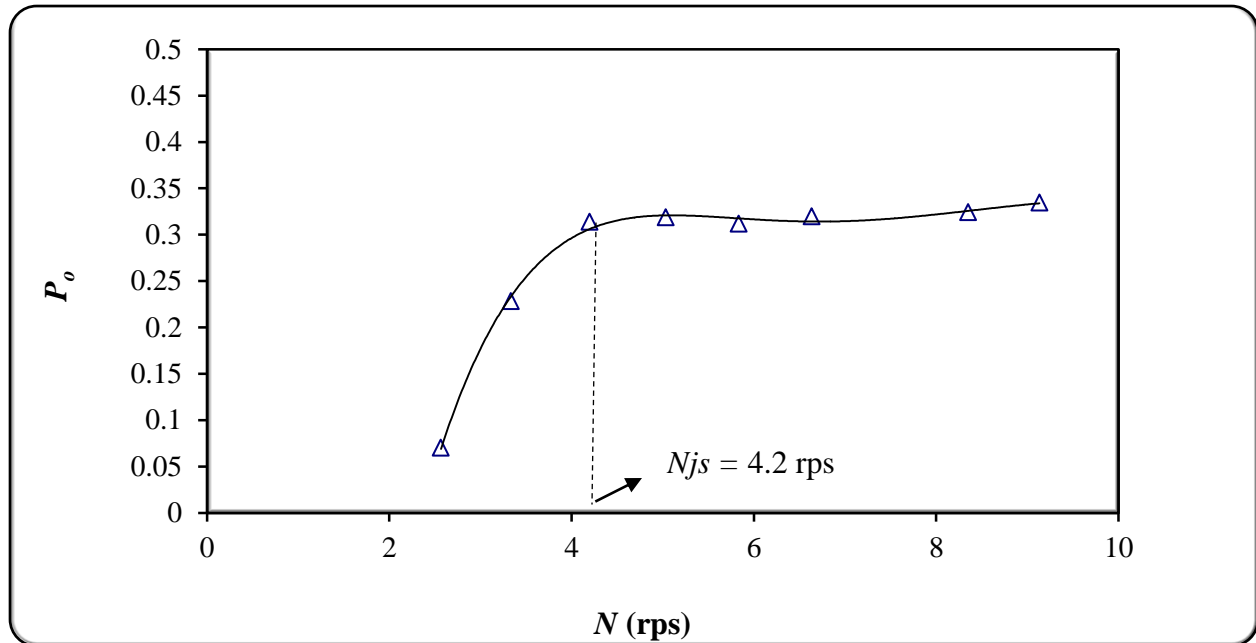

Figure 4.2 Just suspended impeller speed (A310 impeller, $X = 15$ wt%, $C = T / 3$, $d_p = 5\,\mu m$)

The calculated just suspended impeller speed, when using the Zwittering' equation was 193 rpm and showed 24% error over the one determined from the measurements of power numbers. The reason for this deviation is that the Zwittering' equation is more effective for a particle size range of 200 – 1000 μm (Paul *et al*., 2004) and has not been validated for fine particles.

4.3 Mixing Time

One of the common variables to evaluate the mixing performance is mixing time. To determine the mixing time 50 mL of 5 w/v% salt solution was injected into the vessel 10 cm below the liquid surface (Figure 4.3). Tracer was distributed all over the tank until the best uniform concentration was achieved. Then, using ERT and 4 measuring planes, the tracer concentration was determined as a function of time. In this study the time required to distribute 50 mL of 5 w/v% salt solution was measured in the range of 154 to 500 rpm.
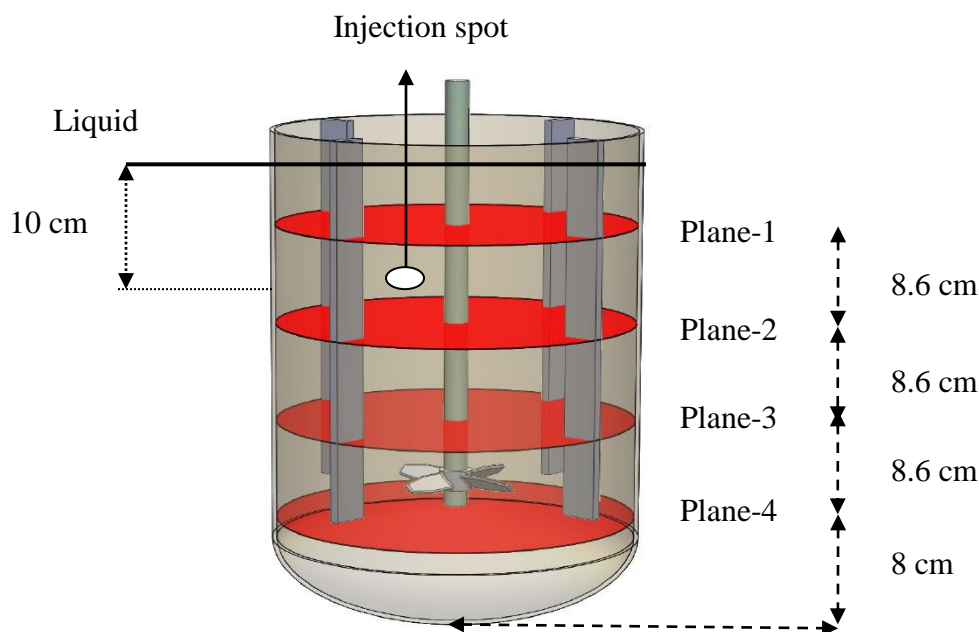
Figure 4.3 The injection location of the 50 ml of the 5 w/v% salt solution in the vessel

Figure 4.4 depicts the responses of 4 planes to the injection of the tracer and shows that 12 sec after the injection of the salt solution at 150 rpm, the contents of the tank reached 95% of the steady-state concentration. Table 4.1 lists the calculated mixing times at each plane. According to this table, plane 3 has the minimum mixing time due to its proximity to the impeller position.

Also, plane 4 shows the maximum mixing time because this plane was located close to the bottom of the tank and encloses the poor mixing area around the baffles. In addition, the overall mixing time declines with the increase of the impeller speed (Figure 4.5). This result is in good agreement with Moo-Young *et al.* (1972) observation.

Moo-Young *et al.* (1972) and Nienow (1997) derived an equation for the mixing time as a function of power consumption per volume as follow:

$$t_m = c \left(\frac{P}{V} \right)^{\frac{-1}{3}} \tag{4.4}$$

where t_m is mixing time (s), P/V is power consumption per volume (W/m^3), c is an equation constant dependent on the geometry of the vessel and impeller. Rewatkar and Joshi (1991), Rzyski (1993) and Foucault *et al.* (2006) obtained the exponent value of -1/3 for most turbulent conditions.

To fit the obtained data to Equation 4.4, log (t_m) was plotted versus log (P/V) (Figure 4.6). According to this graph, the mixing times and power consumptions per volume fitted well with Equation 4.4. The slope and the *c* value were obtained -0.32 and 29.27, respectively.
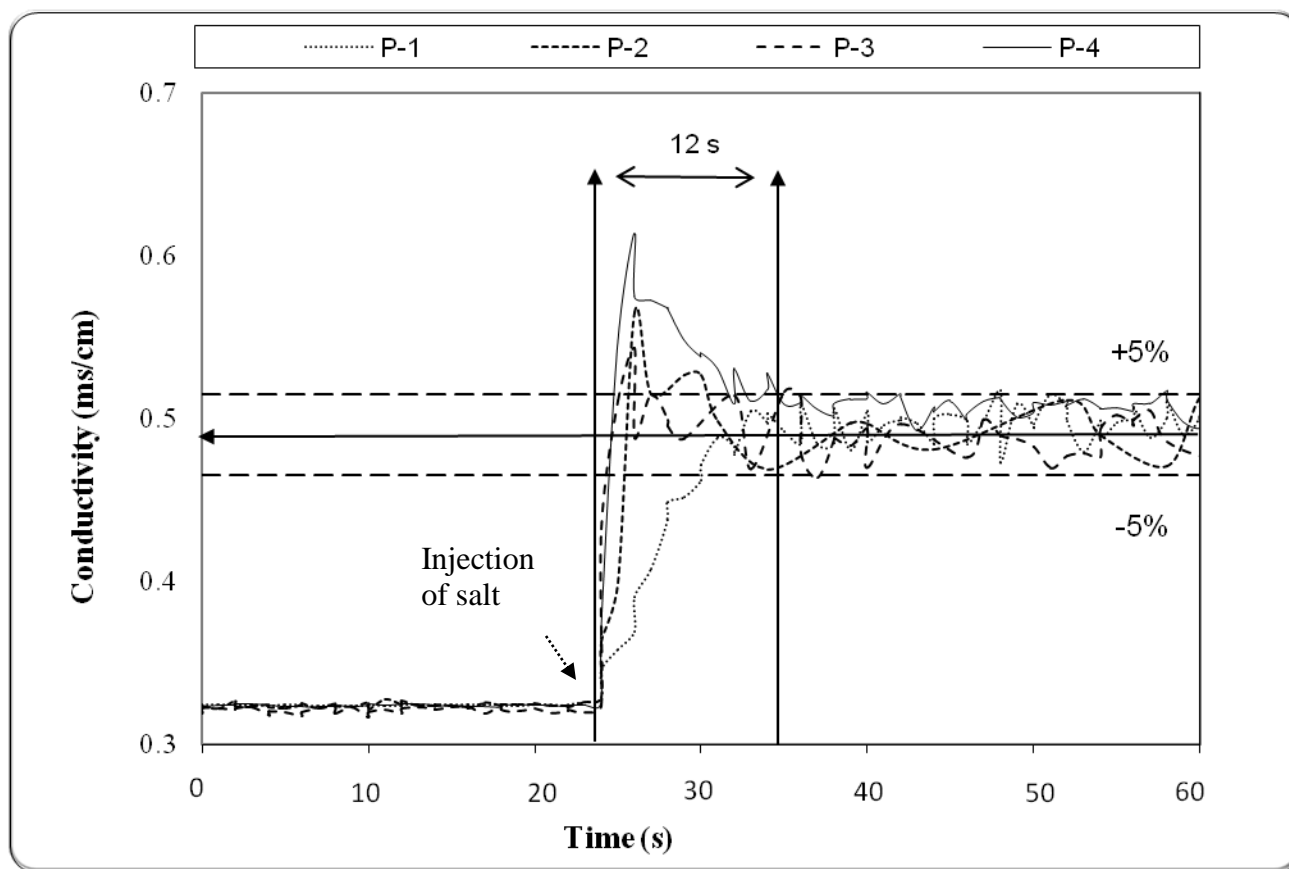
Figure 4.4 Plane conductivity following addition of tracer (X =15 wt%, N = 150 rpm), Plane 1: (z = 0.388 m), Plane 2: (z = 0.252 m), Plane 3: (z = 0.166 m) and Plane 4: (z = 0.08 m).

Table 4.1 Mixing time measured at each ERT plane (A310 impeller, X = 15 wt%, $C = T / 3$, d_p = 5 µm, 150 rpm)

Plane number	Plane mixing time(s)
1	6.5
2	5
3	3
4	12
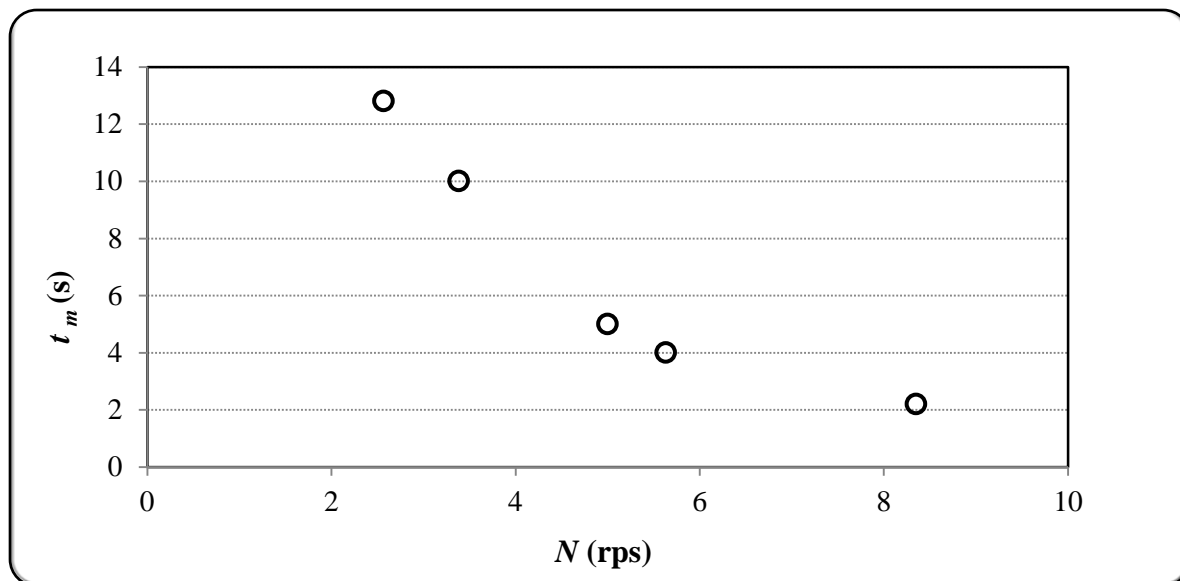
Figure 4.5 Overall mixing time as a function of the impeller speed (A310 impeller, $X = 15$ wt%, $C = T / 3$, $d_p = 5$ μm)
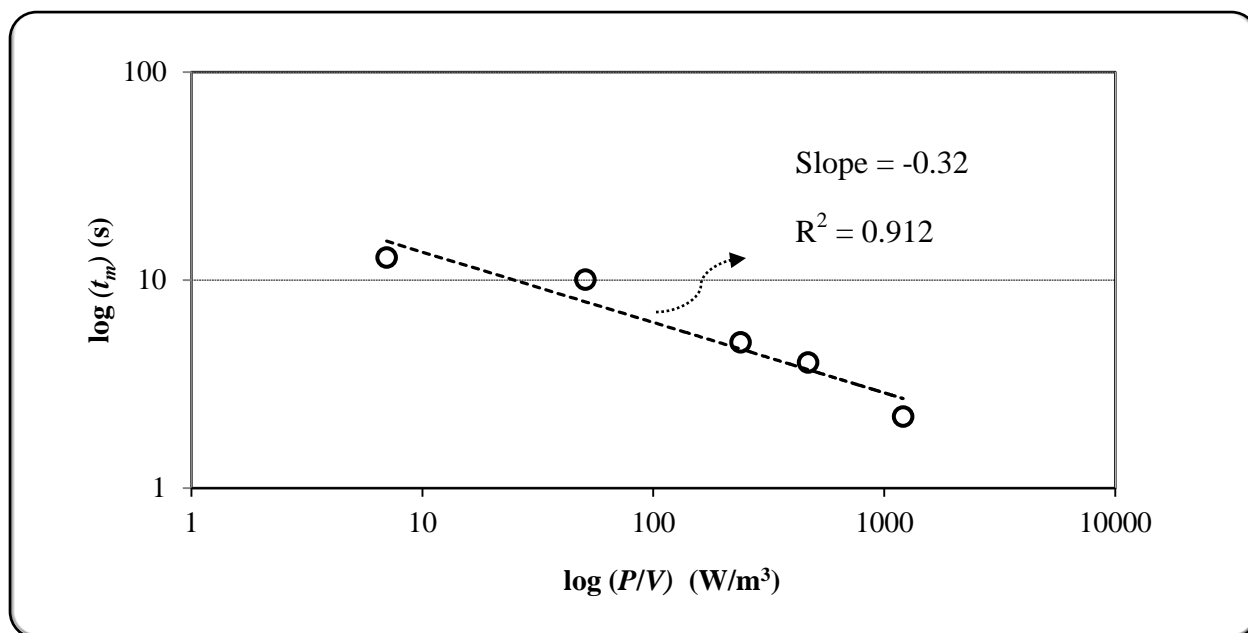
Figure 4.6 Mixing time versus power consumption per unit volume (A310 impeller, $X = 15$ wt%, $C = T / 3$, $d_p = 5$ μm)

4.4 Axial Concentration

To extract the axial concentration profile, the average solid volume concentration of each plane at the steady state was taken into account and the results were normalized to the average concentration to reduce numerical errors. Figure 4.7 shows the deviation of normalized solid volume fraction from the ideal homogeneity value which is one. As the impeller speed increases the magnitude of the deviation decreases and the solid distribution becomes more homogeneous. In this case (15 wt% solid concentration), the minimum deviation from the perfect homogeneity was achieved at 300 rpm. For the impeller speeds greater than 300 rpm, the centrifugal force overcame the gravity force and drove the particles above the impeller and reduced the homogeneity. Thus, the deviation from the perfect homogeneity increased.

Figure 4.8 illustrates the tomograms obtained for the solid suspension at 30 wt% concentration. Latex particles had lower conductivity than water. So, the regions with blue color show the accumulation of latex particles. As the impeller speed increased, more solid particles were suspended. Thus, the amount of solid particles sitting on the bottom of tank decreased and finally disappeared at Njs (252 rpm). Further rise in the impeller speed increased the level of homogeneity only slowly until the solid suspension reached its maximum homogeneity. At this point the blue color regions showing the accumulation of latex particle disappeared. In this case, the maximum homogeneity was achieved at 377 rpm. Any further increase in the impeller speed caused more accumulation of latex particles around the impeller region and reduced the level of homogeneity.
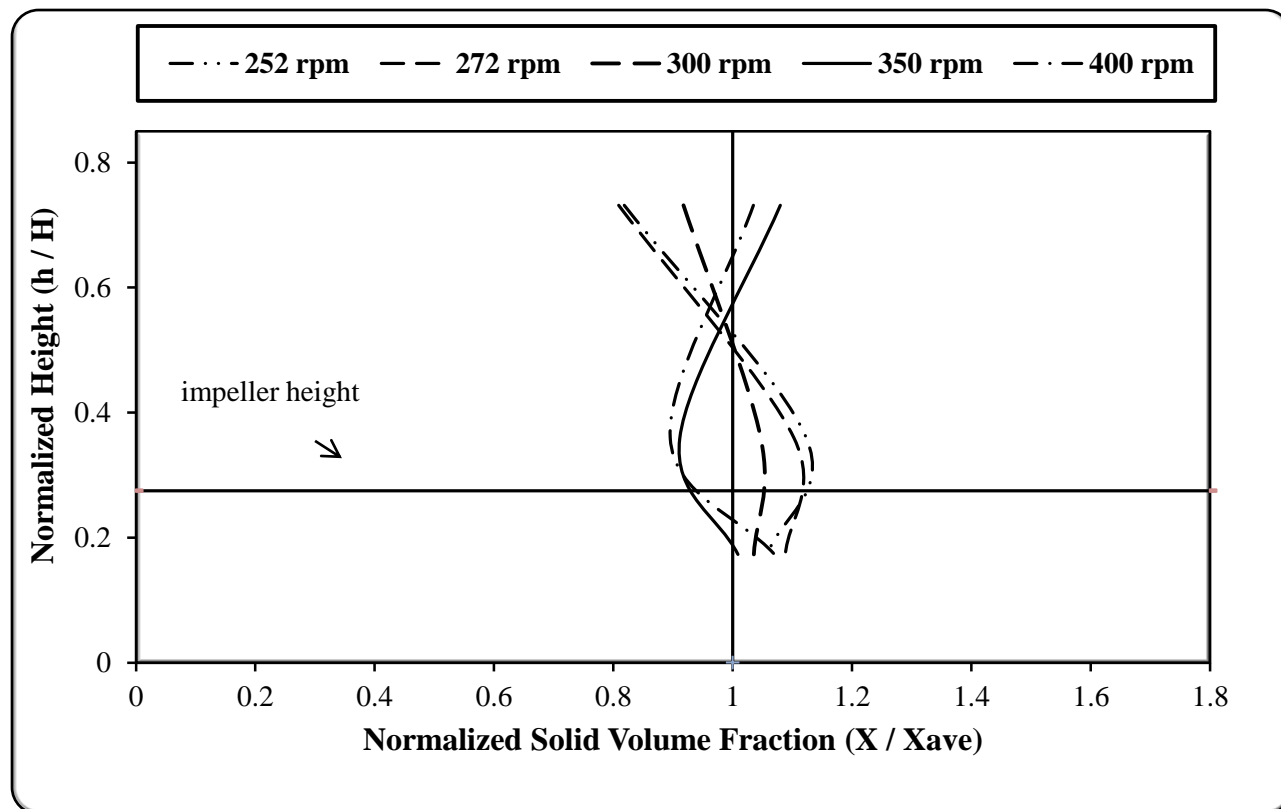
Figure 4.7 Axial concentration profile (A310 impeller, $X = 15$ wt%, $C = T / 3$, $d_p = 5$ µm)

252 rpm P1 P2 P3 P4

300 rpm P1 P2 P3 P4

377 rpm P1 P2 P3 P4

400 rpm P1 P2 P3 P4

0.250   0.338 (mS/cm)
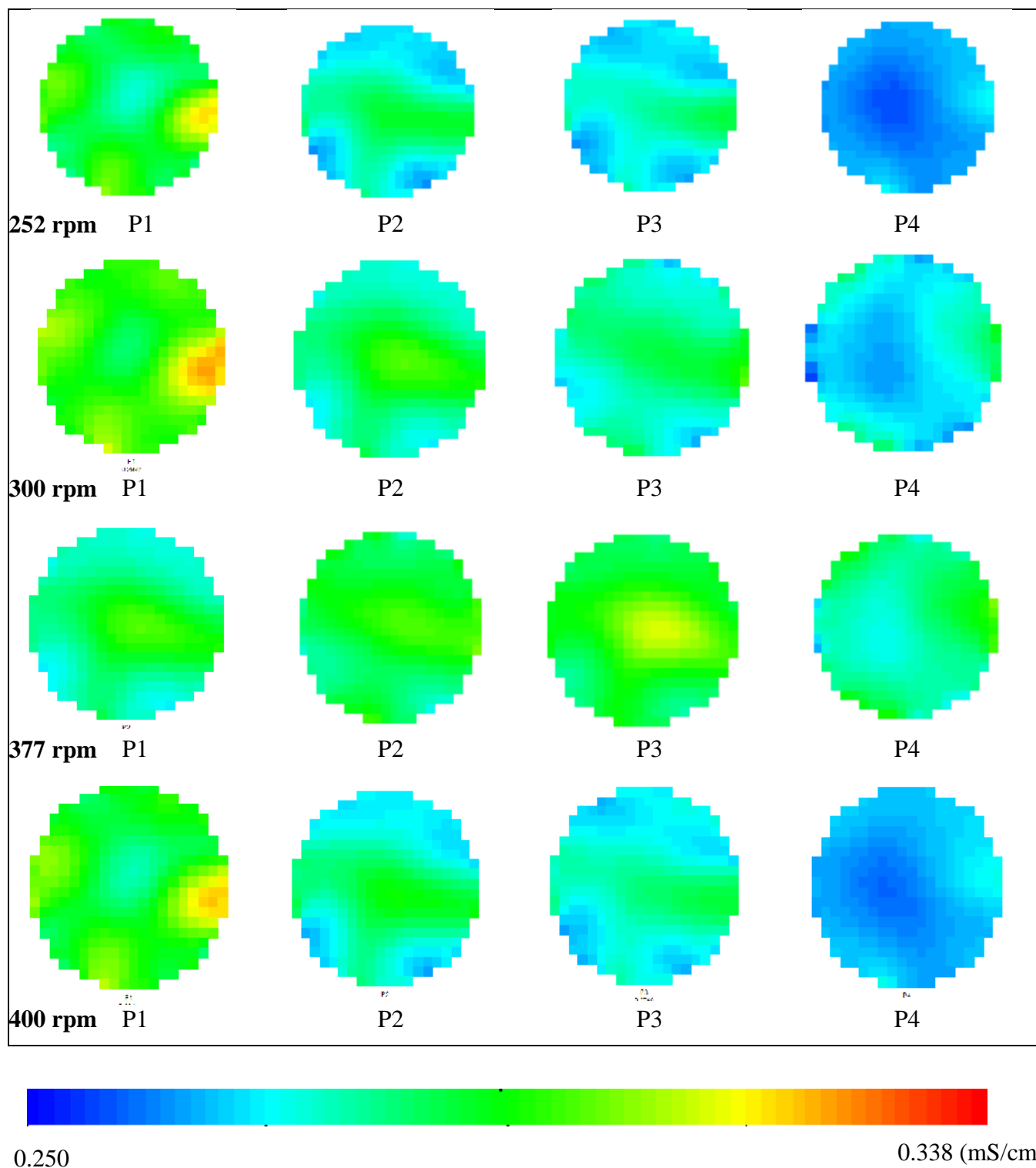
Figure 4.8 Tomogram obtained for the solid suspension (A310 impeller, $X = 30$ wt%, $C = T / 3$, $d_p = 5$ μm)

4.5 Effect of Operating Condition and Design Parameters on Solid-Liquid Mixing

The performance of a solid-liquid mixing system is influenced by operating conditions such as impeller speed, impeller pumping direction and geometric parameters such as impeller clearance, impeller type and impeller diameter. In this section, the significance of these parameters on the mixing quality has been investigated.

4.5.1 Impeller Speed

Impeller speed has a considerable effect on the level of homogeneity in a solid-liquid mixing system. In order to measure the homogeneity level of a system at various impeller speeds, the homogeneity parameter based on variance was defined as (Mak, 1992):

$$\text{Homogeneity} = 1 - \sqrt{\frac{\sum_1^n \left(X_V - \overline{X_V}\right)^2}{n}} \tag{4.5}$$

where n, X_V and $\overline{X_V}$ are the number of planes, solid volume concentration for each plane and average solid volume concentration (the concentration of prepared sample), respectively.

According to Equation 4.5, the minimum variance generates the maximum level of homogeneity and occurs once the concentration gradients are at minimum values. Thus, the objective of each mixing process is to obtain the homogeneity with a unit value.

In this study, the effect of the impeller speed on the level of homogeneity in the range of 252 - 400 rpm was investigated. Figure 4.9 presents that the maximum homogeneity occurred at a specific impeller speed (300 rpm) above which the homogeneity decreased.
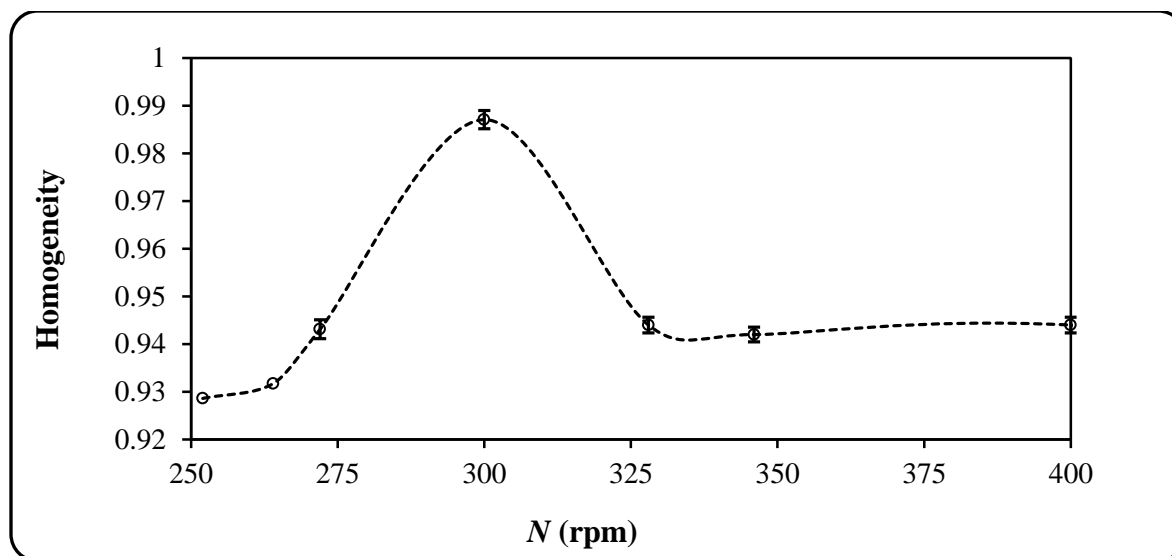
Figure 4.9 Effect of impeller speed on homogeneity (A310 impeller, $X = 15$ wt%, $C = T / 3$, $dp = 5$ µm)

In fact, for impeller speeds greater than 300 rpm, the centrifugal force overcame the gravity force and drove the particles (with higher density than water) to the impeller region, the area with highest circulation velocities, and consequently decreased the homogeneity. Hence, it is required to select the impeller speed above the N_{js} and around the impeller speed which gives the maximum homogeneity. This behaviour is well confirmed in the literature (Einenkel, 1980 and Hosseini, 2008). Einenkel, and Hosseini, reported an optimum impeller speed for the maximum homogeneity in a solid- liquid mixing system above which the homogeneity decreased.

Also, the effect of the impeller speed on the homogeneity was observed at higher concentrations using the vertical slice images and 3D images (Figure 4.11). In order to observe the mixing performance inside the tank, the mixing tank was sliced vertically from two different positions; X=10 and Y= 8 (Figure 4.10).
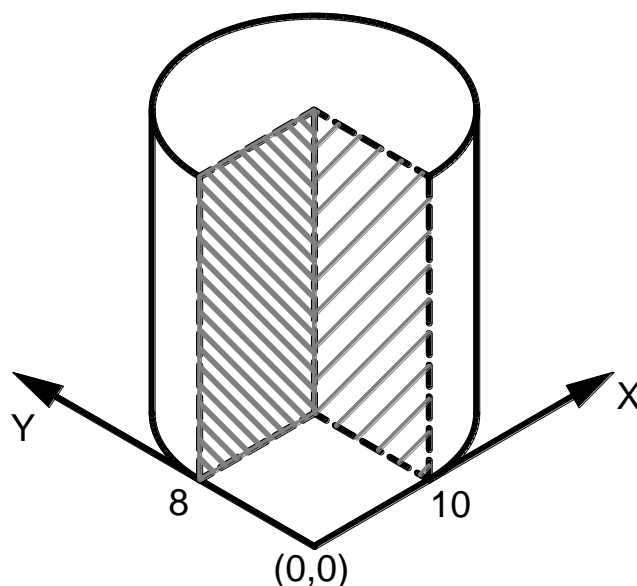
Figure 4.10 The position of vertical slice in the mixing tank

Latex particles had the lower conductivity than water, thus, the regions with lower conductivity (blue color regions) show the accumulation of latex particle. Figure 4.11 (a) illustrates that there was an accumulation of latex particles on the bottom of the tank when there was no agitation. As the impeller speed increased, more latex particles were suspended and the level of homogeneity increased. Thus, the areas showing the accumulation of latex particles (dark blue area) are gradually disappeared. Figure 4.11 (b) shows 3D images of the same information presented in Figure 4.11 (a). These two figures show that for the solid suspension with the concentration of 30 wt%, the maximum homogeneity was achieved at 377 rpm. At this impeller speed, there was a balance between the centrifugal force and the gravity force. Then, any further increase in the impeller speed reduced the homogeneity because the centrifugal force overcame the gravity force and drove the particles to the impeller region, the area with highest circulation velocities. Finally, at 400 rpm, the regions show the accumulations of particles observed on the tomograms which indicates the homogeneity was reduced.

.
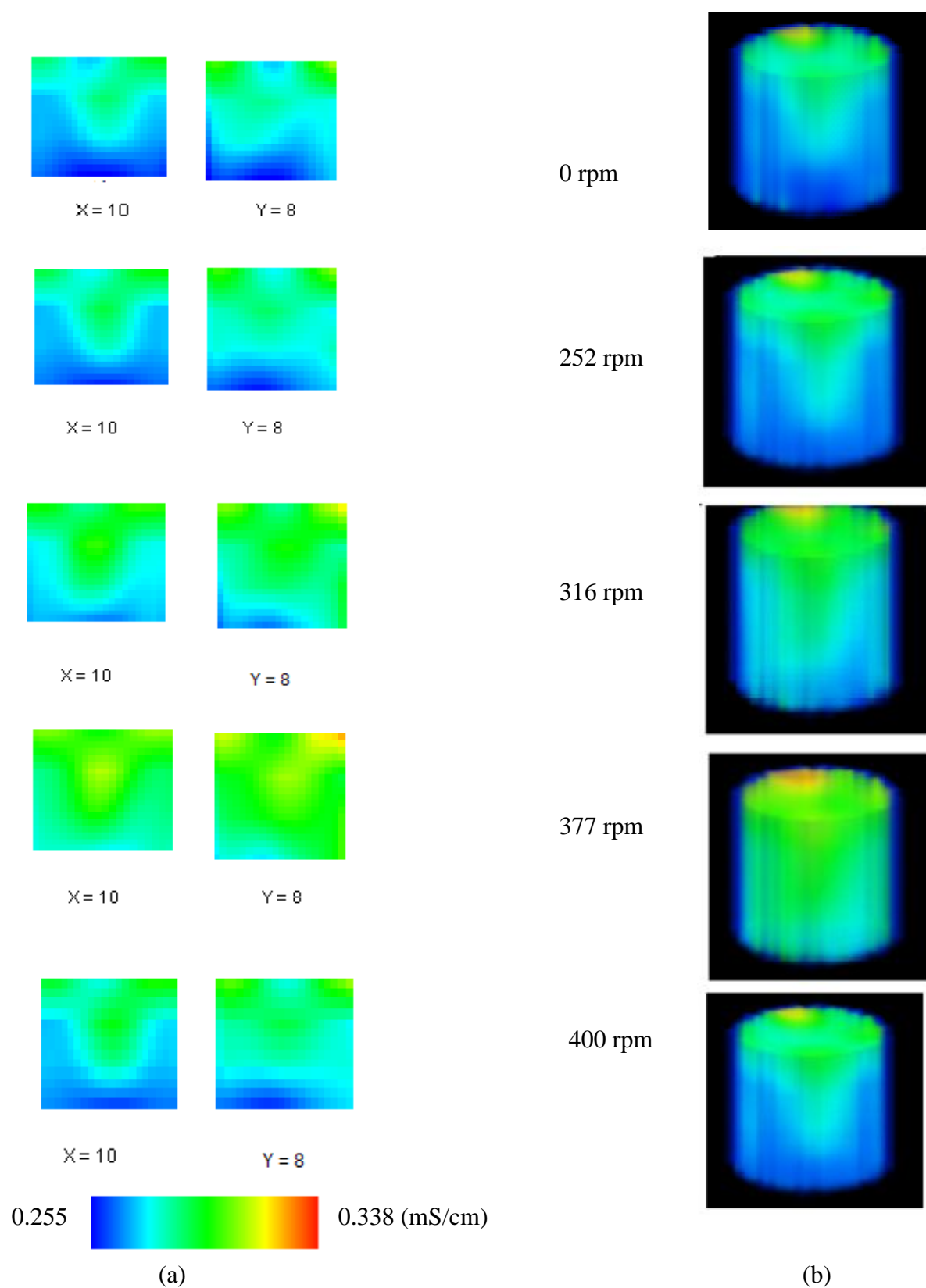
Figure 4.11 vertical slice image (a) and 3D image (b) of solid homogeneity at different impeller speeds (A310 impeller, $C = T / 3$, $X = 30$ wt%, $d_p = 5\mu m$)

4.5.2 Impeller Pumping Direction

In this study, in order to investigate the effect of impeller pumping direction on the mixing performance, A200 impeller with upward and downward directions was utilized. When an impeller is pumping upward, the generated flow acts on the surface of liquid and enhances the motion at top part of a vessel. Unlike the upward impeller, downward impeller directs fluid to the bottom of a vessel (Figure 4.12) and increases the fluid velocity at this area. These impellers are suitable to lift heavy particles from the bottom of a tank. In this work, the impeller was located close to the bottom of the tank ($C = T/3$). It was obvious that the top region of the tank was deprived of having a sufficient motion. Thus, upward impeller could affect the dead zones, which were close to the liquid surface and consequently could improve the homogeneity. In addition, the solids were polymeric micron sized latex particles which could disperse in the fluid (water) easily, thus, upward impeller could disperse these particles from the bottom of the tank while directing the fluid to the surface of the liquid. On the other hand, the density of particles was 1.05 g/cm^3 and the density of water was 0.998 g/cm^3 at the room temperature. Due to the small difference between the density of water and particles, there was slow sedimentation velocity of particles in the mixing vessel. Therefore, downward impeller which directed the fluid to the bottom of the tank was not as suitable as upward direction. As a result, it was concluded that the homogeneity achieved by the upward impeller was higher than that obtained by downward one (Figure 4.13).

In addition, at a fully turbulent flow regime, a power number of 0.6 was obtained for upward impeller and 1.0 for downward impeller. Therefore, comparing to the downward impeller, upward impeller had a lower power number and consumed less energy to achieve a certain homogeneity level making it more energy efficient to suspend the solid particles (Figure 4.14). Since the sedimentation velocity of particles was very slow over the time, the outcome of this section is similar to the results reported by Ozcan-Taskin about the floating particles (2006). Ozcan-Taskin observed the dominant advantages of the upward pumping mode against the downward pumping mode for floating particle suspension.

Downward pumping   Upward pumping
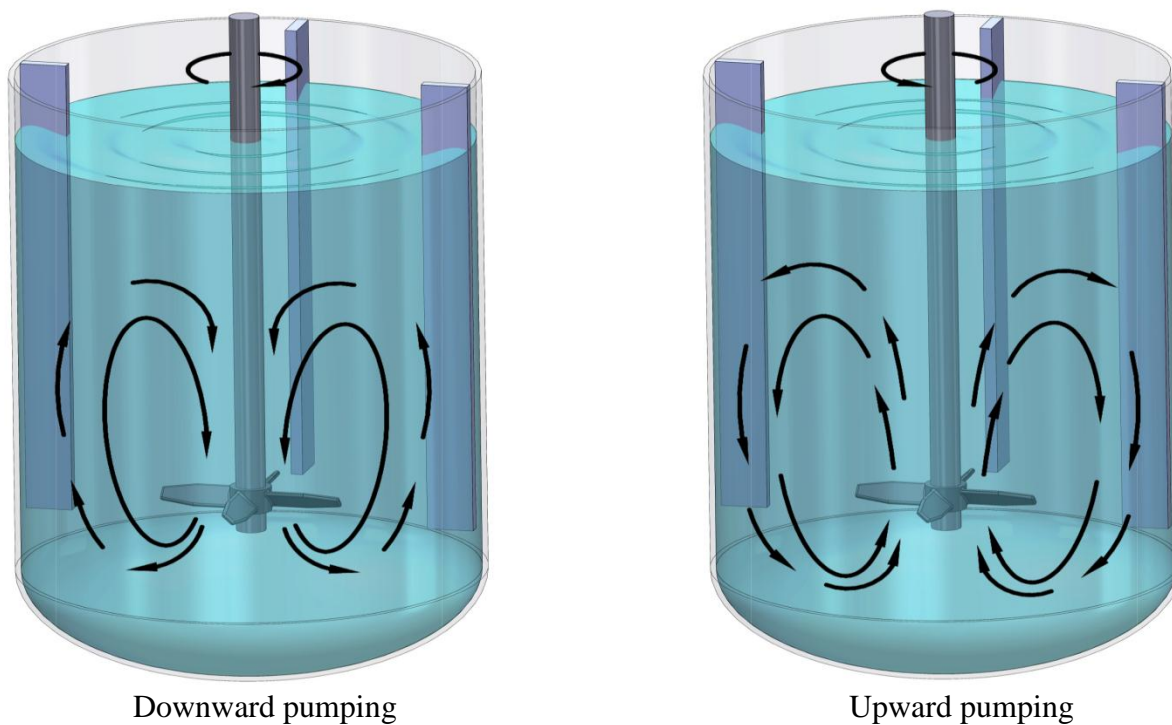
Figure 4.12 The flow pattern of upward and downward direction of an impeller
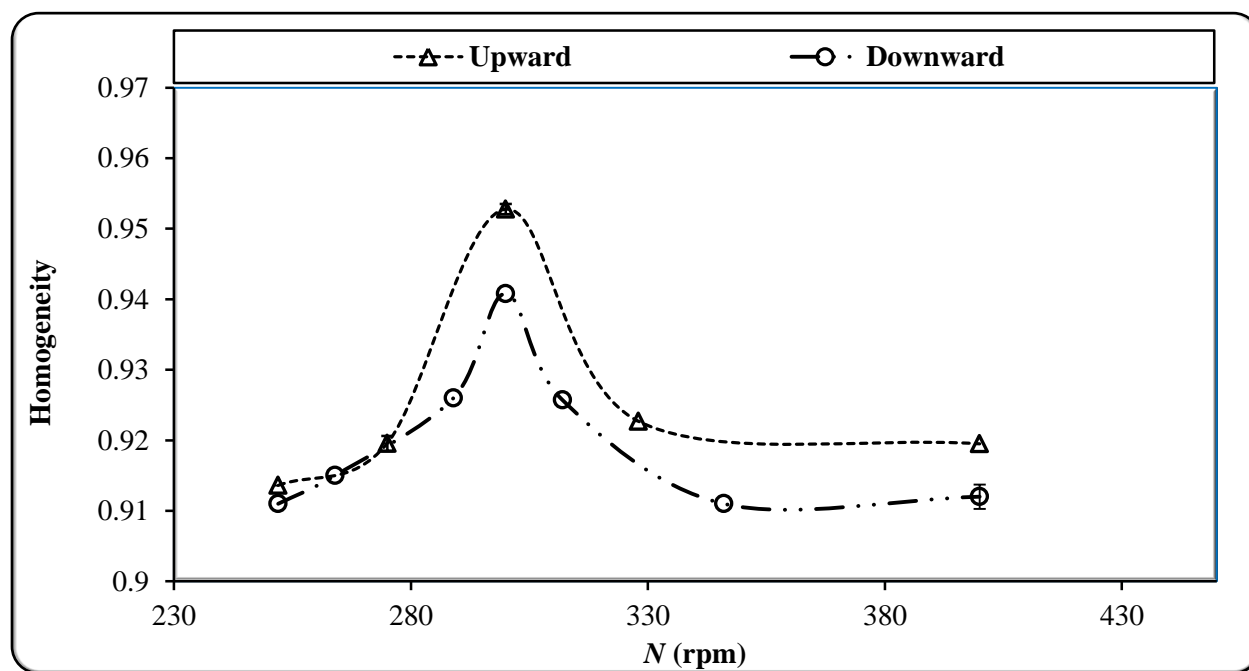
Figure 4.13 Effect of impeller direction of rotation on homogeneity (A200 impeller, $C = T / 3$, $X = 15$ wt%, $d_p = 5$ μm)
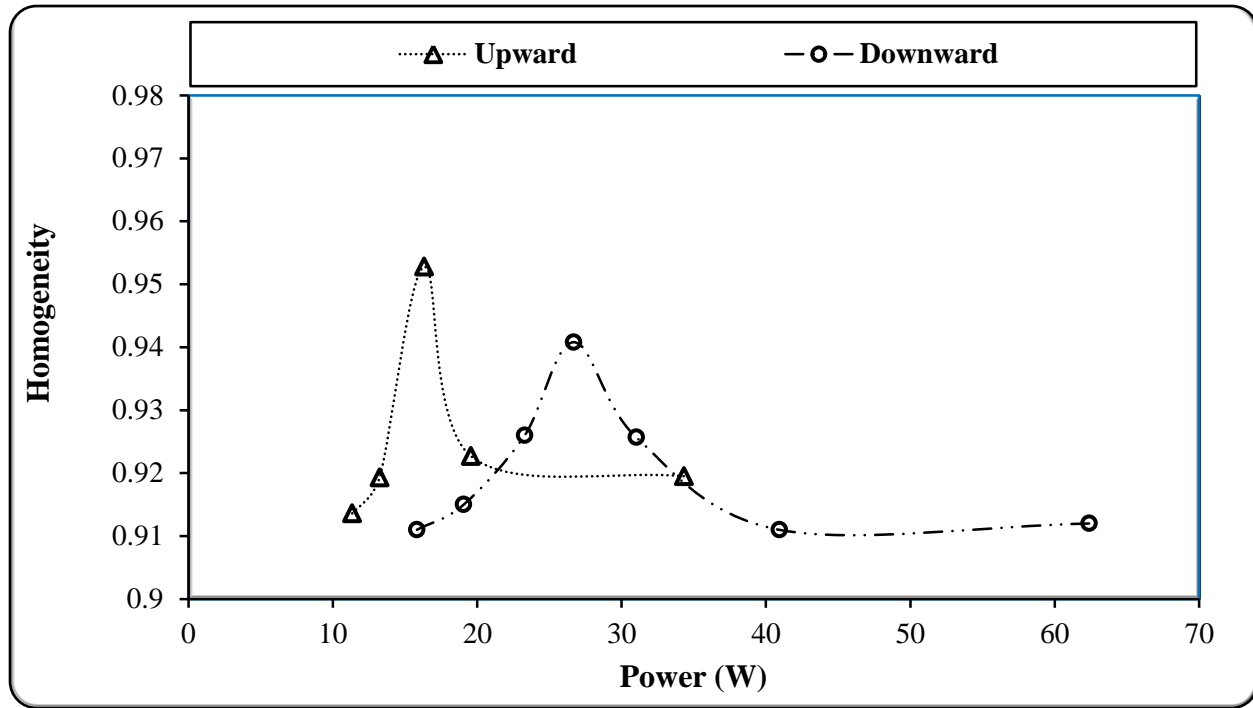
Figure 4.14 Effect of impeller direction of rotation on power (A200 impeller, $C = T / 3$, $X = 15$ wt%, $d_p = 5 \mu m$)

4.5.3 Impeller Clearance

Clearance is the distance between the impeller and the bottom of tank and has substantial effect on the mixing quality. In this study, using A310 impeller, three various impeller positions were applied on the shaft. Plotted on the Figure 4.15, the results illustrate that at the clearance $C = T/3.8$, since the impeller was located very close to the bottom of the tank, it could not generate enough motion across the tank. As a result, the homogeneity achieved at this clearance was low. As the clearance increased from $C = T / 3.8$ to $C = T / 3$, the level of homogeneity increased and achieved its highest level at the clearance $C = T / 3$. As a result, the best homogeneity was obtained at clearance $C = T / 3$. In this clearance, the created flow pattern balanced all existing forces in a way that particles were distributed more uniformly compared to the other clearances. Any further increase in the clearance, from $C = T / 3$ to $C = T / 2.5$, reduced the homogeneity. In fact, at $C = T / 2.5$, the generated flow pattern changed from axial to radial-flow pattern and consequently dropped the homogeneity. Also,, the level of homogeneity was plotted versus normalized clearance in Figure 4.16. According to this graph, the maximum level of homogeneity was achieved when C / T = 0.33. For C / T > 0.33, the level of homogeneity

decreased due to the flow transaction from axial to radial. This behaviour was also observed by Armenate *et al.* (1998). They reported that for $\dfrac{C}{T} > 0.35$, the flow pattern acts radial.

In addition, Figure 4.15 shows that the impeller speed to achieve the maximum homogeneity was independent of impeller clearance for the range of 252 - 400 rpm. The outcome of this study is in good agreement with that reported by Hosseini *et al.* (2010).

Also, Figure 4.18 shows that once the clearance increases, the power consumption shifts to a higher value. In fact, at a high impeller clearance, there are two circulation flows above and below the impeller. At a low clearance, there is only one circulation flow above the impeller (Figure 4.17). In the former case, the power dissipated at constant impeller speed is higher. (Nienow, 1968 and Conti *et al.*, 1981). In this work, the circulation flow generated below the impeller at high clearance, forced the solids to pile-up near the center of the tank. As the clearance increased, the circulation flows generated below the impeller were widened and led to the increasing of the power consumption. As a result, as the impeller clearance increased from T/3.8 to T/2.5, the corresponding power consumption shifted to the higher values. The outcome of this section is in agreement with the results reported by Nienow (1968) and Conti *et al*. (1981).
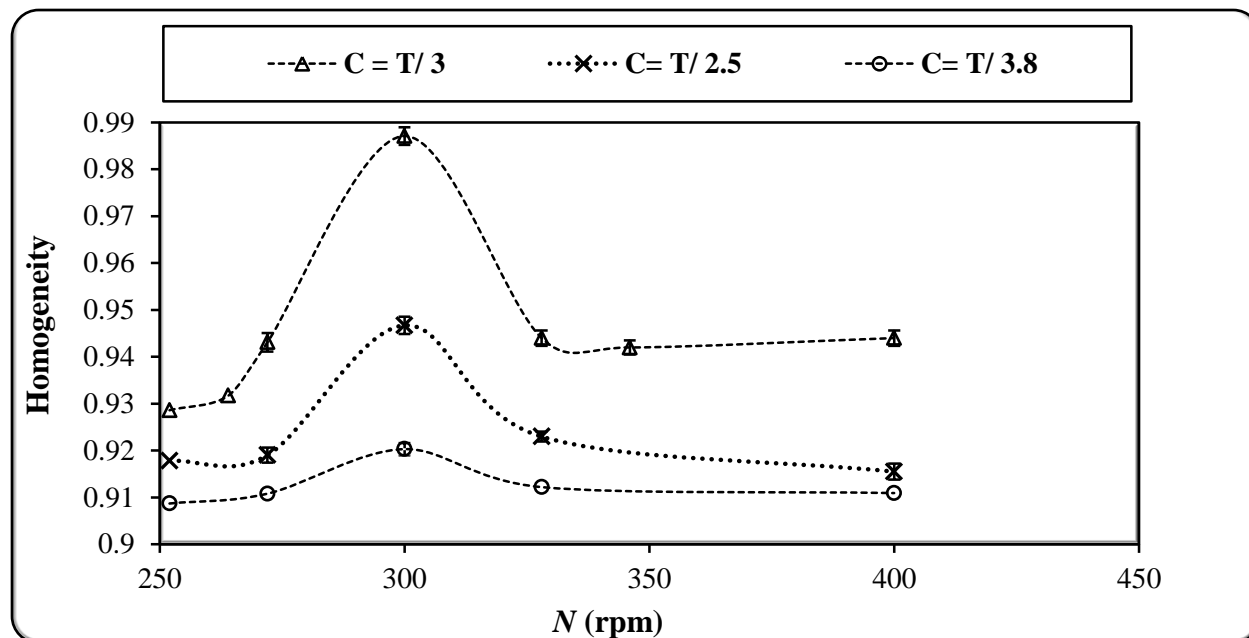
Figure 4.15 Effect of impeller clearance on homogeneity (A310 impeller, $X = 15$ wt%, $dp = 5$ μm)
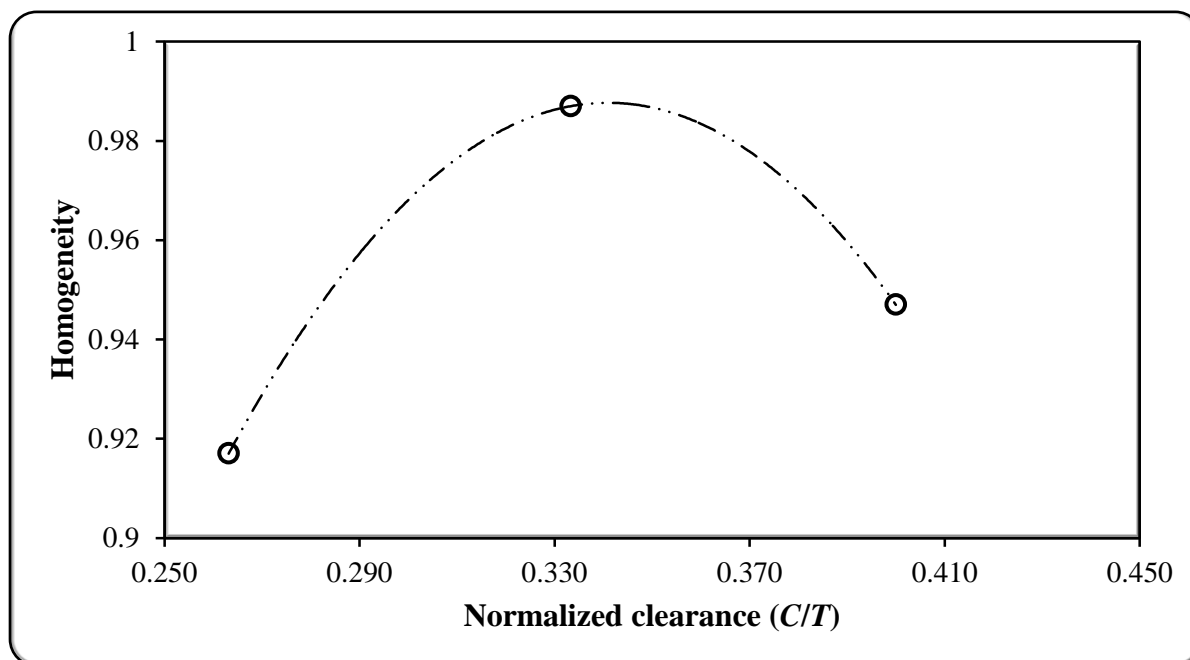
Figure 4.16 Normalized clearance effect on homogeneity (A310, $N = 300$ rpm, $X = 15$ wt%, $d_p = 5$μm)
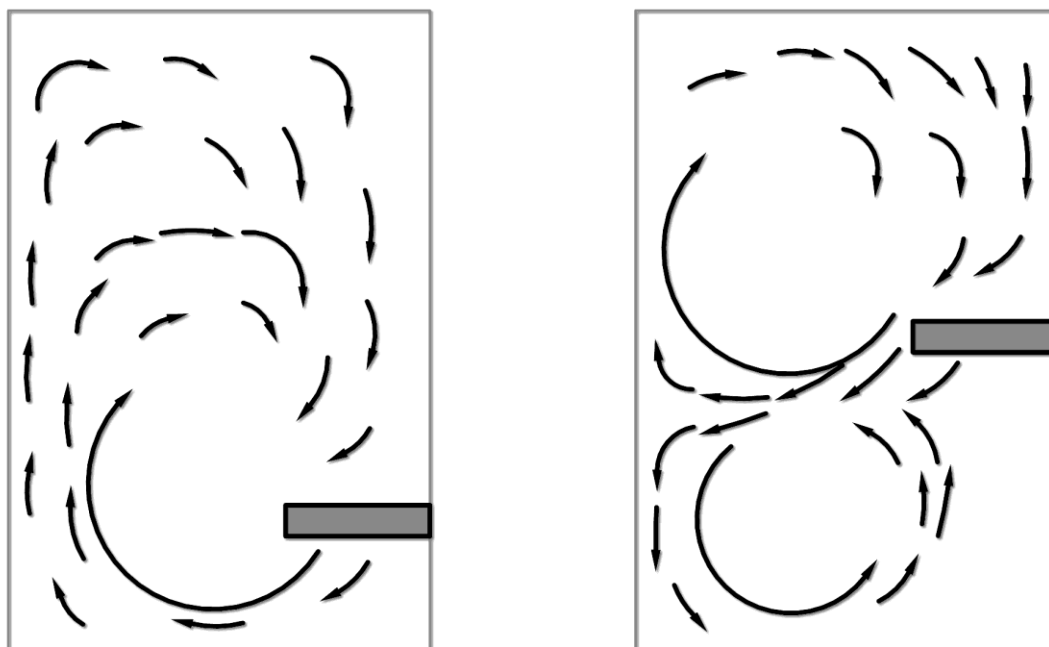
Figure 4.17 Flow circulation pattern in an axial impeller, left to right: low clearance to high clearance
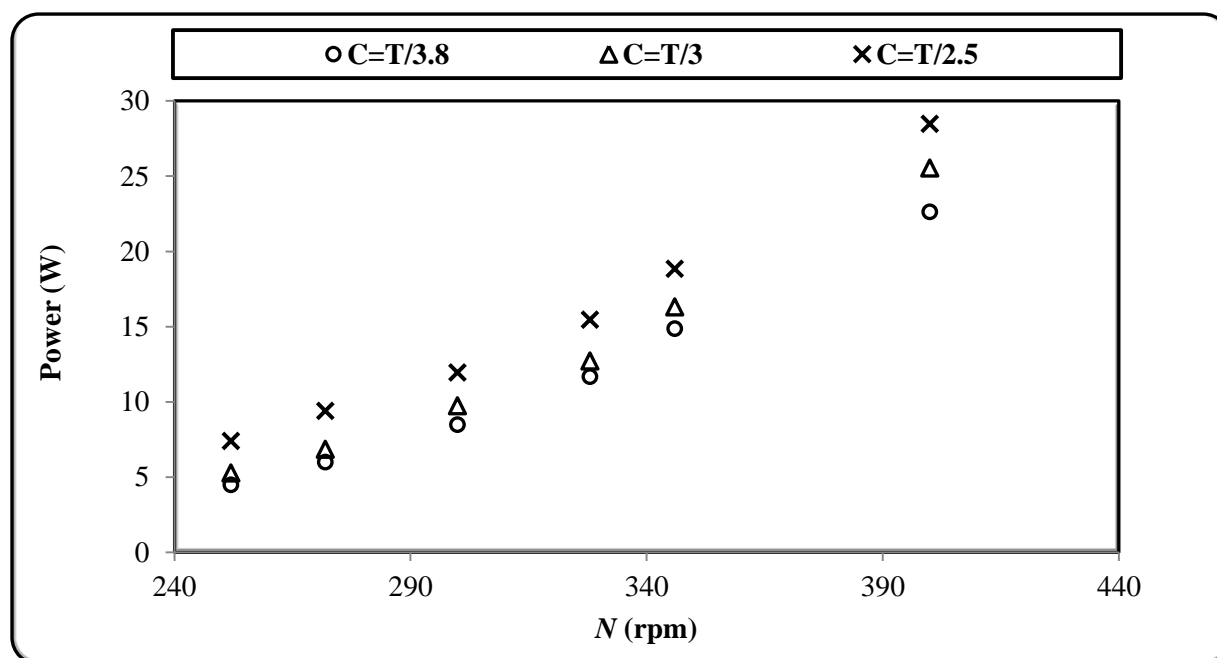
Figure 4.18 Effect of impeller clearance on power consumption (A310 impeller, $X = 15$ wt%, $dp = 5$ μm)

4.5.4 Effect of Impeller Type on the Level of Homogeneity

Impeller type is a geometrical parameter of a mixing system with a crucial effect on the mixing performance and is selected differently for various mixing systems. The previous studies show that axial-flow impellers are the most suitable group of impellers for solid-liquid systems (Paul *et al*., 2004). The six different axial- flow impellers used in this study were: A315, A200, A320, A310, A100, 3AM (Figure 4.19).

| A310 | A320 | A200 |

| A315 | 3AM | A100 |

Figure 4.19 Different axial-flow impellers employed in this study

4.5.4.1 Impeller Power Number

The most important characteristics of impellers are power, flow and circulation numbers. In this study, power number for six axial-flow impellers was experimentally obtained and compared with power numbers reported in the literature.

In Figure 4.20, the power numbers for A310 impeller are plotted against Reynolds numbers for water and 30% latex concentrations. Definition of Reynolds number used for Newtonian fluids in this work is:

$$\mathrm{Re} = \frac{ND^2\rho}{\eta} \tag{4.6}$$

where η, N, D, ρ, are Newtonian viscosity, impeller rotational speed, impeller diameter, and fluid density, respectively.

Figure 4.20 depicts that at fully turbulent condition, the power number is independent of the sample type and concentration.

Impeller turbulent power number is a characteristic of the impeller geometry and does not depend upon the rheological properties of the material (Tatterson, 1994). Thus, to obtain the turbulent power number for each impeller, 30 wt% latex suspension was used. Then power number was plotted versus Reynolds number for each impeller (Figure 4.21). At the fully turbulent regime, the power number of each impeller was independent of Reynolds number and remained constant. The value of the constant power number was read from the Figure 4.21 and listed in the Table 4.2. The Figure 4.21 presents that A200 consumed the highest amount of power at a specific speed (Ibrahim and Nienow, 1995), while A100 consumed the least power.
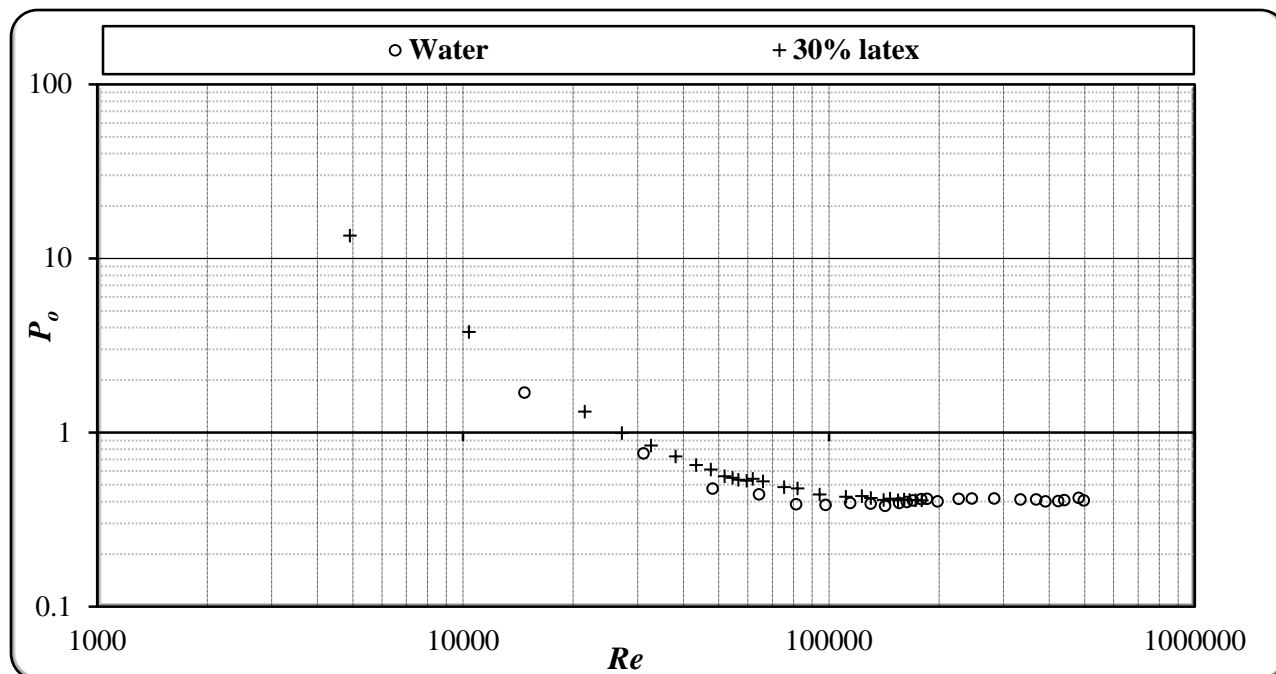
Figure 4.20 Experimental Power Curve (A310 impeller, $C = T / 3$, $dp = 5$ µm)
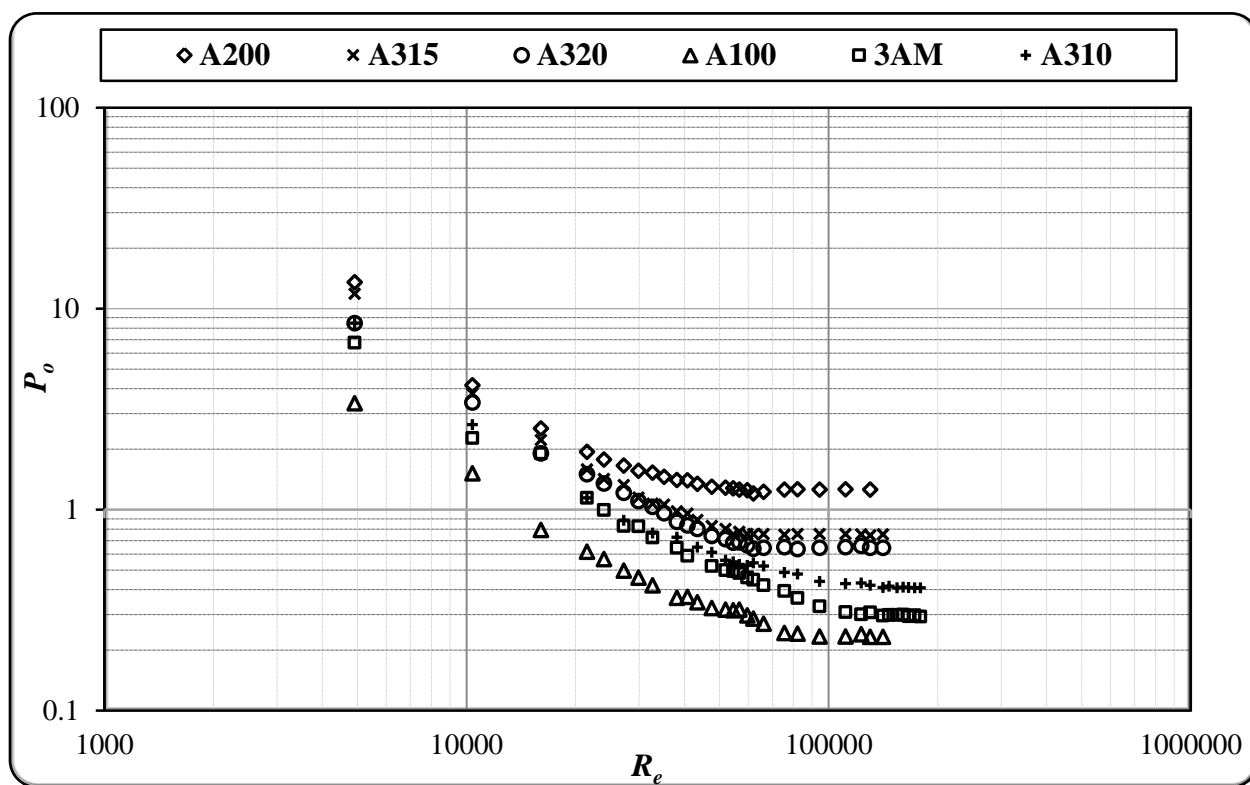
Figure 4.21 Experimental power curve for various axial impellers ($X = 30$ wt%, $C = T / 3$, $dp = 5$ µm)

The reported power numbers for A310 are as follow: 0.37 (Wyczalkowski, 2004), 0.29 for A310 impeller (Ibrahim & Nienow, 1995), 0.33 (Wu and Pullum, 2000), 0.40 (Mavros *et al.,* 1996), 0.34 (Patwardhan and Joshi, 1999), 0.32 (Wu *et al.,* 2001), 0.3 (Edward *et al.,* 2004), 0.3-0.4 (Kumaresan & Joshi, 2006), and 0.31 (Wu *et al*., 2006 A) and 0.28-0.35 (Kumaresan *et al.,* 2005).

For an A200 impeller, the reported power numbers are: 1.3 (Kumaresan & Joshi, 2006), 2.21 (Ranade & Joshi, 1989), 1.26 (Houcine *et al*., 2000), 1.27 (Nienow, 1990), 2.1 (Ranade *et al.,* 1992), 1.7 (Jaworski *et al*., 1996), 1.8 (Ranade and Dommeti, 1996), 2.1 (Mishra *et al.,* 1998), 2.2 (Sahu *et al*., 1999), 1.93 (Patwardhan and Joshi, 1999), 1.93 (Aubin *et al.,* 2001), 1.22 (Wu *et al*., 2001), 1.6 (Wyczalkowski, 2004), 1.27 (Edward *et al.,* 2004), 1.6 (Kukukova *et al*., 2005), and 1.27 (Oldshue, 1983).

The reported power numbers for A100 are as follow: 0.34 (Edward *et al*., 2004), 0.87 (Oldshue, 1983), 0.89 (Mishra *el al*., 1998), 0.23 (Nienow, 1990), 0.89 (Ranade *et al.,* 1992), 0.89 (Sahu *et al*., 1999), and 0.87 (Oldshue, 1983).

For an A320 impeller, the reported power number is 0.64 (Weetman and Coyle, 1989).

For A315, the reported power number was 0.76-0.84 (Macfarlane *et al.,* 1995), and 0.75 (weetman and Gold, 1993).

For 3AM impeller, the reported power number is 0.30 (Paul *et al.,* 2004).

Table 4.2 compares the experimentally obtained power number of impellers with those reported in the literature.

Table 4.2 Impellers Turbulent Power Number

Impeller	Power number reported in literature	Power number obtained experimentally
A100	0.23 – 0.89	0.23
A200	1.22 – 2.21	1.25
A310	0.29 – 0.40	0.40
A320	0.64	0.64
A315	0.75 – 0.84	0.75
3AM	0.30	0.30

The power numbers obtained experimentally for all impellers are in good agreement with values reported in the literature.

4.5.4.2 Impeller Type

According to the studies have been done so far, the best group of impellers suitable for the solid-liquid suspension is axial- flow impellers (Paul *et al.,* 2004). Axial - flow impellers are designed differently for various industrial purposes. In this work, the six axial impellers considered were: A100, A310, A320, A315, A200, 3AM.

A suitable impeller for the mixing of a solid-liquid suspension is one that can generate maximum homogeneity using minimum power. Thus, in order to compare the efficiency of these six impellers, the maximum homogeneity generated by each impeller is plotted against the impeller power consumption (Figure 4.22).

Figure 4.22 presents that the highest levels of homogeneity, achieved by A200 and A320 were lower than those achieved by the other impellers. Also, the powers used by these two impellers to reach the maximum homogeneity were high in comparison with other impellers. In fact, the generation of eddies at the end of each blade caused the A200 (Kresta and Wood, 1993) and

A320 to have the worst efficiency in the mixing of fine particle suspensions. Therefore, in this study, A200 and A320 were not suitable impellers for the solid- liquid suspension. A100, A315 and 3AM were able to generate a maximum homogeneity of 95%. Among these three impellers, A100 used the least power to reach 95% of homogeneity. Thus, A100 was more suitable than A315 and 3AM. The A310 impeller could produce the homogeneity of 99%. However, the power required to reach this homogeneity was more than that used by A100, to reach its 95% of homogeneity. Thus, in this study, A100 demonstrated the best performance. Meanwhile, A310 impeller showed the best efficiency since it could achieve approximately 99% of the homogeneity in solid-liquid mixing system consuming a moderate power. As a matter of fact, having tapered blades caused the generation of fewer eddies at the blade tips of impeller A310. The levels of homogeneities achieved by theses impellers are ranked as follow:

A310 > A100 >A315 >3AM > A200 >A320

The results related to the comparison of A310, A100, and A200 impellers, with respect to the levels of homogeneity, agree with the results reported by Hosseini *et al*. (2010)

Figure 4.23 illustrates the power consumption of each impeller and the achieved level of homogeneity by each impeller. According to this graph, A100 consumed the least power while A200 used the most. The power consumptions of the impellers are rated as follow:

A100 < 3AM < A315 < A310 < A320 < A200

The results related to the comparison of A100, A310, and A200 impellers, with respect to power, are also confirmed by the results reported by Hosseini *et al*. (2010)

Corpstein *et al*. (1994) realized that the high efficiency impellers (HF-3) are more advantageous than pitched blade turbines (A200) in solid-liquid mixing, since they use less power to reach the desired homogeneity. Considering the high efficiency impellers have approximately similar characteristics as A310 impeller, it can be concluded, the results related to the comparison between A310 and A200 impellers are in good agreement with the results reported by Corpstein *et al*. (1994).

The outcome of this section is that A310 and A100 have the best efficiency and performance, respectively.
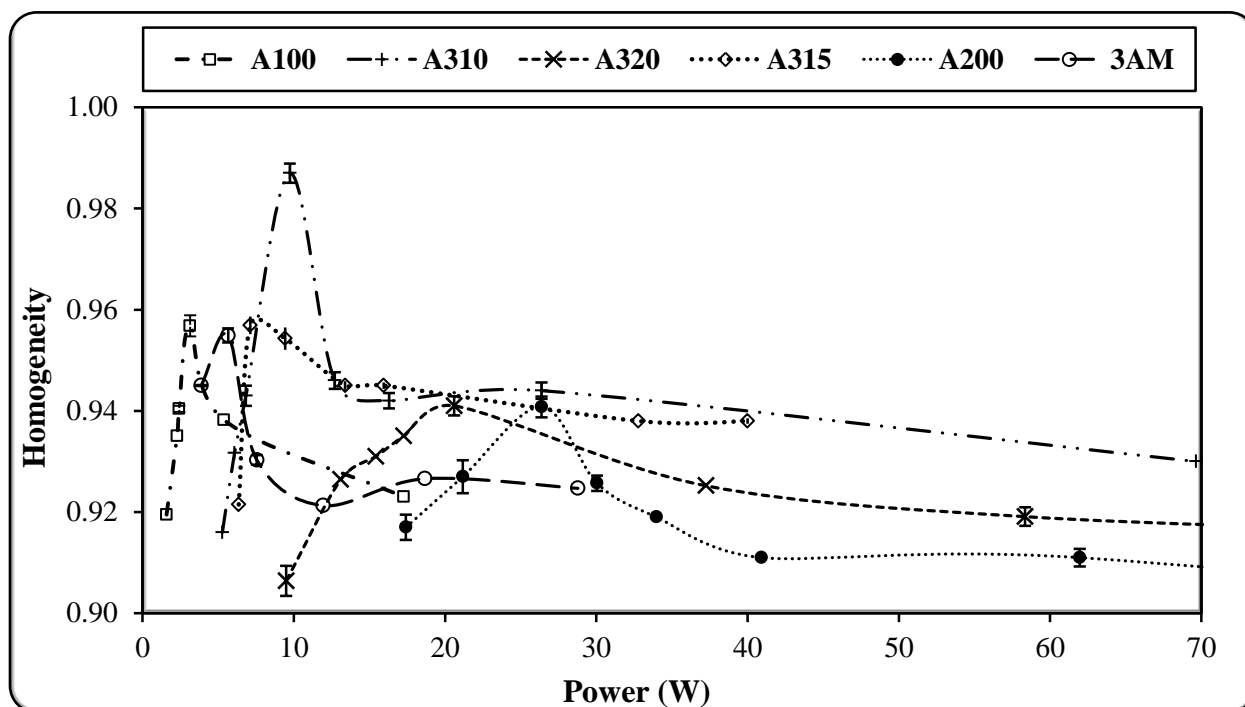
Figure 4.22 Effect of impeller type on homogeneity ($C = T / 3$, $dp = 5$ μm, $X = 15$ wt%)
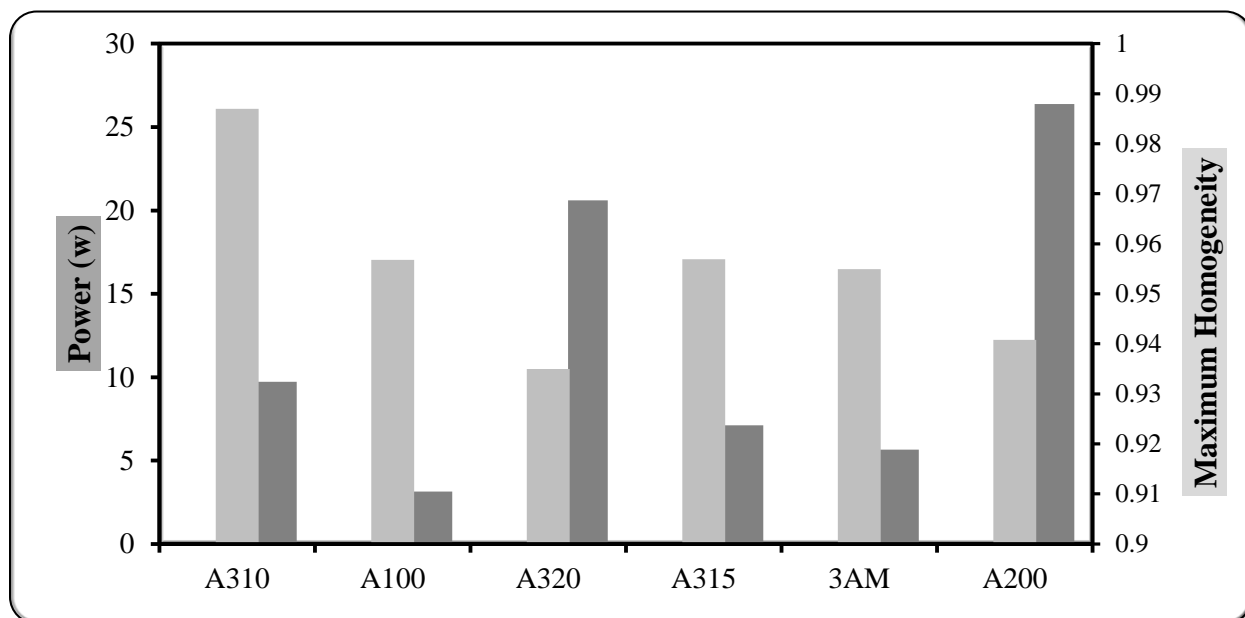
Figure 4.23 Maximum homogeneity versus power consumption for different axial-flow impellers ($C = T / 3$, $dp = 5$ μm, $X = 15$ wt %)

4.5.5 Impeller Diameter

The ratio of the impeller diameter to the vessel diameter is a crucial parameter that greatly influences the flow pattern and solid distribution. In this study, four different impeller to vessel diameter ratios (D/T = 0.47, D/T = 0.39, D/T = 0.31, D/T = 0.29) were selected for A200 impeller. At the constant clearance of *T/3* and downward rotational speed, Figure 4.24 presents that the impeller (D/T = 0.31) generated the strongest axial-flow and achieved the highest level of homogeneity. As the impeller diameter increased (D/T > 0.31), the impeller started to direct the fluid to the vessel wall and changed the axial flow to radial flow (Bakker *et al*., 1994). Therefore, the direction of the flow at the bottom of the tank was reversed from outward to inward. Since the velocity at the bottom of the tank was decreased, more solid particles were accumulated at the base of the tank. Hence, the level of homogeneity was reduced. As the impeller diameter decreased (D/T < 0.31), the primary flow and motion in the tank were reduced resulting in a decrease in the achieved level of homogeneity. The outcome of this study is in agreement with the results from Bakker *et al.* (1994). They found that, there is an optimum value for impeller diameter to tank diameter ratio. Once the impeller diameter to tank diameter ratio increases beyond the optimum value, a flow transition takes place and the flow pattern of the impeller acts radially and directs the fluid to the vessel wall. In addition, the impeller with D/T = 0.31 consumed the least power to achieve the highest level of homogeneity and was more energy efficient. This is also confirmed by Paul *et al.* (2004).
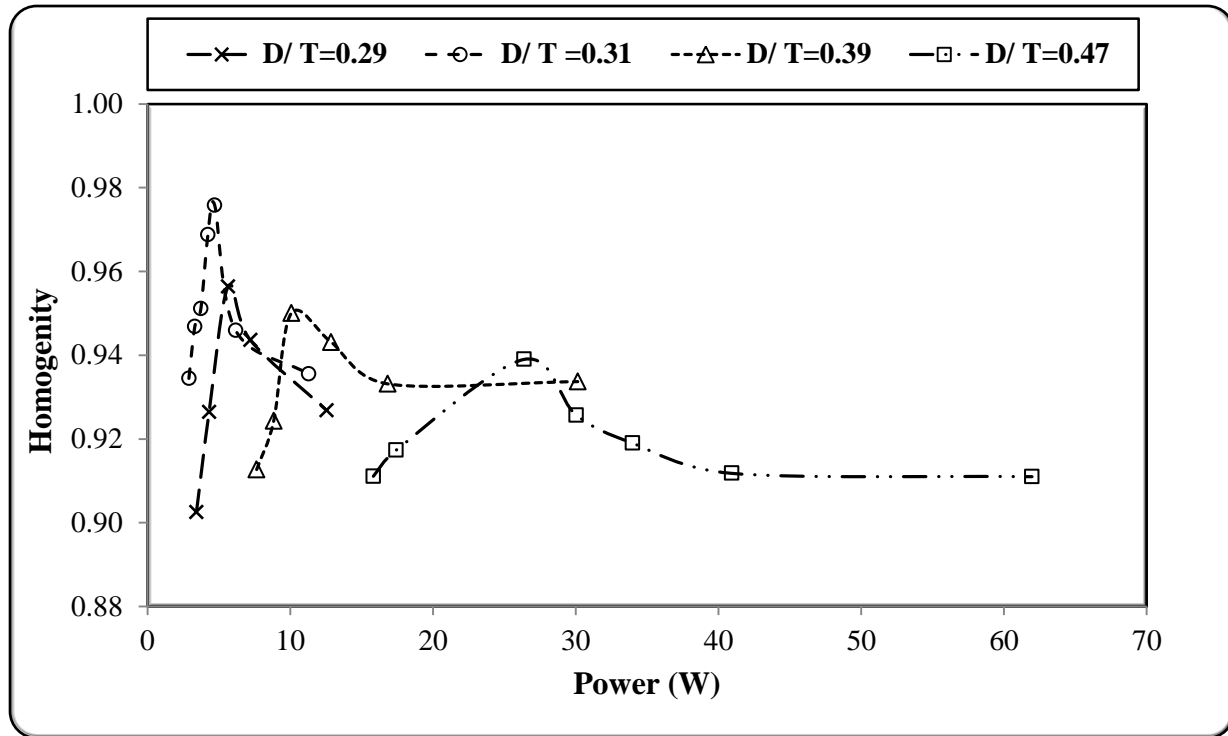
Figure 4.24 Effect of impeller diameter on homogeneity (A200 impeller, *C= T / 3, dp = 5 μm,*
X = 15 wt%)

4.5.6 Concentration

Concentration is one of the influential parameters affecting the homogeneity of the solid-liquid suspension. Hosseini *et al.,* (2010) studied the effect of concentration on the homogeneity of the glass bead suspension. They observed that as the concentration increases, the interaction between the glass bead particles increases. This interaction prevents particles from settling down and improves the homogeneity. In this study, to investigate the effect of the concentration on the level of homogeneity, the homogeneity of different weigh concentrations of 15%, 20%, 25%, 30% were plotted versus power consumption in Figure 4.25. This figure presents that as the concentration increased the level of homogeneity decreased. In this work, the settling velocity of particles was low because the density of latex particles (1.05 g/cm^3) was very close to the density of water (0.998 g/cm^3) at room temperature. Thus, at higher concentrations, the increase of the particle-particle interaction, which prevents particles from settling down, didn't improve the homogeneity. But, as the concentration was raised, the number of particles, viscosity, and density increased. This caused the impeller to require more power to suspend particles. Therefore, at the

constant power consumption, the homogeneity achieved at higher concentration was less than that achieved at lower concentration. As expected, Figure 4.25 demonstrates that the concentration of 15 wt% and 30 wt% had the highest and the lowest level of homogeneity, respectively. Also, Figure 4.26 depicts that the increasing of the solid concentration reduced the maximum level homogeneity, linearly.

In addition, as the concentration increased, the power required to achieve the maximum level of homogeneity shifted to a higher value. In other words, the power required to achieve the highest level of homogeneity, at low concentration of particles, was able to suspend only parts of particles in higher concentration. Therefore, higher concentration of particles needed more power to achieve the maximum level of homogeneity. This fact was previously confirmed by Hosseini *et al.* (2010).
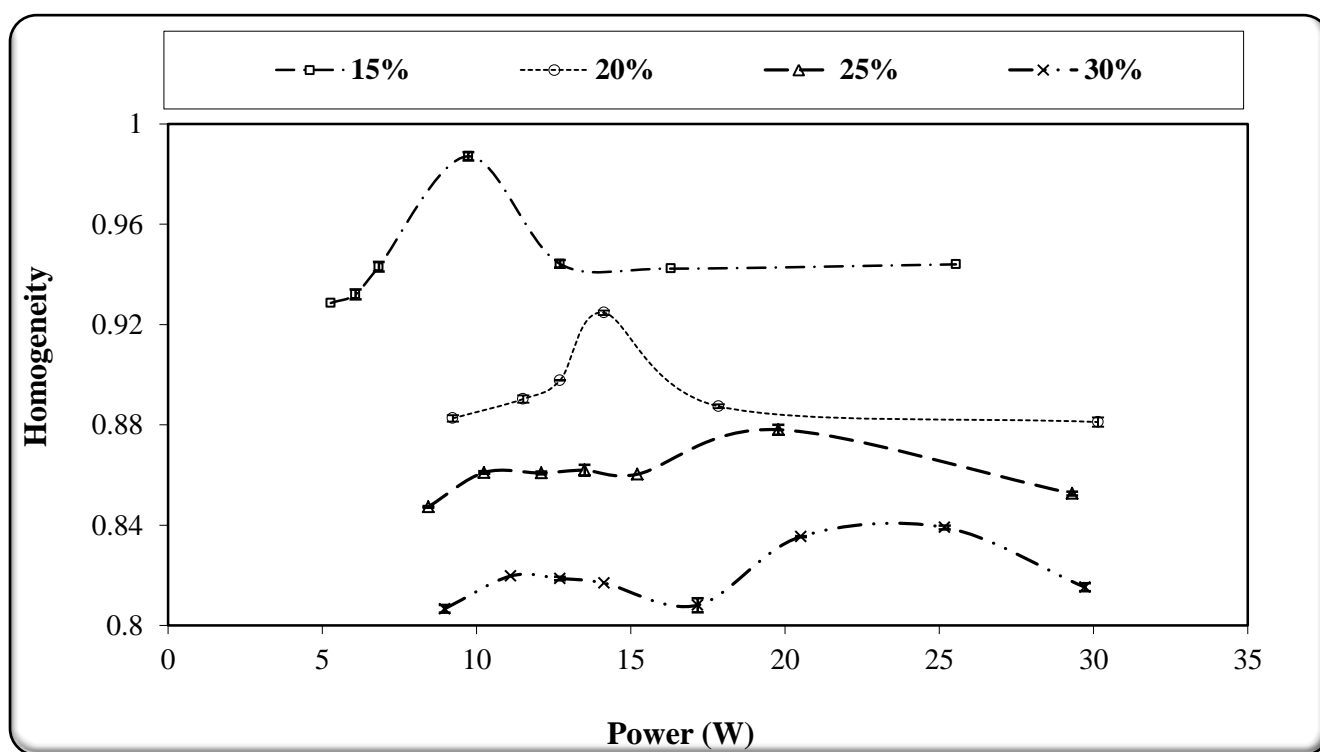
Figure 4.25 Effect of concentration on homogeneity (A310 impeller, *C = T / 3*, *dp* = 5 μm)
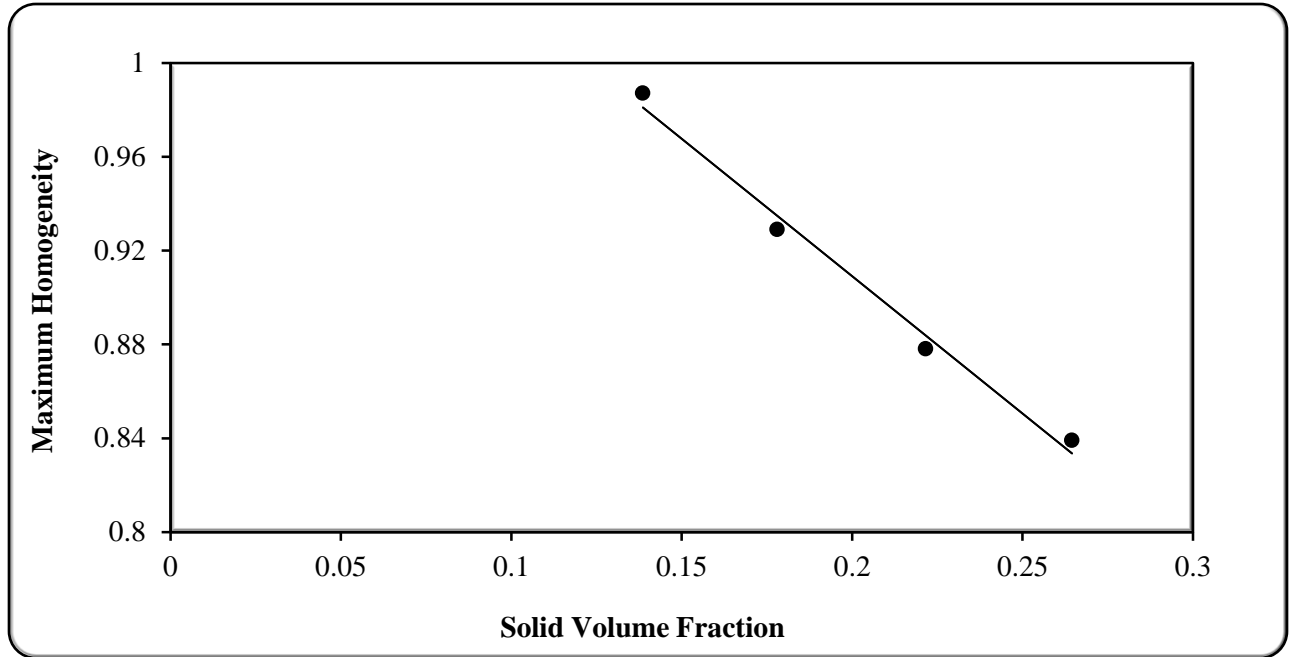
Figure 4.26 Effect of concentration on maximum homogeneity (A310 impeller, *C = T / 3*, *dp =* 5 μm)

4.6 Effect of Particle Size on the Solid-Liquid Mixing

4.6.1 Particle Size

One of the substantial parameters influencing the homogeneity of solid-liquid suspension is the size of particles. Small particles have greater exposure area than large particles when in contact with the fluid. The high exposure surface area reduces terminal velocity, constant settling velocity of particles with zero acceleration. This makes the suspension of particles easier and drives the suspension to a more homogeneous mixture (Peker and Helvaci, 2008). For the Newtonian turbulent regime, $Re_p > 1000$, the expression to calculate terminal velocity V_t is defined as follows (Perry & Green, 1984):

$$V_t = 1.73 \left(\frac{g_c d_P (\rho_s - \rho_l)}{\rho_l} \right)^{\frac{1}{2}} \tag{4.7}$$

where, g_c is the gravitational constant, d_p is the particle diameter, ρ_s is the particle density, and ρ_l is the liquid density.

To investigate the effect of particle size on the homogeneity level of solid-liquid suspension, the axial change in solid volume concentration with various particle sizes were plotted in Figure 4.27. This figure shows that the homogeneity of particle size of 5.2 μm has the least deviation from homogeneity level of one, the perfect homogeneity. As the size of particles increases, this deviation also increases. Thus, the homogeneity of particle size of 9.1 μm has the most deviation from the homogeneity level of one. This phenomenon agrees well with the results reported by Hosseini *et al.* (2010), Peker *et al.* (2008) and Selima *et al.* (2008).

Figure 4.28 presents the homogeneity of three different sizes of particles, 5.2, 8.5, and 9.1 μm versus impeller speed. This graph demonstrates that the particle size of 5.2 μm generated the highest level of homogeneity. Also, as the particle size increased the suspension of particles became harder and led to the reduction of homogeneity. Figure 4.29 shows the reduction of maximum level of homogeneity with the increase of particle size.

In addition, the size of particles influences the impeller speed required to achieve the maximum level of homogeneity. Paul *et al.* (2004) revealed that the just suspended impeller speed is directly proportional to the particle size. In other words, he realized that as the particle size increases, higher impeller speed is required to completely suspend all particles. Similar to the results of Paul *et al.* (2004), Figure 4.28 presents that as the particle size increased, the impeller speed for the maximum homogeneity shifted to the higher speeds.
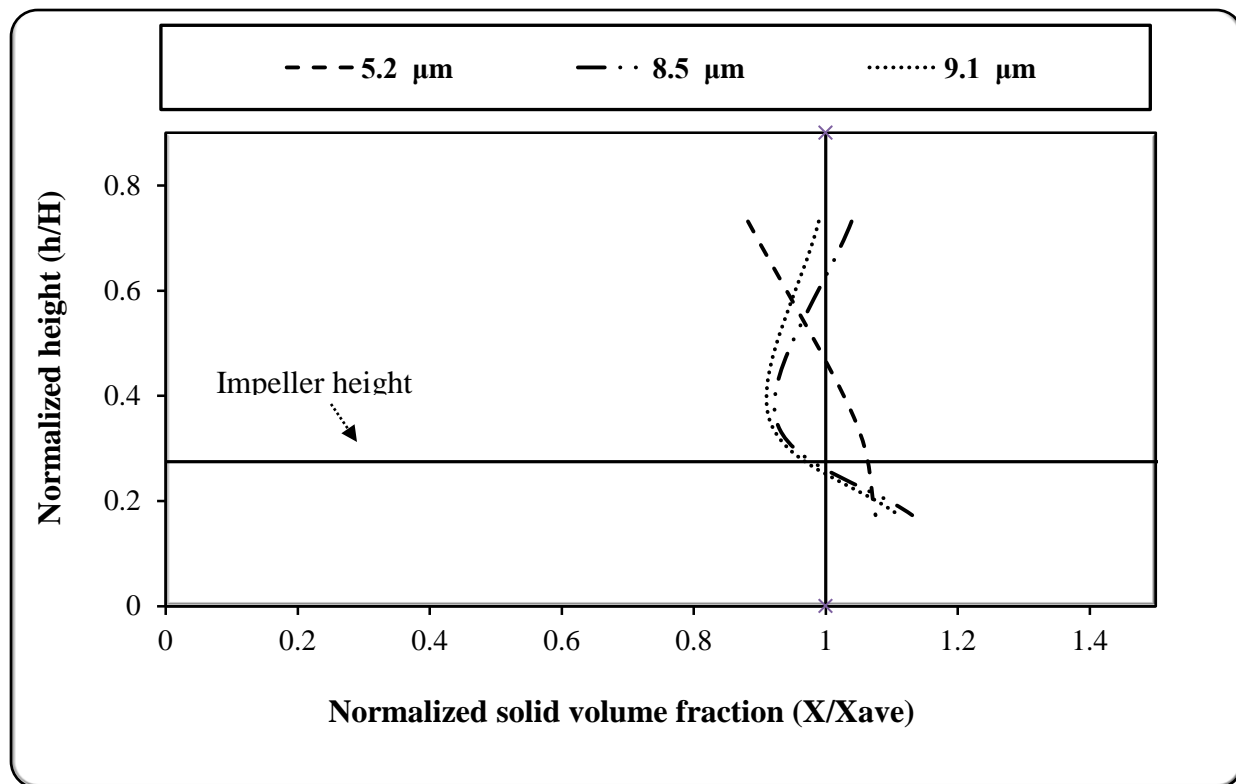
Figure 4.27 Effect of particle size on axial concentration profile (A310 impeller, $C = T / 3$, $X = 15$ wt%)
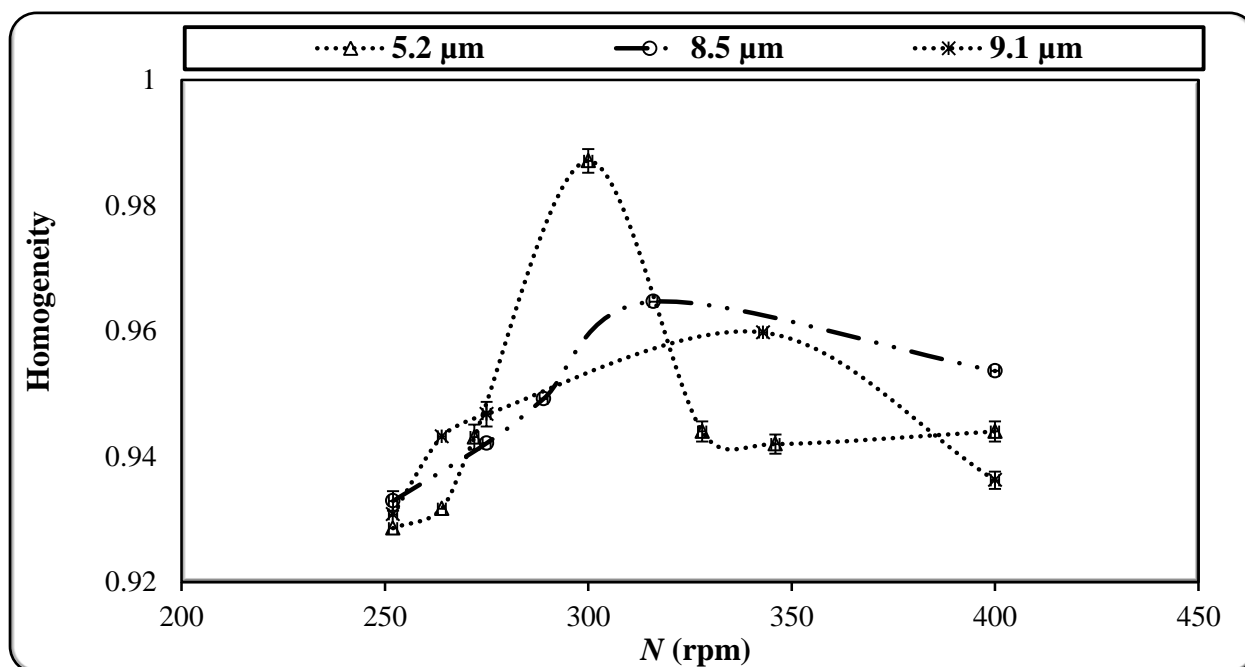

**Figure 4.28** Effect of particle size on homogeneity (A310 impeller, $C = T / 3$, $X = 15$ wt%)
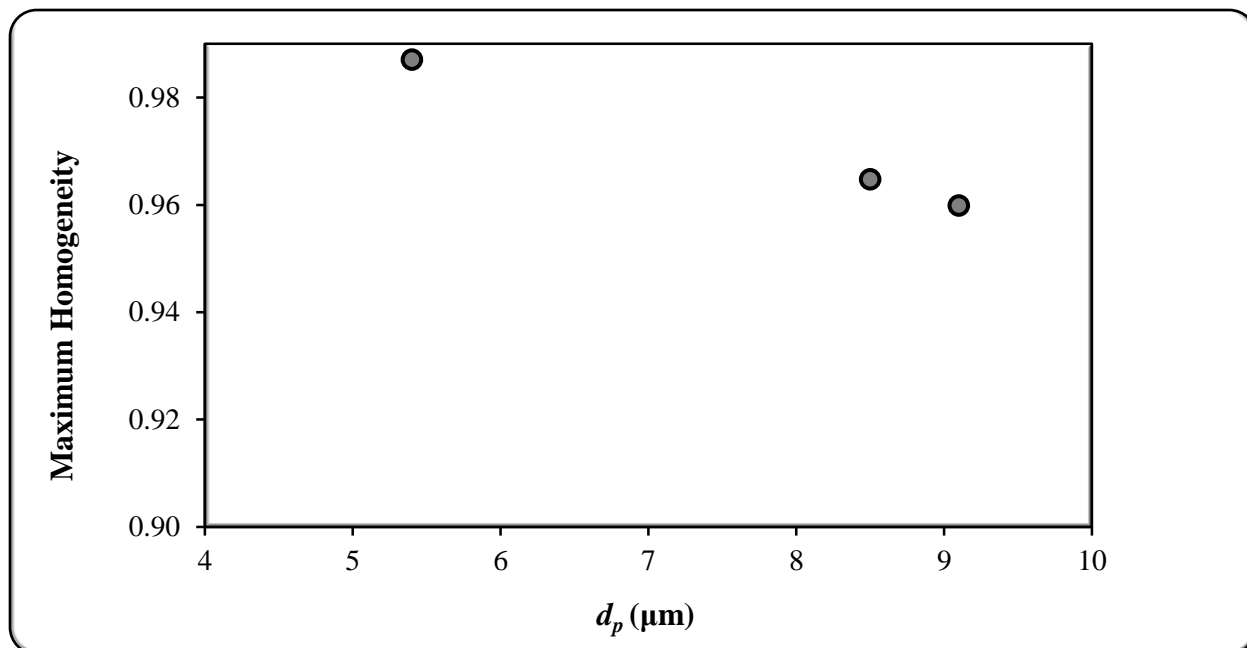
Figure 4.29 Effect of particle size on maximum homogeneity (A310 impeller, $C = T / 3$, $X = 15wt\%$)

Chapter 5
Conclusions and Recommendation

5.1 Conclusions

In this study, the Electrical Resistance Tomography was successfully used to investigate the quality of solid-liquid mixing in response to any changes in design parameters such as impeller type, impeller diameter, and impeller clearance, as well as operating conditions (e.g. impeller speed, impeller pumping mode, solids concentration), and particle size. The level of homogeneity was calculated using the concentration distribution data obtained from ERT measurements. In this study, six axial impellers (A310, A100, A200, A320, A315, 3AM) were used and the level of homogeneity achieved by each impeller was calculated. A310 impeller was found to be the most effective, and A320 and A200 the least effective impellers, in terms of achieving homogeneity. Meanwhile, A100 showed better efficiency than A315 and 3AM impeller.

The results demonstrated an optimal impeller speed for the maximum degree of homogeneity. Also, the effect of off-bottom impeller clearance (*C/T*) on the level of homogeneity, in the range of T/3.8-T/2.5 was investigated. The results showed that the maximum homogeneity was achieved at *C=T/3*, which is within the recommended range in the literature. The impeller diameter to tank diameter ratio (*D/T*) was ranged from 0.29 to 0.47. However, an impeller diameter to tank diameter ratio of 0.31 proved to produce the maximum level of homogeneity.

The effect of downward and upward pumping direction on the level of homogeneity was also studied and the results showed that upward pumping direction was more effective in providing better homogeneity. The level of homogeneity was calculated using three different sizes of latex particles (5.2 µm, 8.4 µm, 9.1 µm). It was found that particle size had an important effect on the quality of solid- liquid mixing. At a constant impeller speed, the level of homogeneity achieved by smaller particles (5.2 µm) was higher than that of achieved by larger particles (9.1 µm). In addition, the concentration of solids had a significant effect on the level of homogeneity. The results demonstrated an increase in the density and viscosity of the solid-liquid suspension as a result of increase in concentration of particles. Thus, the suspension of particles with higher

concentration was more difficult than that with lower concentration. Therefore, for a given power consumption, a rise in concentration of particles resulted in a drop in the level of homogeneity.

Applying the finding of this study will lead to improved equipment design, chemical cost reduction, increased production rate, improved quality of products, and more efficient use of power in slurry reactors.

5.2 Recommendation for Future Work

With respect to solid-liquid mixing, the following suggestions are offered for further studies:

➢ Study of the effect of design related parameters, operating conditions and physical properties on the mixing of micron sized particles with Computational Fluid Dynamics (CFD).

➢ Study of the effect of all geometrical parameters, required for scaling up such as size, shape, number and angle of impeller, number of impeller blades, shape of the tank bottom, and height and clearance of baffle on the mixing of micron sized particles with CFD modeling and ERT experiments.

➢ Study of solid-liquid mixing behavior in a continuous mixing process.

➢ Study of rheological behavior of multi-phase mixing system in a non-Newtonian medium.

Nomenclature

C	Impeller clearance off vessel bottom, m
D	Impeller diameter, m
dp	Particle size, μm
g	Gravitational acceleration, m/s^2
H	Impeller head, m
K	Consistency index , $Pa.s^n$
k_s	Proportionality constant in Metzner and Otto relationship
M	Torque, N.m
N	Impeller rotational speed, rpm
Njs	Just suspended impeller speed, rpm
n	Total number of planes
P	Power, W
t	Time, s
T	Vessel diameter, m
t_m	Mixing time in a batch mixing vessel, sec
t_s	Sampling time, s
V_t	Terminal velocity, m/s
X	Solid concentration, wt%

X_{ave}	Average solid concentration in entire the vessel
Z	Liquid depth in mixing vessel, m
$(N\theta)$	dimensionless mixing time
$(N\theta)_{CS}$	dimensionless mixing time at critical impeller speed from bottom

Greek Letters

$\dot{\gamma}_{avg}$	Average Shear rate, s^{-1}
$\dot{\gamma}$	Shear rate, s^{-1}
η	Apparent (non-Newtonian) viscosity, Pa.s
μ	Fluid viscosity, Pa.s
ρ_L	Fluid density, Kg/m^3
ρ_s	Particle density, Kg/m^3
τ	Shear stress, Pa
τ_y	Yield stress, Pa

Dimensionless Numbers

Fr	Froude number
Po	Power number
Re	Reynolds number

References

Angst, R., Kraume, M. (2006). Experimental investigations of stirred solid/liquid systems in three different scales: Particle distribution and power consumption. *Chem. Eng. Sci*., 61(9), 2864-2870.

Armenante, P. M., Nagamine, E. U. (1998). Effect of low off-bottom impeller clearance on the minimum agitation speed for complete suspension of solids in stirred tanks. *Chem. Eng. Sci.,* 53(9), 1757-1775.

Aubin, J., Mavros, P., Fletcher, D. F., Bertrand, J., Xuereb, C. (2001). Effect of Axial Agitator Configuration (Up-Pumping, Down Pumping, Reverse Rotation) on Flow Patterns Generated in Stirred Vessels. *Chem. Eng. Res. Des*. 79, 845-856.

Bakker A., Fasano, J. B., Myers, J. K. (1994). Effect of Flow pattern on the Solid Distribution in a Stirred Tank. *Proc 8th Europ Mixing Conf*, IChemE Symp Series No. 136, Cambridge, Sep. 21. IChemE Rugby, UK, 1-8.

Baldi, G., Conti, R., Alaria, E. (1978). Complete suspension of particles in mechanically agitated vessel. *Chem. Eng. Sci*., 33, 21-25.

Barresi, A., Baldi, G. (2000). Power consumption in slurry systems. *10th Europ Mixing Conf*, Jul. 3. Delft, the Netherlands.

Beck, M. S., Campogrande, E., Morris, M. A., Williams, R. A., Waterfall, R. (1993). *Tomography Techniques and Processes Design and Operation.* Computational Mechanics Publications.

Bittorf, K. J., Kresta, S. M. (2002). Prediction of Cloud Height for Solid Suspension in Stirred Tanks. *Chem. Eng. Res. & Des.*, 81(A5), 568-577.

Bouaifi, M., Roustan, M. (2001). Power consumption, mixing time and homogenization energy in dual-impeller agitated gas–liquid reactors. *Chem. Eng. Process*. 40, 87–95.

Bourne, J. R., Sharma, R. N. (1974). Homogeneous Particle Suspension in Propeller-Agitated Flat Bottom Tanks. *Chem. Eng. J*., 8, 243–250.

Brucato, A., Micale, G., Rizzuti, L. (1997). Determination of the Amount of Unsuspended Solid Particles Inside Stirred Tanks by Means of Pressure Measurements. *Récentprogrès en génie chimique*, 11, 3–10.

Bubicco, R., Di Cave, S., Mazzarotta, B. (1997). Influence of solid concentration and type of impeller on the agitation of large PVC particles in water. *Recents Prog. Genie Procedes*, 11(52), 81-90.

Bujlaski, W., Takenaka, K., Paolini, S., Jahoda, A., Paglianti, A., Takahashi, A. W.(1999). Suspension and Liquid Homogenization in High Solids Concentration Stirred Chemical Reactor. *Chem. Eng. Res. & Des*., 77, 241-247.

Calderbank, P. H., Moo-Young, M. B. (1959). The prediction of Power Consumption in the Agitation of Non- Newtonian fluids. *Trans I. Chem. Eng*., 37, 26-33.

Conti, R., Sicardi, S., Specchia, V. (1981). Effect of the stirrer clearance on suspension in agitated vessels. *Chem. Eng. J*., 22, 247-249.

Corpstein, R. R., Fasano, J. B., Myers, K. J. (1994). The high-efficiency road to liquid-solid agitation. *Chem. Eng. J*, 72, 138-144.

Dickin, F., Wang, M. (1996). Electrical resistance tomography for process applications. *Meas. Sci. Technol.,* 7(3), 247-260.

Dierick, M., Vlassenbroeck, J., Masschaele, B., Cnudde, V., Van Hoorebeke, L., Hillenbach, A. (2005). High-speed neutron tomography of dynamic processes. *Nucl. Instrum. Methods*, 542 (3), 296-301.

Distelhoff, M. F. W., Marquis, A. J., Nouri, J. M., Whitelaw, J. H. (1997). Scalar Mixing Measurements in Batch Operated Stirred Tanks. *Can. J. Chem. Eng.,* 75, 641-652

Dohi, N. Y., Matsuda, N., Itano, N., Minekawa, K., Takahashi, T., Kawase, Y. (2001). Suspension of Solid Particles in Multi- Impeller Three-Phase Stirred tank Reactors. *Can. J. Chem. Eng*., 79, 107-111.

Drewer, G. R., Ahmed, N., Jameson, G. J. (1994). Suspension of high concentration solids in mechanically stirred vessels. *AIChE Symp*.,136, 41-48.

Edward, L. P., Atiemo-Obeng, V. A., Kresta, S. M. (2004). *Handbook of Industrial Mixing Science & Practice*. Wiley-Interscience.

Einenkel, W. (1980). Influence of physical properties and equipment design on the homogeneity of suspensions in agitated vessels. *German Chem. Eng*., 3, 118-124.

Foucault, S., Ascanio, G., Tanguy, P. A. (2006). Mixing Time in Coaxial Mixers with Newtonian and Non-Newtonian Fluids. *Ind. Eng. Chem. Res*., 45, 352-359.

Fox, E. A., Gex, V. E. (1956). Single Phase Blending of Liquids. *AIChE J.,* 2 (4), 539-544.

Fransolet, F., Crine, M., Marchot, P., Toye, D. (2005). Analysis of Gas Holdup in Bubble Columns with Non-Newtonian Fluid Using Electrical Resistance Tomography and Dynamic Gas Disengagement Technique. *Chem. Eng. Sci.,* 60, 6118-6123.

Geselowitz, D.B. (1971). An application of electrocardiographic leaded theory to impedance plethysmography. *IEEE Trans. Biomed. Eng.,* BME-S8, 38-41.

Gisser, D. G., Issacson, D., Newell, J. (1987). Current Topics in Impedance Imaging. *Clin. Phys. Physiol. Meas*., 8 (A), 36-46.

Guiraud, P., Costes, J., Bertrand, J. (1997). Local measuremts of fluid and particle velocities in a stirred suspension. *Chem. Eng. J., 68*(2-3), 75-86.

Hackl, A., Wurian, H. (1979). Determination of Mixing Time. *Ger. Chem. Eng.* 2, 103-110.

Harrop, K. L., Spanfelner, W. H., Jahoda, M., Otomo, N. A., Etchelles, W., Bujalski, W., Nienow, A. W. (1997). Impact of suspended solids on the homogenization of the liquid phase

under turbulent conditions in a stirred vessel, *Recents Progres an Genie des Procedes* ,11(52), 41–48.

Hicks, M. T., Myers, K. J., Corsptein, R. R., Baker, A., Fasano, J. B. (1993). Cloud height, fillet volume, and the effect of multiple impellers in solid suspension. *Mixing XIV conf*., Jun 20. Santa Barbara, CA.

Holden, P. J., Wang, M., Mann, R., Dickin, F. J., Edwards, R. B. (1998). Imaging Stirred-Vessel Macromixing Using Electrical Resistance Tomography. *AIChE J*., 44 (4), 780-790.

Hosseini, S., Patel, D., Mozaffari, E. F., Mehrab, M. (2010). Study of solid–liquid mixing in agitated tanks through electrical resistance tomography. *Chem. Eng. Sci*., 65(4), 1374-1384.

Houcine, I., Plasari, E., David, R. (2000). Effects of the Stired Tank's Design on Power Consumption and Mixing Time in liquid Phase. *Chem. Eng. Technol*., 23(7), 605-613.

Hoyle, B. S. (2005). A schema for generic process tomography sensors. *IEEE Sens. J.,* 5(2), 117-124.

Hua, P., Woo, E J., Webster, J. G., Tompkins, W. J. (1993). Using Compound Electrodes in electrical impedance tomography. *IEEE Trans.Biomed. Eng*., 40, 29-34.

Ibrahim, S., Nienow, A. W. (1996). Particle suspension in the turbulent regime: the effect of impeller type and impeller/vessel configuration. *Chem. Eng. Res. & Des*, 74(6), 679-688.

Ibrahim, S., Nienow, A.W. (1995). Power Curves and Flow Patterns for a Range of Impellers in Newtonian Fluids 40<Re<5x105. *Chem. Eng. Res. Des*.,73(5), 485-491.

Industrial Tomography System Ltd. (2006). Operating Manual. *Industrial Tomography System Ltd.*

Jahoda, M., Machon,V. (1994). Homogenization of liquids in tanks stirred by multiple impellers, *Chem. Eng. Technol*. 17, 95–101.

Jaworski, Z., Nienow, A. W., Dyster, K. N. (1996). An LDA Study of Turbulent Flow in Field in a Baffled Vessel Agitated by an Axial, Down Pumping Hydrofoil Impeller. *Can. J. Chem. Eng*., 74, 3-15.

Jaworski, Z., Nienow, A.W., Koatsakos, E., Dyster, K., Bujalski, W. (1991). Effect of Flow Pattern on the Solid Distribution in a Stirred Tank. *Trans. I. Chem. Eng*., 69(A), 313-320.

Javorski, Z., Nienow, A., W. Koutsakos, E., Bujalski, W. (1991). LDA study of turbulent flow in a baffled vessel agitated by a pitched blade turbine. *Chem. Eng. Res. Des*., 69, 313-320.

Kamiyama, M., Taguchi, S., Misumi, R., Nishi, K. (2005). Monitoring stability of reaction and dispersion states in a suspension polymerization reactor using electrical resistance tomography measurements. *Chem. Eng. Sci.,* 60(20), 5513-5518.

Kee, N. C. S., Tan, R. B. H. (2002). CFD simulation of solids suspension in mixing vessels. *Can. J. Chem. Eng*., 80(4), 721-726.

Kotre, C. J. (1989). A sensitivity coefficient method for the reconstruction of electrical impedance tomograms. *Clin.Phys. Physiol. Means.,* 10 (3), 275-281.

Kramers, H., Baars, G. M., Knoll, W. H. (1953). A comparative study on the rate of mixing in stirred tanks*. Chem. Eng. Sci*. 2, 35-42.

Kraume, M. (1992). Mixing Times in Stirred Suspensions*. Chem. Eng. Technol*., 15, 313-318.

Kukukova, A., Mostek, M., Jahoda, M., Machon, V. (2005). CFD Prediction of Flow and Homogenization in a Stirred Vessel: Part I Vessel with One and Two Impellers. *Chem. Eng. Technol.* 28(10), 1125-1133.

Kumaresan, T., Joshi, J. B. (2006). Effect of impeller design on the flow pattern and mixing in stirred tanks. *Chem. Eng. Sci*., 115, 173-193.

Kumaresan, T., Nere, N. K., Joshi, J. B. (2005). Effect of Internals on the Flow Pattern and Mixing in Stirred Tanks. *Ind. Eng. Chem.,* 44, 9951-9961.

Kuzmani´c, N., Zaneti´c, R., Akrap, M. (2008). Impact of floating suspended solids on the homogenization of the liquid phase in dual-impeller agitated vessel. *Chem. Eng. and Process*, 47, 663–669.

Lee, K. C., Yianneskis, M. (1997). Measurement of Temperature and Mixing Time in Stirred Vessels with Liquid Crystal Thermography. *Proc. 9th Europ. Conf. Mixing,* Paris, France.

Mak, A.T.C. (1992). *Solid–liquid mixing in mechanically agitated vessels*. Ph.D. Dissertation, University of London.

Mak, A. T. C., Ruszkowski, S. W. (1991). Scaling up solids distribution in stirred vessels. IV Fluid Mixing, *AIChE Symp*. Ser.121, 379-395.

Mann, R., Williams, R. A., Dyakowski, T., Dickin, F. J., Edwards, R. B. (1997). Development of mixing models using electrical resistance tomography. *Chem. Eng. Sci.,* 52 (13), 2073-2085

Masiuk, S., Lacki, H. (1993). Power Consumption and Mixing Time for Newtonian and Non-Newtonian Liquids Mixing in a Ribbon Mixer. *Chem. Eng. J*., 52, 13-17.

Mavros, P., Xubereb, C., Bertrand, J. (1996). Determination of 3-D Flow Fields in Agitated Vessels by Laser-Doppler Velocimetry. Effect of Impeller Type and Liquid Viscosity on Liquid Flow Patterns. *Chem. Eng. Res. Des*., 74, 658-668.

Menisher, T., Metghalchi, M., Gutoff E. B. (2000). Mixing Studies in Bioreactors. *Bioprocess Eng.*, 22, 115-120

Mewes, D., Schmitz, D. (2000). Analysis of the flow patterns in pipes and packings using tomographic methods. *Am. Soc. Mech. Eng,* 253, 487-500.

McCabe, W. L., Smith J. C., Harriott, P. (2005). *Unit Operations of Chemical Engineering* (7th Edition). New York: McGraw-Hill.

McFarlane, M. C., Zhao, X., Nienow, A. W. (1995). Studies of high solidity ratio hydrofoil impellers for Aerated bio reactors.2. air-water studies. , *Biotechnol prog*., 11, 608-618.

Michelletti, M., Nikiforaki, L., Lee, K. C., Yianneskis, M. (2003). Particle concentration and mixing characteristics of moderate-to-dense solid-liquid suspensions. *Ind. Eng. Chem. Res*., 42, 6236-6249.

Mishra, V. P., Dyster, K. N., Jaworski, Z., Nienow, A. W., Mckemmie, J. (1998). A Study of an Up- and a Down-Pumping Wide Blade Hydrofoil Impeller: Part I. LAD Measurements. *Can. J. Chem. Eng.*, 76, 577-588.

Montante, G., Micale, G., Magelli, F., Brucato, A. (2001). Experiments and CFD predictions of solid particle distribution in a vessel agitated with four pitched blade turbines. *Chem. Eng. Res. & Des*., 79(A8), 1005-1010.

Moo-Young, M., Tichar, K., Dullib, A. L. (1972). The Blending Efficiencies of Some Impellers in Batch Mixing. *AIChE J*., 18(1), 178-182.

Musil, L. (1976). Hydrodynamics of Mixed Crystallizers. *Collection of Czechoslovak Chem. Commun*. 41(3), 839-852,

Myer, K. J., Reeder, M. F., Bakker, A., Rigden, M. (1996). Agitating for Success. *Chem. Eng. J.* Oct.10, 39-42.

Myer,.K. J. (1996). The Performance of Multiple Impeller System in Solids Suspension. Industrial Mixing and scale up. *AIChE. Annual Meeting*, Nov.13. Chicago,USA.

Myers, K. J., Corpstein, R. R., Bakker, A., Fasano, J. B. (1993). Solids suspension agitator design with pitched blade and high efficiency impellers. 1st Industrial Chem Eng Tech Topical Conf, *AIChE. Annual Meeting*, Nov.7. St. Louis, Missouri, USA.

Myers, K. J., Corpstein, R. R., Bakker, A., Fasano, J. B. (1996). The effect of flow reversal on solids suspension in agitated vessels. *Can. J. Chem. Eng*., 74, 1028-1033.

Myers, K. J., Fasano, J. B., Corpstein, R. R. (1994). The influence of solid properties on the just suspended agitation requirements of pitched-blade turbines and high efficiency impellers. *Can. J. Chem. Eng*., 72, 745-748.

Nere, N. K., Patwardhan, A. W., Joshi, J. B. (2003). Liquid Phase Mixing in Stirred. *Ind. Eng. Chem. Res.* 42 (12), 2661-2698.

Nienow, A. W. (1990). Agitators for Mycelial Fermentations. *Trends. Biotechnol.*, 8, 224-233.

Nienow, A. W. (1997). On impeller circulation and mixing effectiveness in the turbulent flow regime. *Chem. Eng. Sci.*, 52, 2557-2565.

Nienow, A. W. (1968). Suspension of solid particles in turbine-agitated, baffled vessels. *Chem. Eng. Sci.*, 23, 1453-1459.

Oldshue, J.Y. (1983). *Fluid Mixing Technology*. New York: McGraw Hill Publications Co.

Ozcan-Taskin, G., Wei, H. (2003). The effect of impeller-to-tank diameter ratio on draw down of solid. *Chem. Eng. Sci.,* 58, 2011-2022.

Pant, H. J., Kundu, A., Nigam K. D. P. (2001). Radiotracer Applications in Chemical Process Industry. *Rev. Chem. Eng.,* 17, 165-252.

Patwardhan, A. W., Joshi, J. B. (1999). Relation between Flow Pattern and Blending in Stirred Tanks. *Ind. Eng. Chem. Res.*, 38, 3131-3143.

Paul, E. L., Atiemo-Obeng, V. A., Kresta, S. M. (2004). *Handbook of industrial mixing: Science and practice*. Wiley-Interscience.

Paulson, K., Breckon, W., Pidcock, M. (1992). Electrode Modeling in Electrical Impedance Tomography. *J. Appl. Math,* 52 (4), 1012-1022.

Peker, S. M., Helvaci S. S., Yener H. B., Ikizler B., Alparslan A. (2008). *Solid-liquid two phase flow* (1st edition). Oxford: Elsevier.

Perry, R. H., Green, D. (1984). *Chemical engineers handbook.* McGraw-Hill: New York.

Pinheiro, P. A. T., Loh, W. W., Waterfall, R. C., Wang, M., Mann, R. (1999). Three-dimensional electrical resistance tomography in a stirred mixing vessel. *Chem. Eng. Commun., 175*(1), 25–38.

Pinelli, D., Nocentini, M., Magelli, F. (2001). Solids distribution in stirred slurry reactors: influence of some mixer configurations and limits to the applicability of a simple model for predictions. *Chem. Eng. Commun*., 188, 91–107.

Raghav Rao, K. S. M. S., Rewatkar, V.B., Joshi, J. B. (1988). Critical impeller speed for solid suspension in mechanically agitated contactors, *AIChE J*. 34 (8), 1332–1340.

Ranade, V. V., Mishra, V. P., Saraph, V. S., Deshpande, G. B., Joshi, J. B. (1992). Comparison of Axial Flow Impellers Using a Laser Doppler Anemometer. *Ind. Eng. Chem. Res*., 31, 2370-2379.

Raghav Rao, K. S. M. S., Joshi, J. B. (1988). Liquid Phase Mixing and Power Consumption in Mechanically Agitated Solid Liquid Contactors. *J. Chem. Eng.,* 39, 111-124.

Ranade, V. V., Dommeti, M. S. (1996). Computational Snapshot of Flow Generated by Axial Impellers in Baffled Stirred Vessels. *Chem. Eng. Res. Des.* 74, 476-484.

Ranade, V. V., Joshi, J. B. (1989). Flow Generated by Pitched Blade Turbines I: Measurements using Laser Doppler Anemometer. *Chem. Eng. Commun*., 81, 197-224.

Reimers, P., Goebblels, J., Weise, H. P., Wilding, K. (1984). Some aspects of industrial non-destructive evaluation by X- and -ray computed tomography. *Nucl. Instr. And Meth*., 221, 201-206.

Rewatkar, V. B., Joshi, J. B. (1991). 1. Critical Impeller Speed for Solid Suspension in Mechanically Agitated Three-Phase Reactors. 2. Mathematical Model. *Ind. Eng. Chem. Res*., 30, 1784-1791.

Rewatkar V. B., Joshi J. B. (1991). Effect of Impeller Design on Liquid Phase Mixing in Mechanically Agitated Reactors. *Chem. Eng. Commun*., 91, 322-353.

Rushton, J. H. (1947). Design and Utilization of Internal Fittings for Mixing Vessels. *Chem. Eng. Prog.*, 43(12), 649-658.

Ruszkowski, S. (1994). A rational method for measuring blending performance, and comparison of different impellers. *Proc 8th Europ Mixing Conf,* IChemE Symp Series No. 136, Cambridge, Sep. 21. IChemE Rugby, UK.

Rzyski, E. (1993). Liquid Homogenisation in Agitated Tanks. *Chem. Eng. Technol*., 16 (4), 229-233.

Sahu, A. K., Kumar, P., Patwardhan, A. W., Joshi, J. B. (1999). CFD Modeling and Mixing in Stirred Tanks. *Chem. Eng. Sci*., 54, 2285-2293.

Sardeshpande, M. V., Sagi, A. R., JuveKar, V. A. (2009). Solid Suspension and Liquid Phase Mixing in Solid−Liquid Stirred Tanks. *Ind. Eng. Chem. Res*, 48(21), 9713–9722.

Selima, Y. S., Fangary, Y. S., Mahmoud N. A. (2008). Determination of minimum speed required for solid suspension in stirred vessels using pressure measurements. *Can. J. Chem. Eng*., 86, 661-666.

Scott, D. M., Sunshine, G., Rosen, L., Jochen, E. (2001). Industrial applications of process imaging & image processing. *Proc. SPIE Int. Soc. Opt. Eng*., 4188, 1-9.

Shervin, C. R., Raughley, D. A., Romaszewski R. A. (1991). Flow Visualization Scaleup Studies for the Mixing of Viscoelastic Fluids. *Chem. Eng. Sci.,* 46, 2867-2873.

Skelland, A. H. P. (1967). *.Non-Newtonian Flow and Heat Transfer.* New York: Wiley.

Tatterson, G. B. (1991). *Fluid mixing and gas dispersion in agitated tanks*. New York: Mc Graw-Hill Inc.

Takenaka, K., Takashi, K., Bujalski, W., Nienow, A. W., Paolini, S., Pagaltini, A., Etchells, A. (2005). Mixing time for different diameters of impeller at a high solid concentration in an agitated vessel. *Chem. Eng. J. of Japan*, 38(5), 309-315.

Thring, R. W., Edwards, M. F. (1990). An Experimental Investigation into the complete Suspension of Flaoting Solids in an Agitated Tank. *Ind. Eng. Chem. Res*. 29, 676-682.

Ulbrecht, J. J., Patterson, G.K. (1985). *Mixing of Liquids by Mechanical Agitation*. Gordon and Brach Science Publishers.

Weetman, R. J., Coyle, C.K. (1989). The Use of Fluidfoil Impellers in Viscous Mixing Application. *AIChE Annual Meeting*. Nov.5. California, USA.

Weetman, R. J., Gold, R., Creek, B. (1993). *Process/Mechanical Design Aspects for Lightnin A315 Agitators in Minerals Oxidation.* Beaver Creek, USA.

Williams, R. A., Mann, R., Dickin, F. J., Ilyas, O. M., Ying, P., Edwards, R. B. (1993). Application of Electrical Impedance Tomography to Mixing in Stirred Vessels. *AIChE J.,* 10, 8-15.

Williams, R. A., Beck, M.S. (1995). *Process tomography: principles, techniques and applications*. 7th ed. Oxford, UK: Butterworth-Heinemann.

Windholz, M., Budavari , S. (Editors) (1989). *The Merck Index*, (11th Edition). NJ: Merck and Company, Inc.

Wu, J., Graham, L. J., Mehdi, N.N. (2006). Performance Estimator of Agitator Flow Shear Rate. *AIChE J.*, 52(7), 2323-2332.

Wu, J., Pullum, L. (2000). Performance Analysis of Axial-Flow Mixing Impellers. *AIChE J.*, 46(3), 489-498.

Wu, J., Zhu, Y., Pullum, L. (2001). Impeller Geometry Effect on Velocity and Solid Suspension. *Chem. Eng. Res. Des*., 79, 989-997.

Wyczalkowski, W. (2004). How Fluid Properties Affect Mixer & Impeller Design. *J. Chem. Eng.*, 111(6), 43-47.

Yamazaki, H., Tojo, K., Miyanami, K. (1991). Effect of power consumption on solids concentration profiles in a slurry mixing tank. *Powder Technol.*, 64(3), 199-206.

Yan, C., Zhong, J., Liao, Y., Lai, S., Zhang, M., Gao, D. (2005). Design of an applied optical fiber process tomography system, Sensors and Actuators. *CIESC,* 104 (2), 324-331.

Zlokarnik, M. (2001). *Stirring: Theory and Practice.* Germany: Wiley-VCH: Weinheim.

Zwietering, T. N. (1958). Suspending of solid particles in liquid by agitators. *Chem. Eng. Sci., 8*(3), 244-253.